UNIVERSITY OF CALIFORNIA,

IRVINE

Eco-driving Strategies based on the Kinematic Wave Model in Various Traffic Situations

THESIS

submitted in partial satisfaction of the requirements

for the degree of

MASTER OF SCIENCE

in Civil Engineering

by

Pengyuan Sun

Thesis Committee:

Professor R. (Jay) Jayakrishnan, Chair

Professor Wenlong Jin

Professor Michael F. Hyland

2020

DEDICATION

Jingle bells, jingle bells,

Jingle all the way.

Oh, what fun it is to ride

in a one horse open sleigh!

------ To me, and to everybody

Life is such a fantastic journey because of you

Contents

List of Figures

List of Tables

Page

ACKNOWLEDGMENT

This is thesis is a summary of my work in the past two years at UC Irvine, and it provides me with an interesting topic for the future study. During the two years, I feel that, for the first time, transportation engineering is such a fantastic world that I can freely explore, while singing the enjoyable Jingle bells. However, as the truth is rarely pure and never simple, I would easily lose without the great helps from all of you.

I would like to thank my advisor, Dr. R. Jayakrishnan for illuminating me to think about the ideas in a network level. He is such an innovation-minded person who enlightens me to explore various interesting topics. I would also thank Dr. Wenlong Jin for his great inspirations on traffic flow theories. His experiences on basic theories make it the initial thesis from a little question in your final exam. I'm also appreciated Dr. Michael Hyland for his great comments on both the thesis and the project.

I would express my gratitude to my colleague and project leader, Dr. Daisik Nam, for his important suggestion on revising the thesis. Other friends in the research team also helped me a lot during this hard time of Covid-19. Finally, I would appreciate my families for supporting and encouragements.

CURRICULUM VITAE

Pengyuan Sun

EDUCATION

MSc in Civil Engineering **2020**

University of California, Irvine *Irvine, California, USA*

BSc in Traffic and Transportation Engineering **2018**

Beijing Jiaotong University *Beijing, China*

RESEARCH EXPERIENCE

Graduate Student Researcher **2018-present**

University of California, Irvine *Irvine, California, USA*

SERVICE

Regular Reviewer **2019-present**

Transportation Research Board/ Transportation Research Record

- AHB 45 2019
- ACP 15, ACP 30, ACP 80 2020

REFEREED PUBLICATIONS

Eco-driving Algorithm with A Moving Bottleneck on A Single-Lane Road **2020**

- Transportation Research Record (doi:10.1177/0361198120961381)
- Transportation Research Board 99th Annual Meeting (TRB 2020)

A Dynamic Real-Time Trajectory Smoothing Algorithm for the Vehicles Behind a Moving Bottleneck in Mixed Traffic **2021**

- Transportation Research Board 100th Annual Meeting (TRB 2021)

Impact of Advisory Speed Limit on the Overall Performance of Signalized Networks: A Network Fundamental Diagram Approach **2020**

- Transportation Research Board 99th Annual Meeting (TRB 2020)

ABSTRACT OF THE THESIS

Eco-driving Strategies based on the Kinematic Wave Model at Various Traffic Situations

By

Pengyuan Sun

Master of Science in Civil Engineering

University of California, Irvine, 2020

Professor R. (Jay) Jayakrishnan, Chair

With connected vehicle technology, eco-driving strategies could bring benefits in decreasing traffic oscillation, reducing fuel consumption along with air pollution, and improving traffic mobility. This thesis proposes an eco-driving strategy to reduce traffic oscillation and smooth trajectories for vehicles at different traffic situations, including highway sections and urban traffic intersections. The eco-driving strategy assumes a connected vehicle environment, in which each vehicle exchanges information in real-time through vehicle-to-infrastructure (V2I) communications and vehicle-to-vehicle (V2V) communications. The proposed strategy devises the advisory speed and the control duration for each vehicle through various control algorithms that are available in different traffic situations. After receiving the information from V2I and V2V communications, each connected vehicle would apply a simple cruise control method during the control duration. The proposed algorithm determines proper advisory speed and control duration through a heuristic solution of the optimization model, which is a tangent line approach. The optimization model, which has the objective function to minimize the speed oscillation of each vehicle, is applied at the origin or estimated trajectories under different traffic situations, including when vehicles are approaching a signalized intersection, non-signalized intersection, and following a moving bottleneck at an arterial road.

Based on the optimization model, this study proposes a heuristic solution which is a tangent line method between control starting point to the estimated objective trajectories, with the slope of the tangent line serving as the static advisory speed applied for the vehicle. The kinematic wave analysis is applied for deriving or estimating vehicle objective trajectories at each traffic situation. In a highway with a slow-moving vehicle, this study solves a more generalized moving bottleneck problem to derive the traffic flow-rate and density upstream of the moving bottleneck, and get the following trajectory for each vehicle after the moving bottleneck. At traffic intersections, the kinematic wave analysis is first applied to describe vehicle start-up behaviors and demonstrate the requirements for improving traffic efficiency. According to the requirements, the estimated time points (i.e., the passing points) are created for vehicles to pass through the intersection. Accordingly, the origin trajectories are estimated in order to make vehicles enter the intersection at each passing point with the designed optimal speed. For a signalized intersection, the passing points are created based on a specific signal plan of a given phasing. In addition, the eco-driving strategy could also be extended into a Cooperative Vehicle Intersection Control (CVIC) algorithm and applied at a non-signalized intersection. In this situation, the passing points are created and updated according to the previous vehicles passing through the intersection from different directions.

The benefits of this strategy are presented from a set of numerical simulations. At the intersection, the benefits are also evaluated with different flow-rate levels of the approaching traffic flows. The simulations are conducted for each traffic situation. In the highway sections, four scenarios with different bottleneck movements are applied, where the moving bottleneck has a constant speed, accelerates, decelerates, and stops-and-goes. The results show that both speed variance and fuel consumption are reduced with the algorithm in each of the scenarios. At the signalized intersections, all vehicles applying the algorithm would never stop before the intersection and would pass through the intersection with the free-flow speed. The number of vehicles that could pass through the intersection also increases. Also, traffic oscillation is reduced when approaching the intersection. With the CVIC algorithm applying at the intersection, all vehicles could pass through the intersection with free-flow speed, and no traffic confliction happens between vehicles. Furthermore, in an illustrative study, the algorithm reduces the total intersection delay by 34.95 % on average, the fuel consumption by 65.79 % on average, and the speed variance by 5.75 % on average. The simulation result shows the algorithm could be beneficial in decreasing traffic oscillation, reducing environmental impact,

and improving traffic efficiency as well when applied at the intersections. The basic idea behind this study is to make a predictable time and speed for the vehicle to eliminate the moving bottleneck effects and to pass through the intersection. This information provides a theoretical basis for further optimizing the traffic flows through the V2I, V2V communications, and CAV technologies, which could be applied to various situations.

Chapter 1

Introduction

1.1 Motivation

Greenhouse gas emissions contribute significantly to global warming and climate change (INRIX, 2019). According to the study of (Rakha *et al.*, 2011), 30% of energy consumption in the US comes from the transportation sector, which is responsible for a significant portion of greenhouse gas emissions as well as air pollution. Transportation is also a primary source of wasted time for the public and energy consumption in urban networks. In 2018, each American lost 97 hours due to traffic congestion, at a total cost of 87 billion dollars (INRIX, 2019). In the European Union, transportation is responsible for 33% of total energy consumption (Cruz, 2013). Fluctuations in traffic flow lead to frequent accelerations and decelerations, which can cause extra greenhouse gas emissions and air pollution and worsen environmental conditions (Yang and Jin, 2014). At the same time, traffic oscillation has been proved to be a major culprit behind high fuel consumption and extra delay (Li *et al.*, 2014).

Extra traffic oscillations could be generated in various traffic situations. In highway sections, smooth flow of traffic could be easily hampered when a moving bottleneck appears. A moving bottleneck is caused by a slow-moving vehicle with speed lower than mainstream traffic (Gazis and Herman, 1992). A moving bottleneck would inevitably force the following upstream traffic to brake, which generates kinematic waves and leads to traffic oscillations. Such traffic oscillations would jeopardize the efficient movement of traffic and build up a queue behind the bottleneck (Li *et al.*, 2014). When the vehicle causing the moving bottleneck leaves the road, queue dissipation requires upstream vehicles to accelerate, which significantly lifts fuel consumption and may potentially incur loss time. For a human driving vehicle (HV), an experienced driver usually gradually reduces the speed while approaching the bottleneck in

order to avoid abrupt deceleration and acceleration. Nonetheless, vehicle speed oscillations are not fully avoidable due to the lack of information on the leading vehicle's movement.

Apart from the slow-moving vehicles that could lead to traffic oscillation, urban traffic flows could also be frequently interrupted by various traffic infrastructures. In traffic intersections, where vehicle trajectories from more than two directions could conflict, proper traffic control methods are necessary to be enforced for safety concerns, such as traffic signals and stop/yield signs. As a price for traffic safety, vehicles traveling through these two kinds of intersections basically experience 'stop-and-go' movements, which create additional traffic oscillations. As a result, traffic delay and extra fuel consumption at traffic intersections is even greater than other traffic infrastructures (Li, Peng and Ouyang, 2010) (Li *et al.*, 2014). The conclusion that the intersections cause a majority of traffic delays for the vehicles is well-known and elaborated in many studies (Hurdle, 1984) (Wolshon and Taylor, 1999) (Ban *et al.*, 2009).

With the objective to decrease the environmental impact in transportation, eco-driving refers to a set of driving modes and strategies which could be applied in vehicles. Eco-driving can be achieved through multiple control mechanisms. Traffic oscillation smoothing is a conventional approach to achieve eco-driving (Ahn *et al.*, 2002). In recent years, with the development of connected and autonomous vehicle (CAV) technology, vehicles could exchange information with others instantaneously through Vehicle-to-Vehicle (V2V) communication. Taking advantage of V2V communication, more accurate and real-time control algorithms could be applied, and effective vehicle control schemes could be developed to further smooth traffic and avoid excessive oscillations. Such kinds of control algorithms could be applied at different traffic situations like signalized intersections (Jiang *et al.*, 2017), freeways (Yang and Jin, 2014), and arterial corridors with intersections (Barth *et al.*, 2011). The algorithm outputs for traffic control are also various, including the advisory speed limit (Al-Dweik *et al.*, 2017), and the optimal speed during adaptive cruise control (Zhou *et al.*, 2020). Although traffic oscillation decrease could be shown from the results, these algorithms apply other objective functions, such as maximize traffic throughput (Ubiergo and Jin, 2016), reach location optimization (Yao *et al.*, 2018), and minimize fuel consumption (Lin *et al.*, 2018). From the results of the previous studies, eco-driving strategies could be proposed and applied to various

traffic situations, and are also potentially beneficial at various aspects, such as becoming more environment friendly, improving traffic mobility, and decreasing traffic oscillation.

The basic idea of eco-driving strategies is introduced into the transportation field for training the drivers how to save the fuel while driving (Dandrea, 1986). Later, the eco-driving is further extended with the combination of control schemes for smoothing traffic oscillation, such as are in the literature for smoothing traffic oscillations, such as setting advisory speed signs (Smulders, 1990), enforcing speed controls policy on different road sections (Vaa, 1997), and installing bumps to adjust vehicle travel speed (Pau and Angius, 2001). In such early studies, the control schemes are usually universal and static, which may not capture the dynamics in traffic flow.

Recent advances in CAV technology enable wireless communications between vehicle to vehicle (V2V) and vehicle to infrastructure (V2I) (Santa, Gómez-Skarmeta and Sánchez-Artigas, 2008). Based on such advanced technologies, CAV could collect extra travel information in advance, and the infrastructure could also obtain more data on the upcoming vehicles. Taking advantage of the detailed traffic information, various driving strategies and control algorithms could be proposed that control the vehicles in real-time and accurately, with the objectives such as improving traffic mobility and reducing traffic oscillation. (Mensing, Trigui and Bideaux, 2011) uses dynamic programming optimization to maximize vehicle costs for the whole system. (Barth *et al.*, 2011) focus on minimizing fuel consumption and gas emissions by real-time vehicle trajectory design in an arterial. At signalized intersections, (Ma *et al.*, 2017) and (Zhou, Li and Ma, 2017) introduce a shooting heuristic algorithm for vehicles to pass the signal with the maximum cruise speed. (Zhao *et al.*, 2018) applies a receding-horizon model-predictive control to achieve minimum energy consumption in mixed traffic flow.

Further extend the eco-driving strategies with CAV technology, the vehicle control algorithms could also lead to novel intersection control methods. The Cooperative Vehicle Intersection Control (CVIC) system can enable connected vehicles to work together with the infrastructure controller via V2I communication to achieve intersection control (Lee and Park, 2012). The

CVIC system provides a new intersection control strategy, through which the controller gathers the information of the upcoming vehicles and guarantees each vehicle passing through the intersection smoothly and safely. Since the vehicles could pass through the intersection purely using other vehicles' real-time travel information, the traffic signals and stop/yields are not necessarily included as a part of the control system. (Lee and Park, 2012) provides an algorithm with CVIC and evaluates the potential benefits. For safety issues, (Lu *et al.*, 2014) proposes a set of rules on the algorithms with CVIC to make connected vehicles pass through unsignalized intersections without potential conflicts.

1.2 Overall layout of the thesis

Based on the previous studies of eco-driving algorithms, this study proposes an advisory speed method that could be applied in highway roads and at traffic intersections. According to the basic idea of the eco-driving strategies, an optimization model is proposed with the objective of minimizing the speed oscillation for each vehicle. In some previous studies (Shamir, 2004) (Li and Li, 2019), the eco-driving algorithms provide each vehicle with a specific trajectory (or the designed speed at each time), and vehicles couldn't adjust their trajectory according to the real-time traffic situation. Safety issues and computational complexity concerns make these algorithms hard to apply in such cases. Instead of continuously controlling vehicle speed at each time, a static cruise speed control method is proposed in this study, which makes the control algorithms less complicated and easy to apply.

The advisory speed for each vehicle is designed from a heuristic solution of the optimization model, based on the vehicle's original traveling trajectory without any eco-driving strategy. When travelling along the highway roads, the following original trajectories after the moving bottleneck vehicle could be derived from the moving bottleneck problem. When the eco-driving strategy is applied at the intersections, the estimated trajectories are created with the objective that vehicles would pass through the intersection most efficiently when traveling along the estimated trajectories. Therefore, the algorithms could potentially improve traffic mobility at the intersections besides traffic oscillation smoothing. Further, the algorithm could also be extended as a CVIC control method, which proposes another intersection control method other than a traffic signal.

The main assumptions of the eco-driving strategy are described as follows:

1. All vehicles are homogeneous in size and travel behavior as long as an algorithm has not applied.
2. The algorithm assumes an uncongested traffic state, where all vehicles could travel with the free-flow speed if not being impeded by the moving bottleneck or intersection controls.
3. A connected vehicle environment is assumed in this study, where all vehicles are connected and autonomous. At the intersections, other connected vehicle environment assumptions shown in (Lee and Park, 2012) are also applied in this study.
4. The travel information and algorithm outputs are conveyed between each vehicle and vehicle-infrastructure via V2V and V2I communications.
5. Delays due to computations, communications and vehicle reactions are omitted in formulating and algorithm designs.
6. Lane changing behaviour is not taken into account in algorithm designs.

The rest of the thesis is organized in the following chapters:

- Chapter 2 provides the methodology on which the rest of the studies is supported. Based on the vehicle start-up behaviour, the requirements for fully minimizing the headway and intersection clearance time are further explored. This section is based on (Sun and Jayakrishnan, 2021). Also, a generalized moving bottleneck problem is solved in order to derive the following vehicle trajectories. This section is based on (Sun, Yang and Jin, 2020). The optimization model is then proposed, and the heuristic solution is presented as the method for advisory speed generation. This section is based on (Sun, Yang and Jin, 2020) and (Sun, Yang and Jayakrishnan, 2021).

- Chapter 3 introduces the simulation testbed (mainly including the car-following model, the acceleration function) which is applied in the numerical experiments for testing the

eco-driving control algorithms introduced in the following chapters. This chapter also introduces the evaluations for testing the algorithm performances. The three evaluations include the speed variance, average speed, and fuel consumption to represent the speed oscillation, traffic efficiency, and environmental impact, respectively.

- Chapter 4 presents the eco-driving algorithm applied in a highway section following a moving bottleneck. The leading vehicle is assumed to pre-plan its leading trajectory on the road as the moving bottleneck trajectory. Based on the leading vehicle moving trajectory, each following vehicle would estimate their following original trajectory by solving the moving bottleneck problem introduced in Chapter 2. The advisory speed and the control duration are generated for each following vehicle according to the original trajectory. This chapter is based on (Sun, Yang and Jin, 2020).

- Chapter 5 presents the eco-driving algorithm applied at the signalized intersections, considering a pre-known signal phasing plan. The study first demonstrates the requirement for fully utilizing the signal capacity given a phasing interval. Based on the requirement, the passing point and the corresponding estimated trajectory are created, which could direct each vehicle entering the intersection most efficiently. Then, the advisory speed and control duration is determined through a control framework according to the chosen estimated trajectory. A set of simulations are conducted to compare the trajectories and evaluate the algorithm performances under different flow-rate levels. This chapter is based on (Sun, Nam and Jayakrishnan, 2021).

- Chapter 6 further proposes an eco-driving CVIC algorithm at the intersection, through which the signal control could be totally replaced by the V2I communications. In this algorithm, the passing points for upcoming vehicles are purely created and updated according to the previous vehicles passing through the intersection from different directions. The estimated trajectory is still generated for each passing point in order to design the advisory speed and control duration for each vehicle. A set of simulations are conducted to compare the trajectories and test the safety of the algorithm. The

sensitivity analysis is also presented to evaluate the algorithm performances under different flow-rate levels in each ring road. This chapter is based on (Sun and Jayakrishnan, 2021).

- Chapter 7 provides the conclusions of the thesis and proposes some further studies.

Chapter 2

Methodology

2.1 LWR model and kinematic wave analysis

The eco-driving strategy introduced in this thesis consists of three algorithms which are all based on kinematic wave analysis. The kinematic waves are applied to model fluctuations of the traffic flows in various situations, such as intersections and highways. In traffic flow analysis, the Lighthill-Whitham-Richard (LWR) model is a traditional model for deriving the kinematic waves(Lighthill *et al.*, 1955) (Richards, 1956). The LWR model is formulated by differentiating the cumulative flow on time and location and can be written as Eq. (2.1).

$$\frac{\partial k(x,t)}{\partial t} + \frac{\partial Q(k(x,t))}{\partial x} = 0 \tag{2.1}$$

Eq. (2.1) has an assumption that the accelerations of vehicles are not limited. From the view of the application, vehicle accelerations should be bounded and could be related with the vehicle speed and the real-time traffic density. Later, the following studies (Jin and Laval, 2018) (Jin, 2019) implement the LWR model with the acceleration function. Eq. (2.2) shows the LWR model considering vehicle acceleration, where $\Psi\left(v, k^{-1}, \left(\frac{\partial v(x,t)}{\partial x}\right)^{-1} k\right)$ is the acceleration equation that satisfies $\Psi(v, k^{-1}, 0) = 0$ with the purpose of avoiding traffic collisions, and ϵ is an infinitesimal number.

$$\frac{\partial v(x,t)}{\partial t} + \frac{\partial v(x,t)}{\partial x} v(x,t) = \max\left\{-\frac{v(x,t)}{\epsilon}, \min\left\{\frac{V(k)-v(x,t)}{\epsilon}, \Psi\left(v, k^{-1}, \left(\frac{\partial v(x,t)}{\partial x}\right)^{-1} k\right)\right\}\right\} \tag{2.2}$$

The LWR model considers a relationship between traffic flow-rate (q) and the density (k), i.e., the fundamental diagram. This thesis applies a triangular fundamental diagram for calculating propagation speeds of kinematic waves in the $x - t$ figure, which is shown in Figure 2.1. Eq. (2.3) presents the triangular fundamental diagram, where v_f is the free-flow speed, w serves as the shock wave speed in congested traffic, and k_j is the jam density.

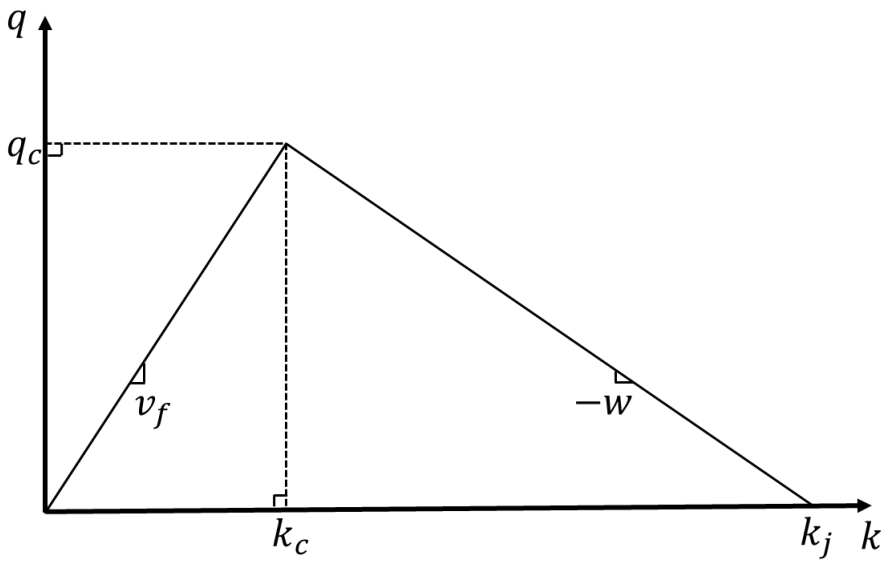

Figure 2.1 The Triangular Fundamental Diagram

$$Q(k) = min\{v_f k, w(k_j - k)\} \tag{2.3}$$

The LWR model with acceleration and the triangular fundamental diagram could be combined to derive kinematic wave propagation speeds between two different traffic states (Leclercq, 2007b). When the upstream traffic is denser than the downstream traffic, a rarefaction wave appears and propagates backward with the speed of $-w$ in an $x - t$ figure. The propagation speed of a rarefaction wave is calculated as Eq. (2.4).

$$w = \frac{q_c}{k_j - k_c} \tag{2.4}$$

When when the downstream traffic is denser than the upstream traffic, a shock wave would appear. The propagation speed of the shock wave is related to the traffic states in downstream traffic (with the flow-rate of q_1 and density of k_1) and upstream traffic (with the flow-rate of q_2 and density of k_2). Eq. (2.5) calculates the propagation speed of the shock wave.

$$v_s = \frac{q_1 - q_2}{k_1 - k_2} \tag{2.5}$$

In the following sections of Chapter 2, the kinematic wave analysis is applied to various traffic scenarios, with the objective of deriving the traffic states $(\tilde{q}, \tilde{k})$ at different locations and times. According to the traffic states, following vehicle trajectories could be derived at the upstream traffic.

2.2 Kinematic wave analysis at intersections

2.2.1 Vehicle start-up behavior

The start-up behaviour is to describe the traffic oscillation when queuing vehicles begin to start up at the intersection. According to the kinematic wave model, when the first queuing vehicle starts to speed up, the downstream traffic (a downside of the first vehicle location) is less dense than the upstream traffic (other queuing vehicles), the rarefaction wave would propagate backward with the speed of $-w$ in $x - t$ space. As the first vehicle accelerates, rarefaction waves keep generating and propagating until the first vehicle reaches a steady speed and stops accelerating. The following vehicles begin to accelerate when the first rarefaction wave reaches their waiting positions. As vehicles are assumed to be homogeneous, following vehicles would have the same acceleration trajectory as the first vehicle, while the accelerating behaviour is along the rarefaction wave. The traffic dynamics and queuing vehicle trajectories in vehicle start-up behaviour are shown in Figure 2.2(a), assuming the queuing vehicles start up from the static state at the intersection.

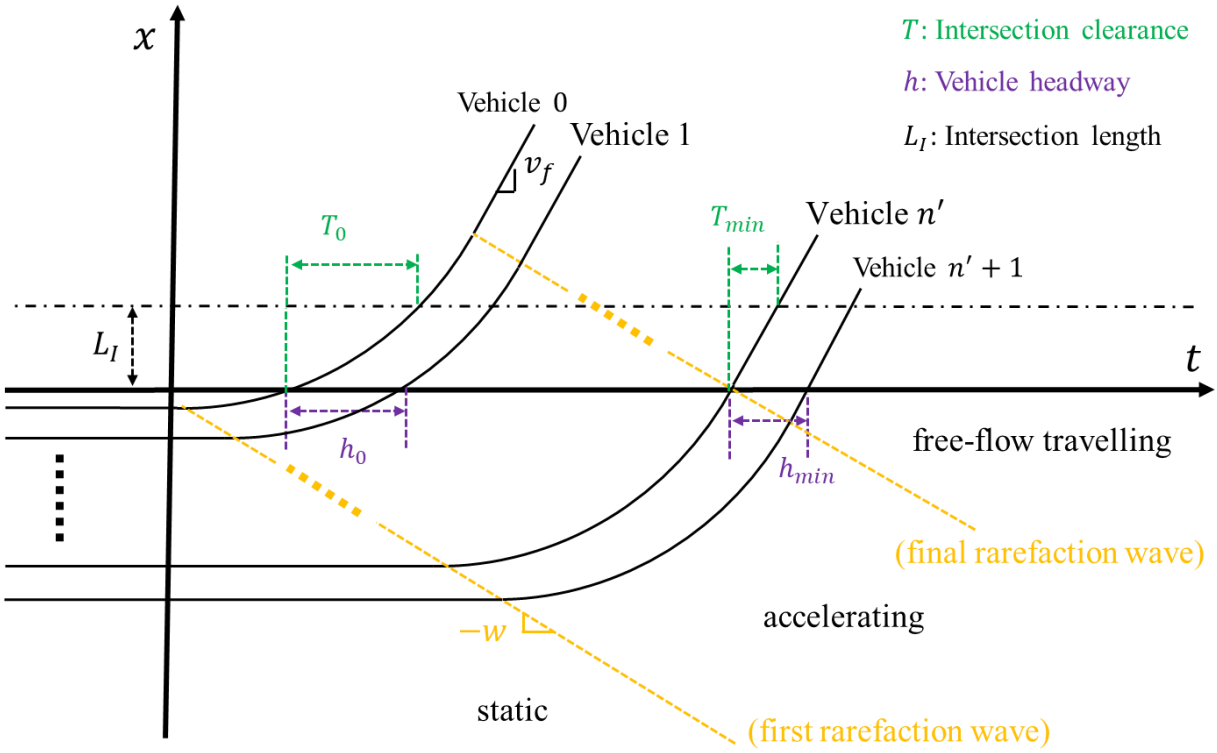

(a)

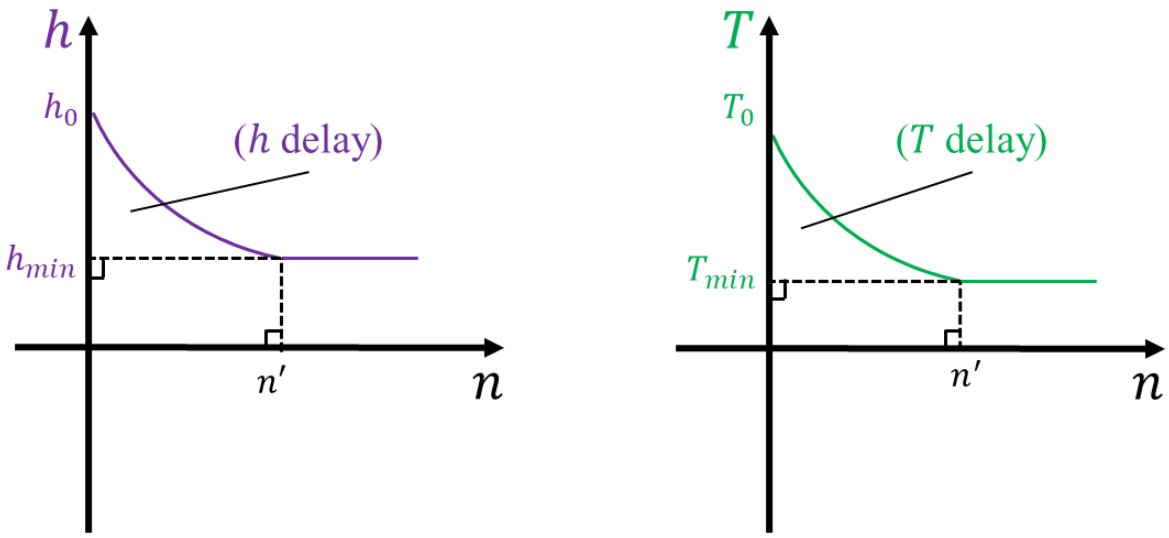

(b) **(c)**

Figure 2.2 Kinematic Wave Analysis at An Intersection

From Figure 2.2(b), vehicle start-up behaviour would lead to an additional time-lost (h delay). The time-lost is embodied in longer headways when vehicles enter the intersection. The headway (h) is a measure of time between the front bumpers of two vehicles. The headway

could be expressed in Eq. (2.6), where $\bar{\tau}$ denote the average time gap between vehicles, and L is the length of the first vehicle. The gap is defined as a measure of time between the rear bumper of the first vehicle and the front bumper of the second vehicle.

$$h = \bar{\tau} + \frac{L}{v} \tag{2.6}$$

The time-lost of the vehicle start-up behaviour could be analysed by the intersection-entering speed (v_I). The intersection-entering speed refers to the instantaneous speed when the vehicle enters the intersection. Theorem 2.1 provides a necessary condition to achieve the minimum headway when vehicles enter the intersection, assuming that vehicles are in the same length of L and the average gap is given.

Theorem 2.1. The headway becomes the minimum if and **only if** the vehicles enter the intersection with the free-flow speed (v_f).

Proof. Let $\bar{\tau}$ be the average time gap between two vehicles. Similar with Eq. (2.6), the headway when vehicles enter the intersection can be expressed as Eq. (2.7).

$$h(v_I) = \bar{\tau} + \frac{L}{v_I} \tag{2.7}$$

Since $v \leq v_f$,

$$\bar{\tau} + \frac{L}{v_I} \geq \bar{\tau} + \frac{L}{v_f} = h(v_f) = h_{min} \tag{2.8}$$

Where $h(v_f)$ denotes the headway when travelling with the free-flow speed.

However, when vehicles begin to accelerate, the intersection-entering speed could not reach the free-flow speed as a result of the bounded acceleration, which leads to the start-up time-lost.

2.2.2 Intersection clearance time

The intersection clearance time (T) refers to the time interval between intersection entering time and exit time. Given a fixed length of the intersection area, the intersection clearance time depends on vehicle average speed when passing through the intersection. If a vehicle enters the intersection with a lower speed, it would occupy the intersection for a long time, and the lagter intersection clearance time would result a time delay. The clearance time-lost is shown in Figure 2.2(a) and 2.2(c). For safety concerns, vehicles from conflicting directions shall not enter the intersection until the vehicle totally leaves the intersection. Therefore, a longer clearance time would potentially make vehicles from other directions wait a longer time before being allowed to pass through the intersection. With the objective of reducing the intersection clearance time-lost, Theorem 2.2 provides a necessary condition to achieve the minimum intersection clearance time (T) when a vehicle enters the intersection, given the vehicle length is L and the travel distance within the intersection L_I.

Theorem 2.2. The intersection clearance time for a vehicle reaches the minimum **only if** the vehicle travels through the intersection with the free-flow speed (v_f).

Proof. Let $\overline{v_I}$ be the average speed when the vehicle is within the intersection, the intersection clearance time for the vehicle could be expressed as Eq. (2.9).

$$T(v_I) = \frac{L+L_I}{\overline{v_I}} \tag{2.9}$$

Since $\overline{v_I} \leq v_f$,

$$\frac{L+L_I}{\overline{v_I}} \geq \frac{L+L_I}{v_f} = T(v_f) = T_{min} \tag{2.10}$$

Where $T(v_f)$ denotes the intersection clearance time when travelling through the intersection with the free-flow speed.

From the analysis shown in section 2.1 and section 2.2, the vehicle bounded acceleration leads to the lost-time from two aspects, including the headway lost-time (h delay) and the intersection clearance lost-time (T delay). From Theorem 2.1 and Theorem 2.2, passing through the intersection with the free-flow speed could make both the headway and clearance time into the minimum at the same time. The eco-driving algorithms designed for intersections are proposed based on the properties analysed above, while the methodology for algorithm design on the freeway section is introduced in the next section.

2.3 The kinematic wave analysis in highway sections (the moving bottleneck problem)

Kinematic wave analysis could be applied to describe the traffic dynamic in a highway section. Smooth-moving traffic in highway sections could be easily hampered when a moving bottleneck appears. In this study, a moving bottleneck refers to a slow-moving vehicle with speed lower than mainstream traffic. Therefore, the moving bottleneck would inevitably force the following upstream traffic to brake, which generates kinematic waves and leads to traffic oscillations. Based on the kinematic wave analysis, the moving bottleneck problem is to derive the traffic flow dynamic and following vehicle trajectories upstream of the moving bottleneck. A great number of previous studies (G. . Newell, 2002) (Leclercq, 2007a) (Leclercq, Chanut and Lesort, 2004) (Fadhloun, Rakha and Loulizi, 2016) have analysed and solved the moving bottleneck problem with the fixed and constantly moving bottleneck as well as considering the vehicle acceleration functions. In this subsection, the trajectories of the following vehicles are derived by solving a generalized moving bottleneck problem where the moving bottleneck

could be either constant or varying speeds. Based on the vehicle following trajectory, the eco-driving algorithm applied, at the moving bottleneck scenario, could be proposed in Chapter 6 for each connected following vehicle.

The slow-moving vehicle could travel with constant speed or varying speeds. When a moving bottleneck enters the road segment with speed lower than the free-flow speed, it begins to create traffic states which are different from the initial uncongested state. As long as the bottleneck is in the road section, it keeps creating traffic states when its speed changes. Since the bottleneck moving speed is less than the free-flow speed, these traffic states are all at lower speeds than the uncongested state. Once a new traffic state is created, characteristic waves are generated between the new traffic state and others. Every time step, these characteristic waves propagate until they merge into other waves. The traffic behind the bottleneck is alternating between different states as the speed of the bottleneck changes.

Figure 2.3(a) shows different traffic states and waves in the fundamental diagram. The initial upstream traffic state is at (k_1, q_1). The moving bottleneck speed is $v_b(t)$, which varies over time. When the moving bottleneck enters the road at $t = 0$ with the speed of $v_b(0)$ ($v_b(0) < u$) between the initial state (k_1, q_1) and the first congested traffic state $\big(k_b(0), q_b(0)\big)$, a shockwave forms the initial propagation speed of $v_s(0)$. Since the bottleneck speeds are varying, congested traffic states are created along the congestion curve (with the slope of $-w$) of the triangular fundamental diagram.

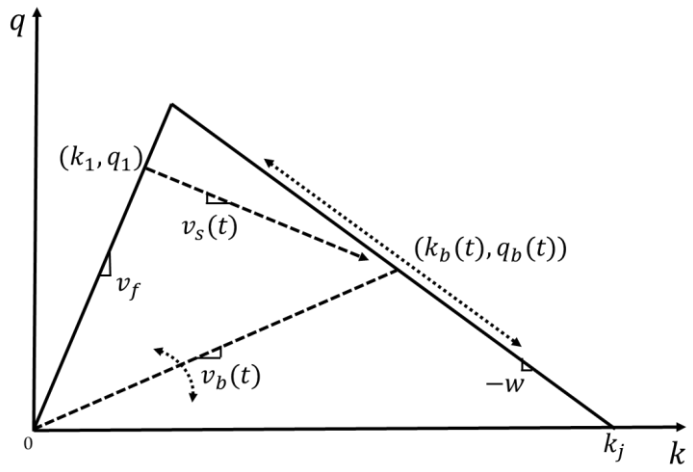

(a)

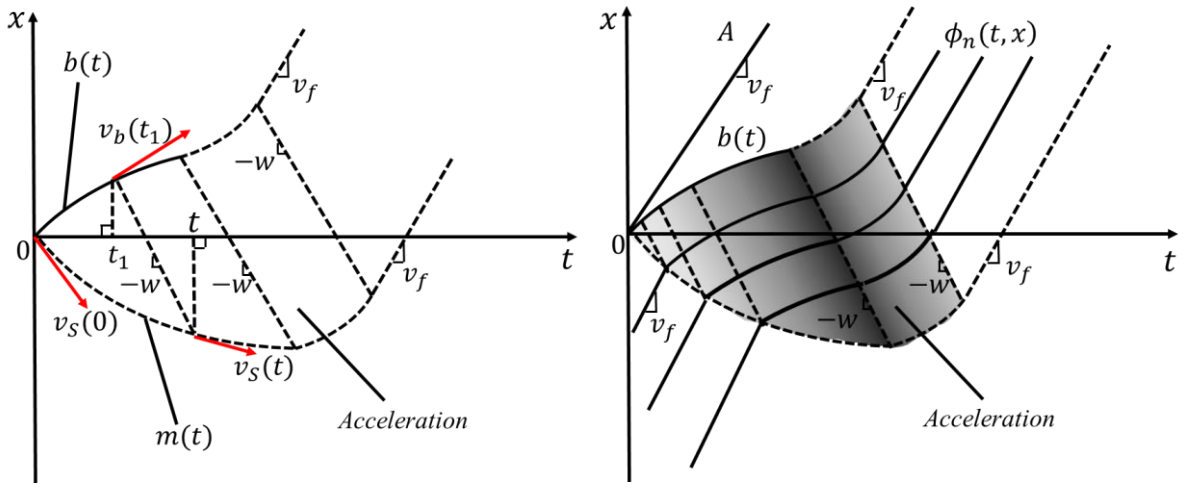

(b) **(c)**

Figure 2.3 Analytical Solution for the Moving Bottleneck Problem

Figure 2.3(b) shows the corresponding traffic states and characteristic waves of Figure 2.3(a) in $x-t$ space. At $t=0$, the bottleneck enters the road with an initial speed $v_b(0)$ ($v_b(0) < u$), and a shock wave with the initial propagation speed $v_s(0)$ is generated. The speed can be derived from Eq. (2.4) and the triangular fundamental diagram. As the bottleneck speed ($v_b(t)$) changes with time, characteristic waves are generated and propagated until they merge into the shock wave curve ($m(t)$). The instantaneous speed of the shock wave at each time is derived from the traffic state generated along with the characteristic wave, and the initial upstream state. In Figure 2.3(a) and 2.3(b), and formulations below, t_1 is the time point when one characteristic wave generates from the bottleneck; t is the time point when this wave merges into the shock wave. q_1 and k_1 are the flow rate and density of upstream flow.

$$\frac{dm(t)}{dt} = v_s(t) \tag{2.11}$$

$$\frac{db(t)}{dt} = v_b(t) \tag{2.12}$$

Eq. (2.11) and Eq. (2.12) describe the relation between speed and trajectory in $x-t$ space. For both bottleneck trajectory ($b(t)$) and shock wave curve ($m(t)$), the speeds at each time, i.e. $v_b(t)$ and $v_s(t)$ respectively, are derived from taking derivatives.

$$\frac{m(t)-b(t_1)}{t-t_1} = -w \tag{2.13}$$

$$v_s(t) = v_b(t_1) \tag{2.14}$$

$$v_s(t) = \frac{q_1-q_b(t_1)}{k_1-k_b(t_1)} \tag{2.15}$$

Eq. (2.13), Eq. (2.14) and Eq. (2.15) demonstrate the features of shock waves and rarefaction waves. In Eq. (2.13), the characteristic wave is generated from the bottleneck at time $t = t_1$ and propagates backward with the speed of w. When the characteristic wave meets and merges to the shock wave ($m(t)$), at the time t, the speed of the shock wave is derived from Eq. (2.14) and Eq. (2.15).

$$q_b(t_1) = k_b(t_1)v_b(t_1) \tag{2.16}$$

$$q = Q(k) \tag{2.17}$$

Eq. (2.16) is the constitutive law to derive the traffic condition including density and flow rate at the time $t = t_1$, when the bottleneck is with the varying speeds of $v_b(t_1)$. To derive $k_b(t_1)$ and $q_b(t_1)$, the relationship between flow rate and density is needed and shown in the fundamental diagram Eq. (2.17).

If the triangular fundamental diagram Eq. (2.3) is applied, we can derive the traffic state at each time caused by the moving bottleneck from Eq. (2.18), where $k_b(t_1)$ and $q_b(t_1)$ are the density and flow rate at the bottleneck location at the time $t = t_1$.

$$\begin{cases} k_b(t_1) = \dfrac{1}{\tau\left(\frac{d(b(t))}{dt}\right)_{t_1} + \tau w} \\ q_b(t_1) = \dfrac{\left(\frac{d(b(t))}{dt}\right)_{t_1}}{\tau\left(\frac{d(b(t))}{dt}\right)_{t_1} + \tau w} \end{cases} \tag{2.18}$$

Finally, based on the traffic states caused by the moving bottleneck at each time $(k_b(t), q_b(t))$, and the initial traffic state (k_1, q_1), the shock wave curve $(m(t))$ could be generalized into the form of a first-order linear differential equation, which is shown in Eq. (2.19). When the moving bottleneck trajectory $(b(t))$ is given, combined with Eq. (2.18) and Eq. (2.19), the shock wave curve could be analytically derived by solving the differential equation.

$$\begin{cases} \dfrac{dm(t)}{dt} = \dfrac{q_1 - q_b(t_1)}{k_1 - k_b(t_1)} \\ \dfrac{m(t) - b(t_1)}{t - t_1} = -w \end{cases} \tag{2.19}$$

At the same time, the moving bottleneck problem analysis could also derive the trajectories of the following vehicles, through the densities and flow rates of traffic states at each time and location. For example, when all the vehicles obey Newell's car-following model with bounded acceleration, and the bottleneck is decelerating and then leaves the road, the following trajectories are shown in Figure 2.3(c). If the following vehicles are being impeded by the moving bottleneck, the following trajectories repeat the moving bottleneck trajectory after entering the shock wave curve. When the bottleneck disappears, if the following vehicle speeds are lower than the free-flow speed, the following vehicles will accelerate at the bounded acceleration rate until reaching the free-flow speed. The following vehicle trajectories, which are derived from solving the moving bottleneck problem, are the foundation of deriving the eco-driving strategy in the next section.

2.4 The optimization model for minimizing the vehicle speed oscillation

The control outputs for the eco-driving algorithms include the static advisory speed for each connected vehicle (v_n^a) and the corresponding ending algorithm time (t_n^*). In optimization language, the objective could be minimizing the level of emissions for various harmful gas, which is shown in Eq. (2.20), where $f(\cdot)$ calculates the emissions for a given vector of advisory speed ($\overrightarrow{v^a}$) under given constraint sets.

$$min\, E = f(\overrightarrow{v^a}) \tag{2.20}$$

However, the relationships between vehicle speed and the fuel consumption are not unique and could also be non-convex. Due to the complexity of the objective function, the optimal solution is hard to obtain. In addition, the objective functions are based on different gas emissions and various emission models, which include parameters with uncertainty. As a result, the optimal solution may not be accurate and universal for different circumstances, and this study proposes a heuristic solution for trajectory design.

We assume that the intersections and moving bottlenecks in highways are considered as the traffic obstructions for smooth-moving traffic flows. When vehicles have travelled through intersections or the highway moving bottleneck leaves/regains the free-flow speed, inevitably, the traffic flow needs to accelerate until it reaches a steady speed. The vehicle's original trajectory ($\phi_n(t)$), which could be optimized in this section, contains a deceleration and oscillation period where vehicle behaviour is impacted by the obstructions (i.e., the impeded period), as well as the acceleration period, where the vehicle is not impacted by the traffic bottleneck and regains the free-flow speed. Considering the factors above, this study proposes an objective function shown in Model 2.1.

Model 2.1. Speed Oscillation Minimization for a Vehicle

min:

$$\sigma = \int_{t_0}^{t_n^2} \left(a_n(t)\right)^2 dt \tag{2.21}$$

$s.t.$

$$\phi_n'(t) - \phi_{n-1}'(t) \geq h_{\min}^{v_n(t)} \quad (\forall t \in [t_0, t_n^2], \forall n \in N) \tag{2.22}$$

$$\frac{d^2(\phi_n'(t))}{dt^2} \leq \Psi\left(v(t), k(t)^{-1}, \left(\frac{\partial v(x,t)}{\partial x}\right)^{-1} k(t)\right) \quad (\forall n \in N,\ \forall t \in [t_0, t_n^2]) \tag{2.23}$$

$$\frac{d(\phi_n'(t))}{dt} = v_n^a \quad (\forall n \in N,\ \forall t \in [t_0, t_n^*]) \tag{2.24}$$

$$\phi_n'(t_n^2) = \phi_n(t_n^2) \quad \forall n \in N \tag{2.25}$$

$$t_n^1 \leq t_n^* \leq t_n^2 \quad \forall n \in N \tag{2.26}$$

- $a_n(t)$ is a set of decision variables representing acceleration rates of each vehicle at each time during the impediment period;
- $\phi_n(t)$ is the input variable, representing each vehicle origin trajectory;
- $\phi_n'(t)$ is the decision variable, representing each vehicle redesigned trajectory;
- t_0, t_n^1, t_n^2 are the algorithm starting time, origin trajectory acceleration period starting time, and origin trajectory acceleration period ending time respectively;
- v_n^a, t_n^* are decision variables, representing the advisory speed and ending application time for vehicle n respectively;
- $\Psi(\cdot), h_{min}^{v_n(t)}$ are input variables, representing the maximum acceleration and the

minimum headway vehicle n could reach at the speed of $v_n(t)$ respectively.

The speed oscillation function is applied as the control objective of each following vehicle (Eq. (2.21)), where t_0 and t_n^2 are the time points when algorithms begin to apply and when the vehicles regain the free-flow speed, respectively; $a_n(t)$ is the following vehicle acceleration at each time between $[t_0, t_n^2]$.

The constraints for setting the static advisory speed limit are shown from Eq. (2.22) to Eq. (2.26), where $\phi_n'(t)$ denotes the redesigned trajectory of the following vehicle n after applying the advisory speed (v_n^a). Among the constraints shown above, Eq. (2.22) ensures that each following vehicle travels safely after applying the advisory speed, with the actual headway no less than the minimum headway at the current speed. Eq. (2.23) restricts that the acceleration, which the vehicle could reach at each time along the redesigned trajectory ($\phi_n'(t)$), cannot exceed the maximum acceleration. Eq. (2.24) sets the advisory speed assuming that the redesigned trajectory ($\phi_n'(t)$) is static during the algorithm control duration ($[t_0, t_n^*]$). Eq. (2.25) directs that the original following trajectory ($\phi_n(t)$) and the redesigned trajectory ($\phi_n'(t)$) meet at the same location when the vehicle regains the free-flow speed at $t = t_n^2$. As a result, Eq. (2.25) ensures that the algorithm does not change vehicle average vehicle speed during the impediment period ($[t_0, t_n^2]$). Finally, Eq. (2.26) restricts the ending application time (t_n^*) should be when the vehicle is regaining its speed to the normal, i.e., the acceleration period.

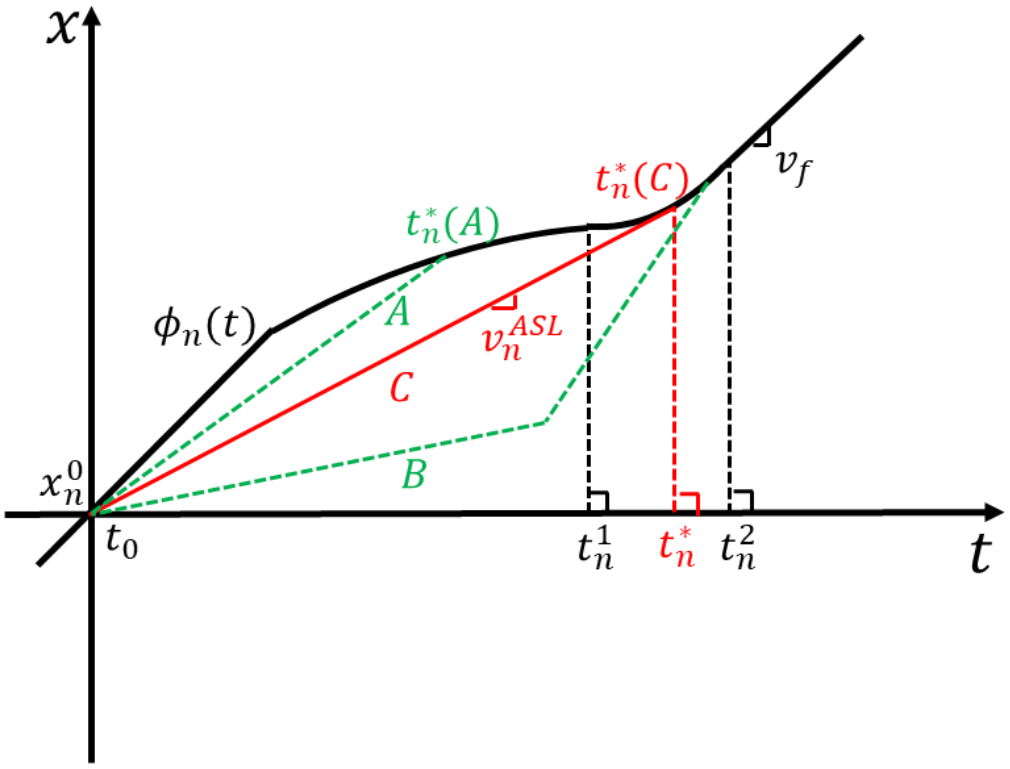

Figure 2.4 The Advisory Speed and End Algorithm Time Designs

In this study, a heuristic solution is considered for setting the advisory speed for the cruise control operations. The design of the advisory speed limit and control duration is shown in Figure 2.4. Obviously, the objective σ in Eq. (2.21) is non-negative and equals zero when the vehicle travels at a constant speed. When the vehicle applies the static advisory speed (v_n^a) during the algorithm application period $[t_0, t_n^*]$, Eq. (2.21) is equivalent to the surrogate objective function in Eq. (2.27), i.e., execute the advisory speed limit algorithm for the longest possible duration in the impediment period $[t_0, t_n^2]$.

$$max\ t_n^*\ \ (t_n^* \in [t_0, t_n^2], \forall n \in N) \tag{2.27}$$

Figure 2.4 demonstrates that the redesigned trajectory will also maximize the surrogate objective function (Eq. (2.27)) when the advisory speed (v_n^a) is designed as the tangent line of the original trajectory (i.e., $max\ t_n^* = t_n^*(C)$). If the advisory speed limit for vehicle n is set to be greater than the tangent line slope (e.g., Trajectory C is the tangent line, and the advisory

speed associated with Trajectory A is greater than the tangent slope), the vehicle would potentially experience another deceleration as well as a longer acceleration period ($t_n^*(A) < t_n^*(C)$). Hence, speed oscillation is not minimized. On the other hand, if the advisory speed limit for vehicle n is smaller than the tangent slope (e.g., Trajectory B), unavoidably, the vehicle would either encounter a further decrease in vehicle average travel speed (violating the constraint Eq. (2.25)); or need to adjust the advisory speed limit for more than once (no longer a static advisory speed limit, violating the constraint Eq. (2.24)). Hence, Trajectory B is not feasible. In contrast, Trajectory C could achieve both operational simplicity and trajectory smoothness without further decrease the average speed of the following vehicle. Therefore, the advisory speed limit should be set to be the slope of the tangent line (Trajectory C).

$$\begin{cases} v_n^a = \frac{\phi_n(t_n^*) - x_n^0}{t_n^* - t_0} \\ \left(\frac{d\phi_n(t)}{dt}\right)_{t_n^*} = v_n^a \end{cases} \quad t_n^* \epsilon [t_n^1, t_n^2] \tag{2.28}$$

According to Figure 2.4, the advisory speed (v_n^a) and the algorithm ending time (t_n^*) for the vehicle n are derived together from Eq. (2.28). The vehicle n travels with the advisory speed limit from (t_0, x_n^0), and its redesigned trajectory tangents to the original trajectory at the algorithm ending point $(t_n^*, \phi_n(t_n^*))$.

In the following chapters, the eco-driving algorithms designed for intersections consider to further optimize the origin trajectory ($\phi_n(t)$) with the objective of minimizing the lost-time resulting from the vehicle start-up and intersection clearance, while the eco-driving algorithm designed for following a moving bottleneck in a highway section considers the natural following trajectory of each vehicle upstream of the moving bottleneck as the origin trajectory.

Chapter 3

Simulation Settings

The settings of the following simulations for each traffic situation are introduced in this section. As the eco-driving strategy is proposed based on the kinematic wave analysis and each vehicle could apply different travel advice, the following simulations are conducted at a microscopic level, which updates the speeds and locations for all vehicles at each time step.

3.1 Vehicle behavior model

Based on the LWR model (Eq. (2.1)) and the triangular fundamental diagram (Eq. (2.3)), Newell's car-following model (G. F. Newell, 2002) is applied to describe the travel behavior of each vehicles. The basic ideas of Newell's car-following model include that each vehicle maintains the minimum time gap (τ) with the vehicle that precedes it, as well as all vehicles could not travel beyond the free-flow speed (v_f). The speed and location for each vehicle (n) are updated at each time step (Δt) according to Eq. (3.1) and Eq. (3.2) respectively.

$$v_n(t+\Delta t) = \min\left\{v_f, \frac{x_{n-1}(t)-x_n(t)-L}{\tau}\right\} \tag{3.1}$$

$$x_n(t+\Delta t) = x_n(t) + v_n(t+\Delta t)\Delta t \tag{3.2}$$

The car-following model shown in Eq. (3.1) and Eq. (3.2) is not applicable for eco-driving designs since it assumes the acceleration to be unbounded. As a result, Newell's car-following model should be implemented with an acceleration function ($\Psi(\cdot)$) (Jin and Laval, 2018). In this study, each vehicle would apply the maximum acceleration that it could reach, i.e., the bounded acceleration rate (a), and the acceleration function is shown in Eq. (3.3).

$$\Psi\left(v, k^{-1}, \left(\frac{\partial v(x,t)}{\partial x}\right)^{-1} k\right) = a \tag{3.3}$$

Each connected vehicle would apply the extended Newell's car-following model with bounded acceleration if its travel behavior is not controlled by the eco-driving strategy. With any control algorithms applied, each vehicle applies a cruise control with setting the speed of v_n^a. Eq. (3.4) shows how each vehicle updates its speed in the following simulations, while the locations are updated according to Eq. (3.2). Eq. (3.5) defines each scenario (Θ) where the eco-driving strategy being applied. $\mathcal{s}, \mathcal{u}, \mathcal{f}$ represent the scenarios of signalized intersection, unsignalized intersection, and highway section with a moving bottleneck respectively.

$$v_n(t+\Delta t) = \begin{cases} v_n^a & (t \in [t_0, t_n^*]_\Theta) \\ \min\left\{v_f, \frac{x_{n-1}(t) - x_n(t) - L}{\tau}, v_n(t) + a\Delta t\right\} & (\text{otherwise}) \end{cases} \tag{3.4}$$

$$\{\mathcal{s}, \mathcal{u}, \mathcal{f}\} \in \Theta \tag{3.5}$$

The eco-driving strategy proposed in this study is beneficial for the traffic flow from three aspects, namely, environmental benefits, reduced speed oscillations, and traffic efficiency improvement. In the following subsections of Chapter 3, the fuel consumption savings, speed variance, and the average vehicle distance travelled during the simulation are introduced as the metrics for the above three aspects respectively.

3.2 Fuel consumption model

To understand the potential environmental benefits of applying the eco-driving strategy, we calculate the fuel consumption in various traffic scenarios in the following simulations. There are a number of models to estimate the gas emissions for vehicles, such as the Comprehensive Modal Emission Model (CMEM) (Ah *et al.*, 1997); VT-Micro Emission Model (Ahn *et al.*, 2002) and SUMO pollutant emission models (Krajzewicz *et al.*, 2015). In this study, we use

the VT-CFPM model because of its simplicity and accuracy (Rakha *et al.*, 2011) (Park *et al.*, 2013).

$$F_n\big(v_n(t), a_n(t)\big) = \begin{cases} \alpha_0 + \alpha_1 P_n(t) + \alpha_2 P_n^2(t) & P(t) > 0 \\ \alpha_0 & P(t) \le 0 \end{cases} \tag{3.6}$$

$$P_n(t) = \frac{R(t)+1.04m}{3600\eta_d} a_n(t) \tag{3.7}$$

$$R(t) = \frac{P_a}{25.92} C_D C_h A_f v^2(t) + 9.8066m \frac{C_r}{1000}(c_1 v(t) + c_2) + 9.8066mG(t) \tag{3.8}$$

The CFPM model estimates the instantaneous fuel consumption based on the vehicle speed ($v_n(t)$) and acceleration rate ($a_n(t)$) every time step (Eq. (3.6)), where $\{\alpha_0, \alpha_1, \alpha_2\}$ are estimated parameters determined by vehicle type, $F_n\big(v_n(t), a_n(t)\big)$ and $P_n(t)$ are instantaneous fuel consumption and vehicle power at time t. The vehicle power $P_n(t)$ is estimated based on Eq. (3.7) and Eq. (3.8). In Eq. (3.7), $R(t)$ is the vehicle resistance force; η_d and m are vehicle mechanical efficiency and vehicle mass. In Eq. (3.8), P_a, C_D, C_h, A_f represent the density of the air in the environment, the vehicle drag coefficient, the correction altitude factor, and the vehicle front area respectively. C_r, c_1, c_2 are rolling resistance parameters that vary as a function of the road surface type, road condition, and vehicle tire type. $G(t)$ is the road grade at time t. The values of the parameters are listed in ***Appendix A***.

This study calculates the fuel consumption during the time when each vehicle is applying the eco-driving strategy, and compares the difference in fuel consumption before and after applying the algorithms in different traffic scenarios. Eq. (3.9) adds up the fuel consumption of vehicles during the impediment period ($[t_0, t_n^2]$).

$$F = \sum_{n=1}^{N} \sum_{t=t_0}^{t_n^2} F_n\left(v_n(t), a_n(t)\right), t \in [t_0, t_n^2]_\Theta \tag{3.9}$$

3.3 Speed oscillation and traffic efficiency evaluations

Although the VT-CFPM model is applied into the evaluation on algorithm performance, due to various objective functions based on different kinds of gas emissions and various emission models, the environmental benefits could not be quantitatively accurate and nor the models are universal for all kinds of emissions and pollutions. However, empirically, reducing traffic oscillation could empirically reduce gas emissions and fuel consumption. To measure the speed oscillations of each vehicle, this thesis calculates the average vehicle speed variance (σ) during the algorithm application time. Eq. (3.10) calculates the variance of an individual vehicle during the impeded period, where t_n^2 is the time when the vehicle regains the initial speed. Eq. (3.11) takes the average value of all the following vehicles.

$$\sigma_n = \frac{\sum_{t=t_0}^{t_n^2} (v_n(t+\Delta t) - v_n(t))^2}{(t_n^2 - t_0)/\Delta t} \tag{3.10}$$

$$\sigma = \frac{\sum_{n=1}^{N} \sigma_n}{N} \tag{3.11}$$

The traffic efficiency improvement in this study is defined as the travel distance increase compared with the same scenario without applying the eco-driving algorithm. In addition to the average speed variance, we also compare the average travel distance increase to evaluate the traffic efficiency improvement provided by the algorithm. As shown in Eq. (3.12), the average travel speed ($\bar{V}$) for a platoon with N vehicles could be calculated, where t_1 and t_2 represent the starting and ending time for calculating the average travel speed respectively.

$$\bar{V} = \frac{\sum_{n=1}^{N} (x_n(t_1) - x_n(t_2))}{N(t_2 - t_1)} \tag{3.12}$$

Chapter 4

The Eco-driving Strategy in Highway Roads after a Moving Bottleneck

4.1. Introduction

In a highway road section, a slow-moving vehicle would occur when the vehicle prepares to stop or leaves the road section. As mentioned in introducing the moving bottleneck problem in Section 2.3, the smoothness of traffic flow in highway could be easily hampered due to the occurrence of the slow-moving vehicle. In addition, the moving bottleneck leads to additional traffic oscillation, and empirically, traffic oscillation leads to extra gas emissions.

Based on the factors shown above, this chapter proposes a control algorithm as the eco-driving strategy, with the objective of minimizing the traffic oscillation for all vehicles upstream of the slow-moving vehicle. This algorithm applies to connected vehicles and operates on a single-lane highway road ($\Theta = \not{f}$), where the traffic flow is uncongested (with the free-flow speed) before being impacted by the moving bottleneck. Such traffic situations could happen when a connected vehicle merges into an uncongested road with the speed less than the free-flow speed or when a connected vehicle begins to decelerate and then leaves the road. Based on Section 2.3, this control algorithm is designed for each vehicle according to its following trajectory without applying any algorithm. Through the V2V communications, each following connected vehicle could real-timely receives the travel information provided by the algorithm.

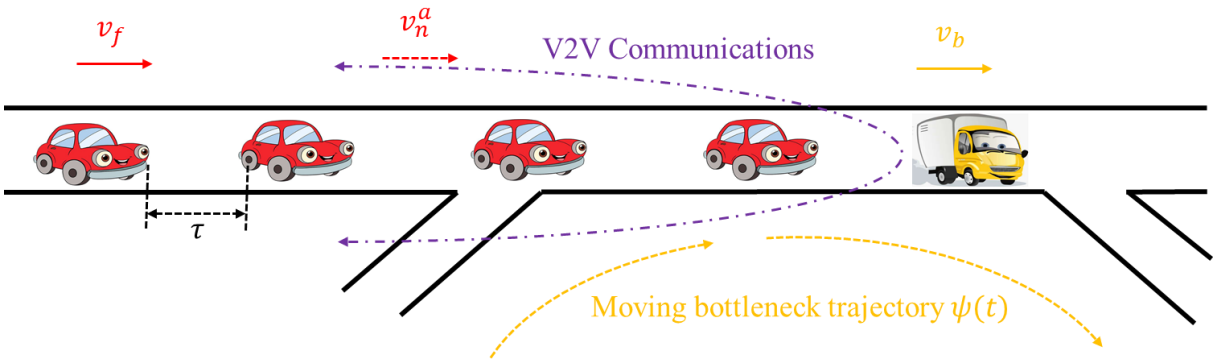

Figure 4.1 The Traffic Scenario in a Highway section for the Algorithm

The algorithm is applied in a highway section shown in Figure 4.1. The leading vehicle, which serves as the moving bottleneck, would come to the highway and begin to impede the upstream traffic from a time point (t_0). As the leading vehicle is connected and autonomous, this study assumes the leading connected vehicle has a planned leading trajectory and will follow the trajectory for the road segment. Delays in communication and computation processes are omittable. Under these assumptions, we could obtain an upper bound performance by applying the algorithm. Based on the kinematic wave analysis of the moving bottleneck problem, the algorithm could calculate the time and location where each following vehicle could start to accelerate after the bottleneck leaves the road. The starting time and location of post-bottleneck acceleration are the input for the eco-driving algorithm.

4.2 Control algorithm operation

4.2.1 Algorithm control framework

In this section, the eco-driving control algorithm is introduced. The control input is the moving bottleneck pre-planned leading trajectory, and the output information includes the advisory speed and the ending application time for each following vehicle. The control objective is to reduce traffic oscillation by applying the heuristic solution of the optimization model (Model 2.1). Each following vehicle would apply the advisory speed (v_n^a) within the algorithm control duration ($[t_0, t_n^*]$) by the algorithm control system, through which, the objective could be realized.

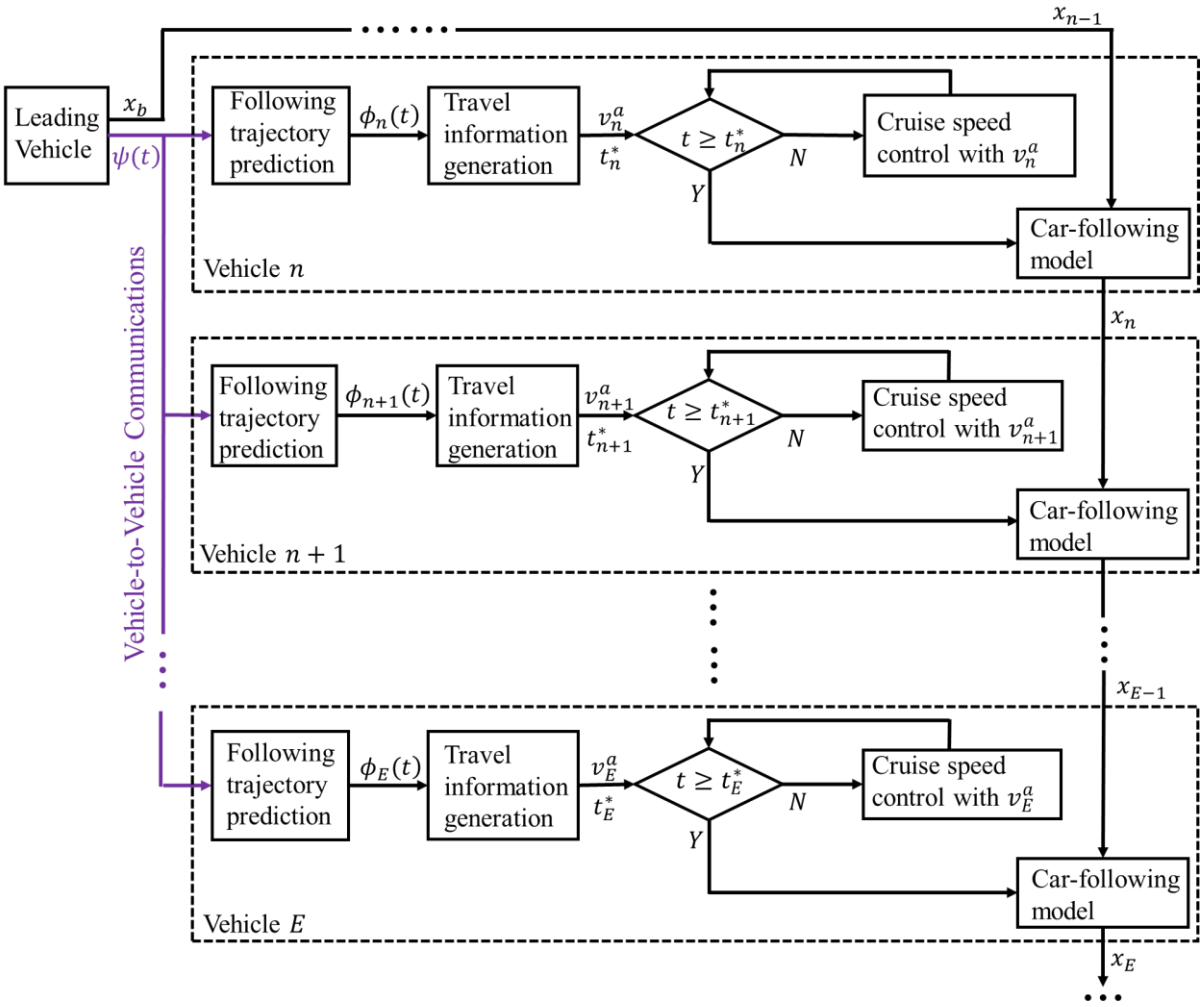

Figure 4.2 The Control System of the Eco-driving Strategy in a Highway Section

The advisory speed for each individual following vehicle is generated through a control framework shown in Figure 4.2. For each following vehicle, the algorithm is operated through the following four steps.

Step 1. Broadcasting the leading vehicle (moving bottleneck)'s trajectory

The leading vehicle shares the estimated trajectory to the following vehicles when it begins to impede upstream traffic flow on the road. It follows the planned movement trajectory ($\tilde{x} = \psi(t)$) until it leaves the road or reaches the free-flow speed.

Step 2. Predicting the following vehicles' trajectories

Based on the leading vehicle trajectory ($\psi(t)$), the following vehicles predict their original following trajectories ($\tilde{x} = \phi_n(t)$) by using the analytical results from the generalized varying speed moving bottleneck problem.

Step 3. Calculating the advisory speed value and the control duration

According the heuristic solution for Model 2.1, the advisory speed for each following vehicle (i.e., v_n^a for the following vehicle n) is decided by taking the tangent line of the following trajectory from Step 2. The duration for applying the advisory speed (i.e., t_n^* for the following vehicle n) can also be derived from the point of tangency which is further elaborated in the advisory speed limit and control duration section.

Step 4. Executing the advisory speed

Each following vehicle adjusts its advisory speed during the execution duration (i.e., from $t = t_0$ to $t = t_n^*$ for the following vehicle n). After that, each following vehicle travelling behaviour is changed back to apply the car-following model.

4.2.2 The Advisory Speed and the Control Duration Design

The design of the advisory speed and the control duration is shown in Figure 4.3. The algorithm begins when the leading vehicle occurs ($t = t_0$). At the same time, the advisory speed limits for each following vehicle are determined according to the estimated leading trajectory. Since the following vehicle speeds are impacted by the leading vehicle ($v_b(t) < v_f$), inevitably from the solution of the moving bottleneck problem, the following vehicles will experience an acceleration period to resume the free-flow speed.

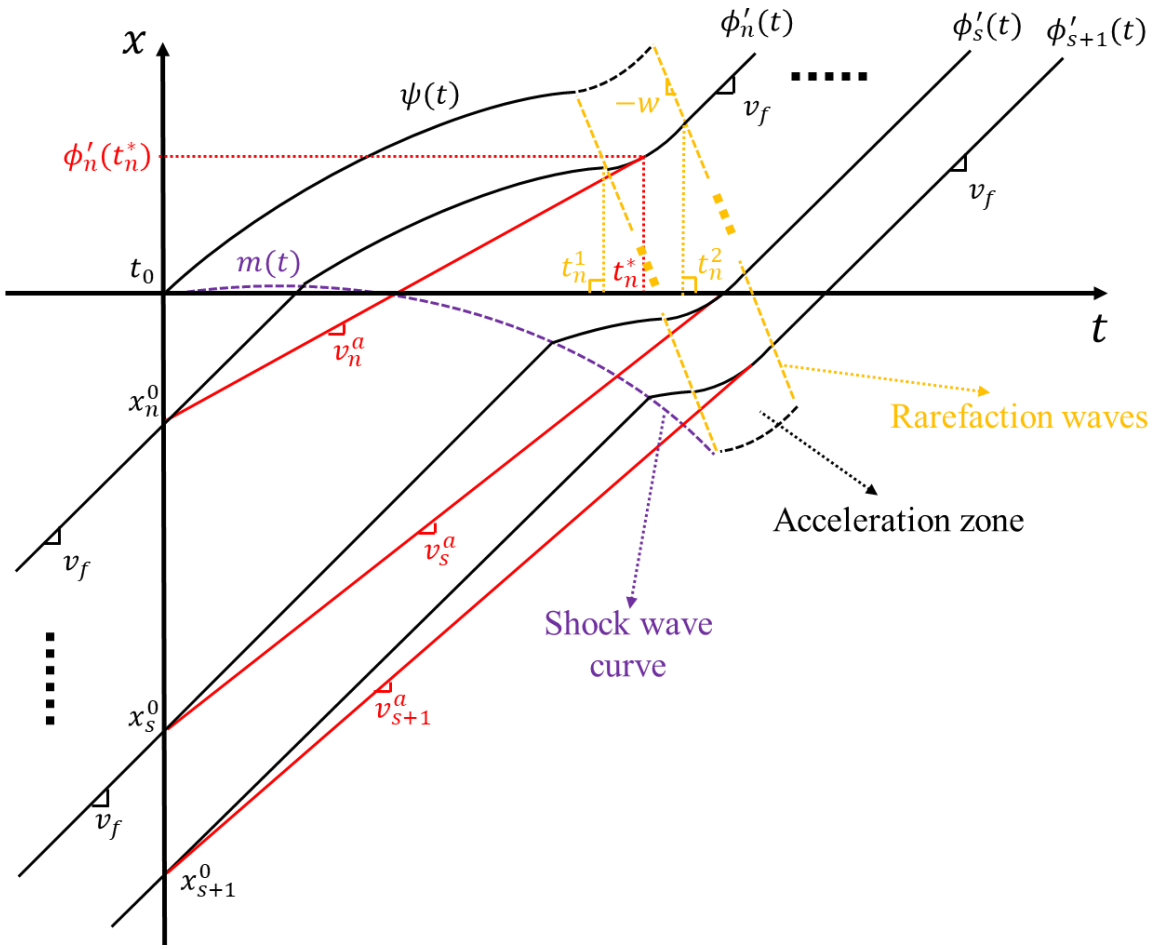

Figure 4.3 The Advisory Speed and End Algorithm Time Operations with the Moving Bottleneck

For vehicle n, the acceleration period is from $t = t_n^1$ to $t = t_n^2$ without the eco-driving strategy. In this case, the advisory speed limit is operated as the slope of the tangent line from (t_0). The tangent point in the acceleration period should be the end time point for applying the advisory speed. The advisory speed limit and control duration are calculated combining Eq. (4.1) and Eq. (4.2).

$$v_n^a = \frac{\phi_n(t_n^*, x) - x_n^0}{t_n^* - t^0} \tag{4.1}$$

$$\left(\frac{d\phi_n(t,x)}{dt}\right)_{t_n^*} = v_n^a \tag{4.2}$$

4.3 Numerical experiments

4.3.1 Simulation setup

In this section, the effectiveness of the eco-driving strategy is presented in four numerical traffic scenarios. The leading vehicle has different movements, namely, traveling at a constant speed (lower than the free-flow speed), accelerating, decelerating, and executing a stop-and-go for pick-up or drop-off. In each scenario, trajectories of following vehicles with and without applying this eco-driving algorithm are compared.

In the simulation, a fleet of connected vehicles is initially travelling with the free-flow speed on a straight single-lane road. The road length is sufficient for all vehicles to apply the algorithm. Newell's car-following model with bounded acceleration is applied to update vehicle speed and location at every time step. The total simulation time is 300 seconds, and the moving bottleneck occurs at $t = 100s$ when the traffic is at an uncongested steady state. The parameter settings for the simulations are shown in Table 4.1.

Table 4.1 Simulation Settings for the Control Algorithm Applied in the Highway

Parameters	Values
v_f, Free flow speed	20 m/s (45 mph)
N, The number of following vehicles	20
a, Bounded acceleration rate	$2m/s^2$ ($6.56ft/s^2$)
Δt, Simulation time step	1 sec

This study compares the trajectories with and without the advisory speed limit from t_0 to t_n^* (Figure 4.3) for all following vehicles in all scenarios. Each simulation includes one leading vehicle and 20 following vehicles.

4.3.2 The Constant Moving Bottleneck

The simulation first tests the highway section with a constant speed moving bottleneck. The moving bottleneck occurs at $t = 100s$ with a speed of $10m/s$ ($22\ mph$). The leading vehicle stays at the road section for 30 seconds and leaves. Figure 4.4(a) and Figure 4.4(b) plot the trajectories of vehicles without and with applying the eco-driving strategy respectively. For both of the two subfigures, the blue line represents the trajectory of the bottleneck, the other lines represent the trajectories of the following vehicles. From the simulation results, the trajectories with the eco-driving control algorithm are smoother than those without the algorithm.

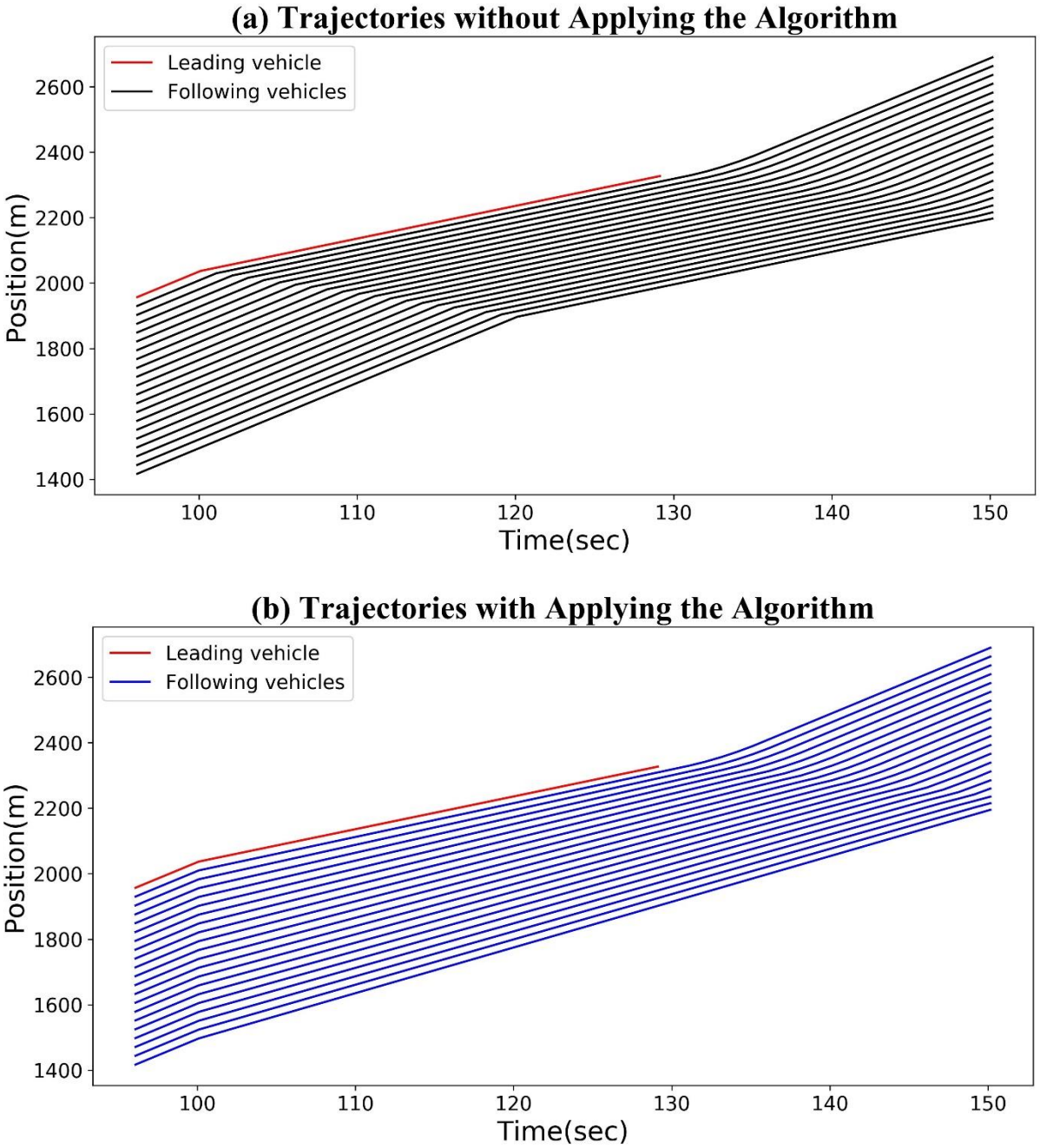

Figure 4.4 A Comparison of Vehicle Trajectories with and without Applying the Eco-driving Strategy with Constant Speed Moving Bottleneck

To further analyse the algorithm performance in vehicle speed oscillation smoothing, this study calculates the standard deviation of speed. By applying this eco-driving strategy, the average speed standard deviation decreases 64.3% comparing with the same scenario without the algorithm. As a result, the overall traffic oscillation has been significantly reduced. The algorithm could also reduce different gas emissions. In addition, the average speeds of all the

following vehicles are calculated during leading vehicle impacted periods, and the result shows the algorithm does not generate an extra decrease in following vehicle speed, which has no impact on traffic efficiency. The statistical results for the constantly moving bottleneck scenario are listed in Table 4.2

Table 4.2 Statistics of Speed and Fuel Consumption with and without Applying the Eco-driving Strategy with Constant Speed Moving Bottleneck

	Non eco-driving	Eco-driving	Improvement
Average Speed (m/s) [mph] ($\bar{V}$)	(12.64) [28.27]	(12.64) [28.27]	0.0%
Speed Standard Deviation (σ)	4.46	1.59	-64.3%
Fuel Consumption (L)	1.670	1.580	-5.39%

4.3.3 Accelerating and Decelerating Bottlenecks

In the second and third scenarios, we test the performance of the eco-driving strategy when the vehicle causing the moving bottleneck is accelerating or decelerating respectively.

For the acceleration scenario, we set the leading vehicle's initial speed to be $10 m/s$ ($22\ mph$). The leading vehicle accelerates with a constant acceleration of $1\ m/s^2$ ($3.28\ ft/s^2$) until it reaches the free-flow speed. After that, since the leading vehicle keeps the free-flow speed afterward and is no impediment for the upstream traffic, the vehicle is not the cause of a moving bottleneck anymore. For the deceleration case, we assume that the vehicle decelerates at a rate of $1\ m/s^2$ for 10 seconds from the free-flow speed, and that it leaves the road after 10 seconds.

The trajectory comparations for accelerating and decelerating moving bottleneck scenarios are shown in Figure 4.5 and Figure 4.6 respectively. Table 4.3 and Table 4.4 list the average speed, speed standard deviation, and fuel consumption values with and without applying this strategy in the two cases, along with the improvements in these three aspects. From these results, when the leading vehicle accelerates and decelerates, this algorithm doesn't change the average speed and it reduces traffic oscillation and gas emissions.

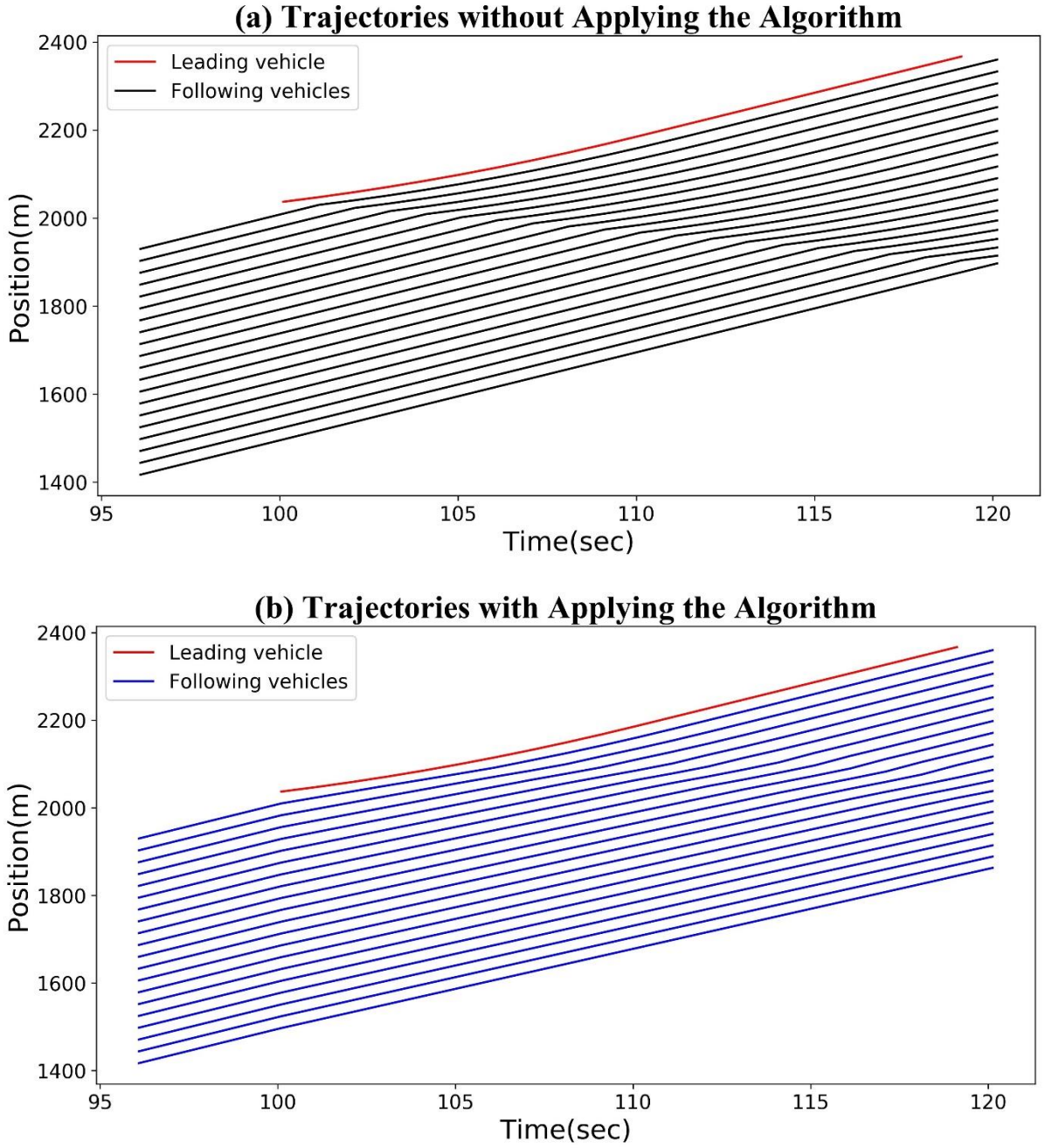

Figure 4.5 A Comparison of Vehicle Trajectories with and without Applying the Eco-driving Strategy with An Accelerating Moving Bottleneck

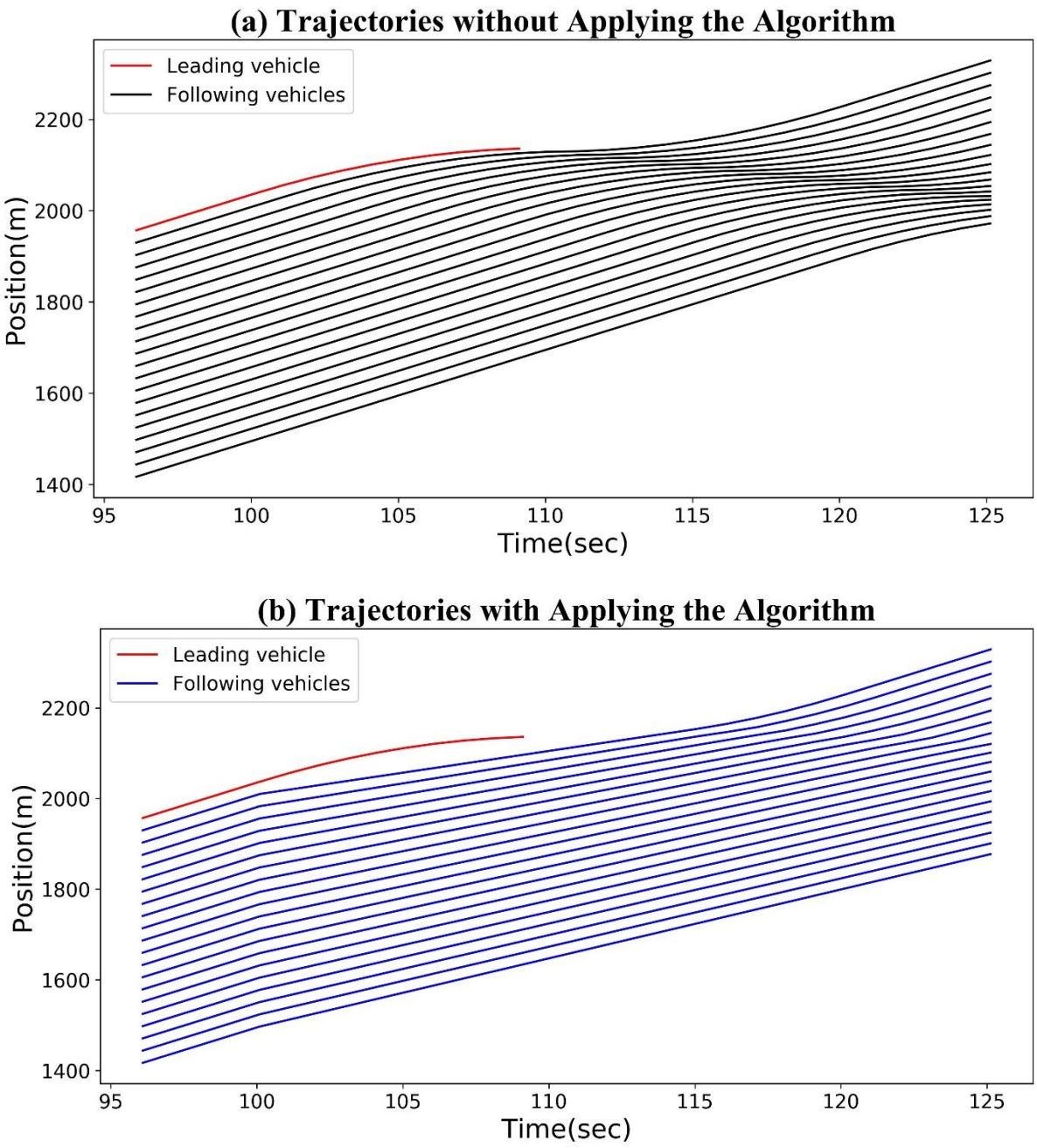

Figure 4.6 A Comparison of Vehicle Trajectories with and without Applying the Eco-driving Strategy with A Decelerating Moving Bottleneck

Table 4.3 Statistics of Speed and Fuel consumption with and without Applying the Eco-driving Strategy with Accelerating Moving Bottleneck

	Non eco-driving	Eco-driving	Improvement
Average Speed (m/s) [mph] ($\bar{V}$)	(17.50) [39.14]	(17.50) [39.14]	0.0%

Speed Standard Deviation (σ)	3.37	1.17	-65.3%
Fuel Consumption (L)	1.140	1.287	-11.4%

Table 4.4 Statistics of Speed and Fuel consumption with and without Applying the Eco-driving Strategy with Decelerating Moving Bottleneck

	Non eco-driving	Eco-driving	Improvement
Average Speed (m/s) [mph] ($\bar{V}$)	(17.26) [38.61]	(17.26) [38.61]	0.0%
Speed Standard Deviation (σ)	3.24	0.983	-69.7%
Fuel Consumption (L)	1.551	1.485	-4.26%

4.3.4 A Stop-and-go Scenario

In the last scenario, this study simulates the leading vehicle travelling with a more complicated movement, i.e., a stop-and-go movement. The leading vehicle begins to decelerate at $t = 100s$. The deceleration rate is $-2\ m/s^2$ ($-6.56\ ft/s^2$). Then the vehicle stops for 5 seconds, at the location $x = 2100m$. At $t = 115s$, this vehicle begins to accelerate with the acceleration rate of $2\ m/s^2$ and reaches the free-flow speed after 10 seconds. This situation happens when a vehicle needs to pick up a passenger for example. Figure 4.7 plots the trajectories with and without applying this eco-driving strategy, and the fuel consumption and speed statistical results are listed in Table 4.5. As the result shows, after applying the algorithm, the following traffic flow is smoother, since the following vehicles don't experience long decelerating and accelerating periods.

Table 4.5 Statistics of Speed and Fuel consumption with and without Applying the Eco-driving Strategy with a 'stop and Go' Bottleneck

	Non eco-driving	Eco-driving	Improvement
Average Speed (m/s) [mph] ($\bar{V}$)	(11.06) [24.74]	(11.06) [24.74]	0.0%
Speed Standard Deviation (σ)	8.17	2.34	-71.4%
Fuel Consumption (L)	1.941	1.757	-9.47%

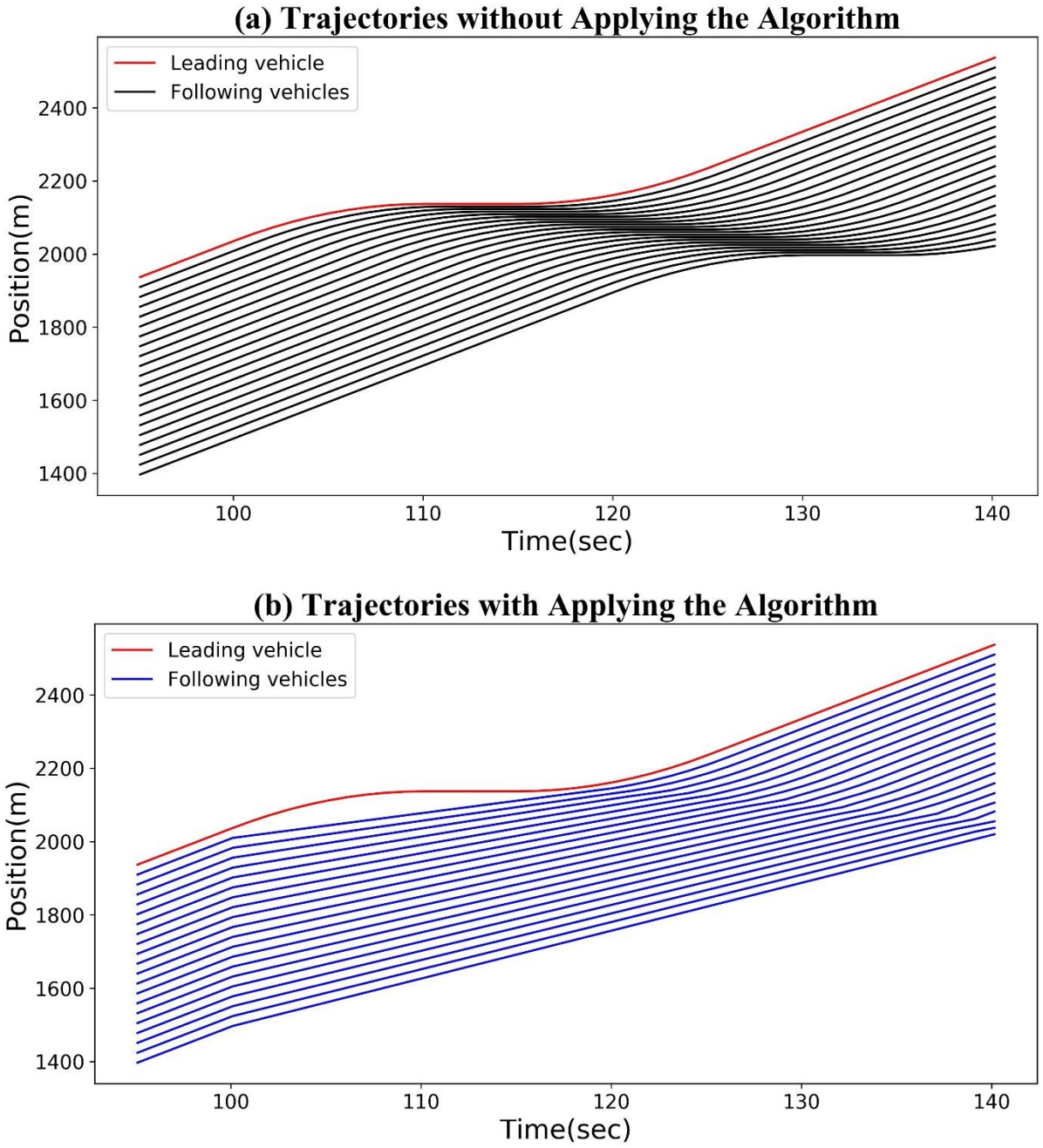

Figure 4.7 A Comparison of Vehicle Trajectories with and without Applying the Eco-driving Strategy with the 'Stop and Go' Bottleneck

4.4 Summary

This chapter introduces one application of the eco-driving strategy proposed in section 2.4. The strategy is applied to a highway section where the smooth traffic flow is impeded by the moving bottleneck. The following vehicle trajectories could be derived from the moving bottleneck problem. Based on the origin trajectory of each following vehicle, this study proposes an eco-driving algorithm that enforces the cruise control with the advisory speed to reduce the traffic oscillation and fuel consumption.

The effectiveness of the eco-driving algorithm is further tested by a set of numerical examples. Various movements of the leading vehicle (serves as the moving bottleneck in the highway) are included in the experiments. According to the simulation results, the vehicle speed variance decreases up to 71.4% after applying the algorithm, and fuel consumption is reduced by 4% to 11%. The results indicate that the eco-driving algorithm is more environmental-friendly and capable of smoothing traffic oscillations.

Chapter 5

The Eco-driving Algorithm at a Signalized Intersection

5.1 Introduction

In this chapter, the proposed eco-driving strategy is applied at signalized intersections through a control algorithm ($\Theta = \mathcal{s}$). Unlike freeway traffic situations, urban arterial traffic flows are frequently interrupted by signalized intersections. As a result, vehicles need to frequently adjust their speeds and travellers need to keep adjusting their travel behaviours when approaching the signal. The traffic oscillation and uncertain behaviours make the traffic less energy-efficient with significant travel time delay. Based on V2I communications, the control algorithm designs advisory speed is real-timely and accurately and each vehicle could apply the cruise control when approaching the signalized intersection.

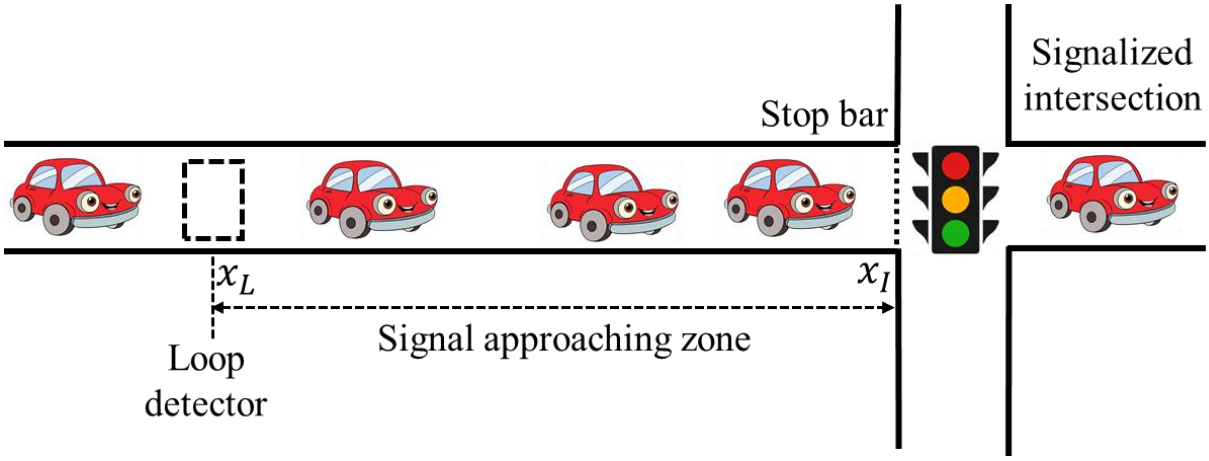

Figure 5.1 The Traffic Scenario at the Signalized Intersection for the Algorithm

The algorithm is applied at a typical signalized intersection, as shown in Figure 5.1. At the signalized intersection, a loop detector is installed ahead of the signal. The loop detector could record the time point when the vehicle covers it. This time point becomes the starting point for the vehicle applying the algorithm. The signal approaching zone is from the detector location to the intersection stop bar, where each vehicle adjusts the travel behaviour under the direction of the control algorithm. In this section, the algorithm doesn't consider spatial channelization of traffic, and makes all turning movements at the intersection identical. Each phasing durations are given within a signal cycle, and the future signal plans are provided to the control system, so that the algorithm could estimate the capacity for each phasing.

The algorithm applied in the signalized intersections could fully improve the capacity of each phasing in each signal cycle. The phasing capacity (c_p) in this study refers to the number of vehicles that could pass through the intersection within a given signal plan. A phasing in one signal cycle consists of three intervals, i.e., the red interval, the green interval, and the yellow interval. Vehicles could pass through the stop line to enter the intersection during the green and yellow intervals. Theorem 5.1 provides a necessary condition that the phasing capacity could reach the maximum given green and yellow intervals of the corresponding phasing p. Based on Theorem 5.1, this algorithm directs the vehicles pass through the intersection by the minimum headway and with the free-flow speed when reaching the stop bar.

Theorem 5.1 The capacity for a given phasing reaches the maximum **only if** all vehicles that passing through the intersection during the phasing time could travel through the intersection with the free-flow speed (v_f).

Proof. Let YL and GL be the length of yellow and green intervals respectively, Eq. (5.1) provides the relation between the phasing capacity (c_p) and the average headway ($\bar{h}$) of the vehicles passing through during the interval $GL + YL$.

$$c_p = \frac{YL+GL}{\bar{h}} + 1 \tag{5.1}$$

Since $\bar{h} \geq h_{min}$,

$$c_p^{max} = \frac{YL+GL}{h_{min}} + 1 \tag{5.2}$$

According to Theorem 2.1, $\bar{h} = h_{min}$ only if the vehicles could pass through the intersection with the free-flow speed (v_f).

In addition, the algorithm could also reduce the traffic oscillation when vehicles travelling at the signal approaching zone. The cruise control speed of each vehicle is designed according to the heuristic solution for solving the Model 2.1. The objectives of the eco-driving strategy at the signalized intersection is realized through a control system shown in the following subsections.

5.2 Algorithm operations

5.2.1 Algorithm control system

In this section, an eco-driving control algorithm is introduced. The control algorithm is applied in a connected vehicle environment with an uncongested traffic condition. The control input is the signal plan information and the time when each vehicle enters the signal approaching zone. The output information which is applied with each vehicle include an advisory speed limit and ending application time. The eco-driving algorithm is operated with a control system framework with feedbacks, as provided in Figure 5.2.

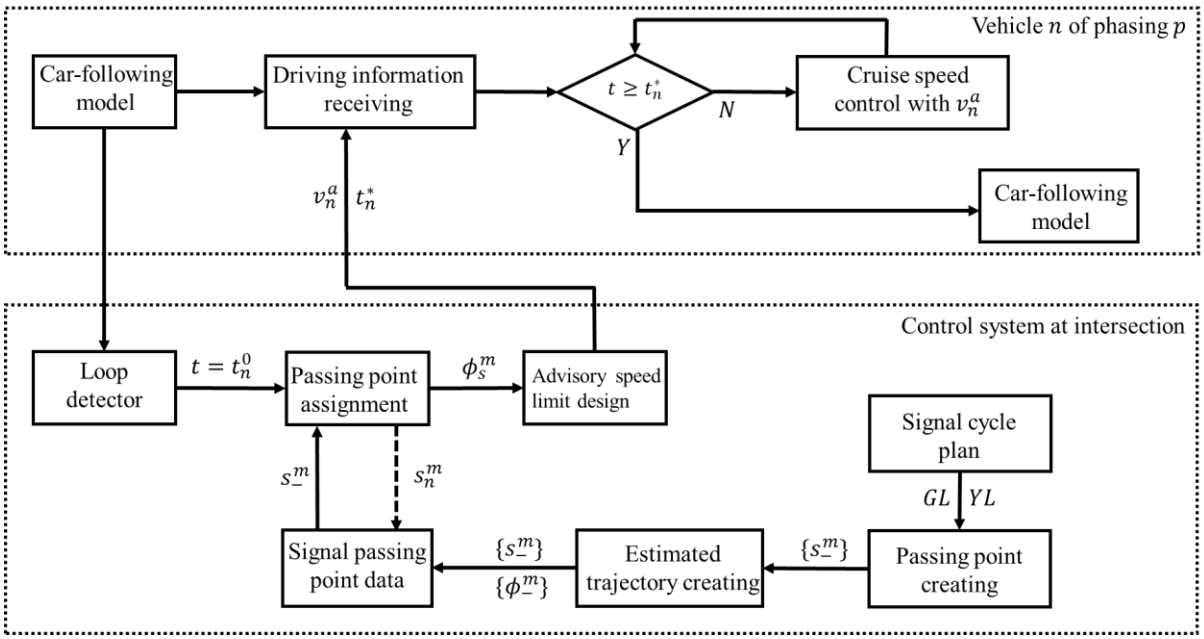

Figure 5.2 The Control System of the Eco-driving Strategy at A Signalized Intersection

Figure 5.2 shows the control algorithm applied at the signalized intersection. Given each signal phase of the signal cycle, the control system creates the passing point for each direction during green and yellow intervals (elaborated in Section 5.2.3). When a vehicle crosses the detector, the detector records the current time as the vehicle's starting point of applying the algorithm i.e., t_0^n. At the same time, the earliest feasible passing point (s_n^m) is assigned for the vehicle, as elaborated in section 5.2.3. In this algorithm, the passing point refers to an estimated moment when a vehicle enters the intersection (passes the stop line). The purpose of setting a passing point is to control the number of vehicles in each phasing entering the intersection given a signal cycle, in order to fully utilize the intersection capacity. Based on the created passing points, the estimated trajectories ($\{\phi_-^m\}$) are also created for letting vehicles pass through the intersection with free-flow speed, and later providing the original trajectory for solving the optimization model shown as Model 2.1.

Based on the assigned passing point (s_n^m) and the corresponding estimated trajectory (ϕ_s^m) an advisory speed (v_n^a) with the ending application time (t_n^*) is generated. Since the delays due to the communication and computation are assumed to be zero, the connected vehicle would apply a cruise control with the advisory speed from when it passes by the loop at $t = t_0^n$, until the ending application time ($t = t_n^*$). Once the control of the algorithm is finished, the vehicle

would travel with the Newell's car-following model with bounded acceleration, and the speed limit is changed back to v_f.

5.2.2 Passing points and estimated trajectories creating

According to Theorem 2.1, the capacity would reach a maximum if vehicles are passing through the intersection with v_f with minimum headway. Therefore, the time interval between each two adjacent passing points should be the minimum headway. In order to make the vehicle reach v_f at the stop bar, each passing point should include a corresponding estimated trajectory. Travelling along the trajectory, the vehicle could reach v_f no later than entering the intersection.

Based on the kinematic analysis, the start-up behaviour and vehicle start-up trajectories are elaborated in Section 2.2. According to the vehicle start-up behaviour, this study pushes back the estimated trajectory of each passing point, so that each vehicle could pass through the intersection by travelling with the pre-designed trajectory. Unlike the natural start-up trajectories, the estimated trajectory could also make the vehicle intersection-entering speed into the free-flow speed, so that vehicles could passing through the intersection with the minimum headway and reach the maximum capacity. With this objective, all estimated trajectories should have the complete acceleration part ($\{\varphi(t)\}$) before reaching entering the intersection at $x = x_I$. Figure 5.3 shows a set of passing points with the estimated trajectories which is pre-created before the beginning of the signal cycle.

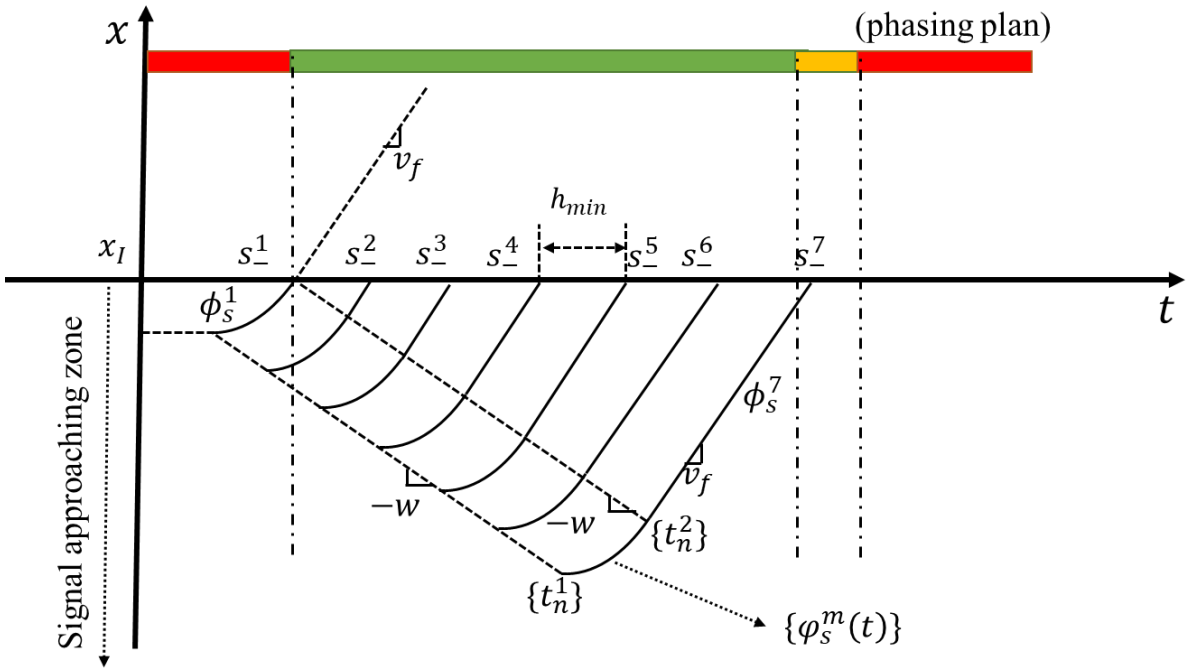

Figure 5.3 Passing Point and Estimated Trajectory Designs

In Figure 5.3, passing points created during one signal cycle (s_-^m) are set during the corresponding green and yellow intervals and divided by the minimum headway (h_{min}). For each passing point, the estimated trajectory has an acceleration part ($\varphi(t)$), which is derived from vehicle acceleration function ($\Psi(\cdot)$) by taking double integral with time (Eq. (5.3)). From Eq. (5.4) and Eq. (5.5), $\varphi(t)$ starts from the static state ($v = 0$) and ends when vehicle speed reaches v_f.

$$\varphi(t) = \iint_{t_n^1}^{t_n^1} \Psi(t) dt^2 \tag{5.3}$$

$$\frac{d\left(\varphi(t_n^1)\right)}{dt} = 0 \tag{5.4}$$

$$\frac{d\left(\varphi(t_n^2)\right)}{dt} = v_f \tag{5.5}$$

Considering the acceleration section ($\varphi_s^m(t)$), the estimated trajectory for each passing point ($\phi_s^m(t)$) is determined from Eq. (5.6) to Eq. (5.8).

$$\phi_s^1(t) = \varphi_s^1(t) \quad (t \le S_-^1) \tag{5.6}$$

$$\phi_s^m(t) = \begin{cases} v_f(t - S_-^m) & (t_s^m < t \le S_-^m) \\ \varphi_s^m(t) & (t \le t_s^m) \end{cases} \quad (m \neq 1) \tag{5.7}$$

$$\phi_s^m(t_s^m) = -w(t_s^m - S_-^1) \quad (m \neq 1) \tag{5.8}$$

According to Eq. (5.6), the first estimated trajectory ($\phi_s^1(t)$) only consists of the acceleration part, i.e., $\varphi_s^1(t)$. For estimated trajectories of the following passing points, Eq. (5.7) illustrates that each of them consists of the acceleration part, and an extra constantly moving part (with the free-flow speed of v_f) after acceleration. The constantly moving part ends at the corresponding passing point. Based on vehicle start-up behaviour, the acceleration part for each following estimated trajectory ($\varphi_s^m(t)$) should be arranged by a rarefaction wave from the first passing point (Eq. (5.8)), where t_s^m presents the ending time of each acceleration trajectory. Eq. (5.8) makes each vehicle could travel along the estimated trajectory without impeding others.

With the creating process analysed above, if vehicles travel along the estimated trajectories, they could reach the free-flow speed before entering the intersection, and pass through the intersection with the minimum headway. In addition, the passing points and estimated trajectories are created based on kinematic wave analysis and start-up behaviour, making sure that no conflict between vehicles when they are travelling along the estimated trajectories. The next section would introduce how vehicles could be directed into the estimated trajectories by applying the control algorithm.

5.2.3 Passing point assignment and the advisory speed operation

After the design of each passing point and the estimated trajectories, the algorithm would make sure vehicles could enter the estimated trajectories smoothly by operating the cruise speed control. This section introduces the passing point assignment process, as well as the advisory speed and algorithm application duration design.

The passing point assignment is the process to choose one of the passing points for each vehicle. Based on the chosen passing point and its corresponding estimated trajectory, the algorithm could generate an advisory speed and the time point for finishing the cruise control. Considering the traffic mobility, the passing point assigned to the vehicle should be the earliest feasible passing point to apply. Figure 5.4 shows the process of the passing point assignment. When the vehicle passes the loop detector, the control system would determine the earliest time it could enter the intersection. The earliest time is when the vehicle travels the signal approaching zone with v_f. Passing points earlier than that time are not feasible. Besides, if a passing point has already been assigned, it is also impossible for other vehicles to apply, and is not feasible either. Except those passing points, the earliest one should be assigned to the vehicle, which makes the vehicle pass the intersection at the earliest time. The passing point assignment could be solved by Eq. (5.9) and Eq. (5.10).

$$E_n = t_n^0 + \frac{x_I - x_L}{v_f} \tag{5.9}$$

$$S_m^n = \max\{\max\{s_-^m\}, E_n\} \tag{5.10}$$

From the equations above, E_n denotes the earliest time that the vehicle n could reach the stop bar (x_I), and $\max\{s_-^m\}$ is the earliest passing point which is not assigned to other vehicles. Figure 5.4 shows two situation of the passing point assignment process. If the vehicle n could follow the free-flow speed without speed decreasing in the signal approaching zone, the passing point of the corresponding cycle length should be re-created as the E_n be first passing point for the rest of the green and yellow intervals. Figure 5.4(a) provides an example for the re-creating

process. Otherwise, the earliest available passing point ($\max\{s_{\_}^m\}$) would be assigned to the vehicle for later generating the advisory speed.

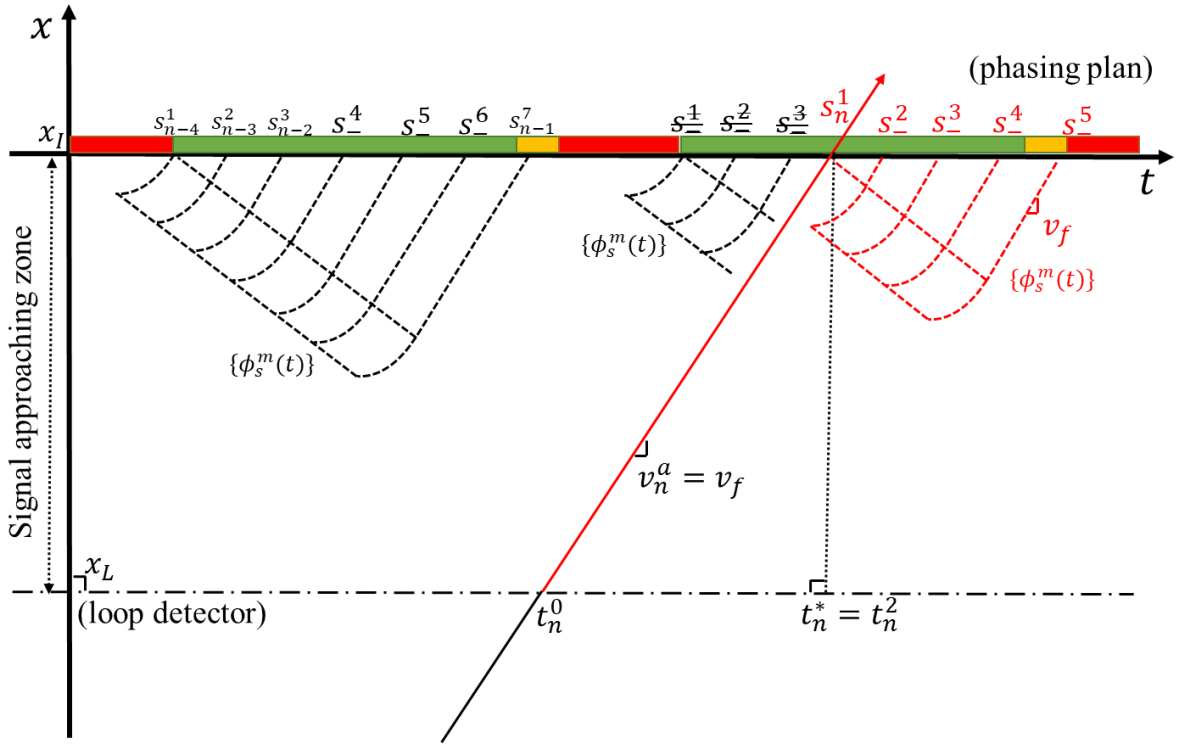

(a)

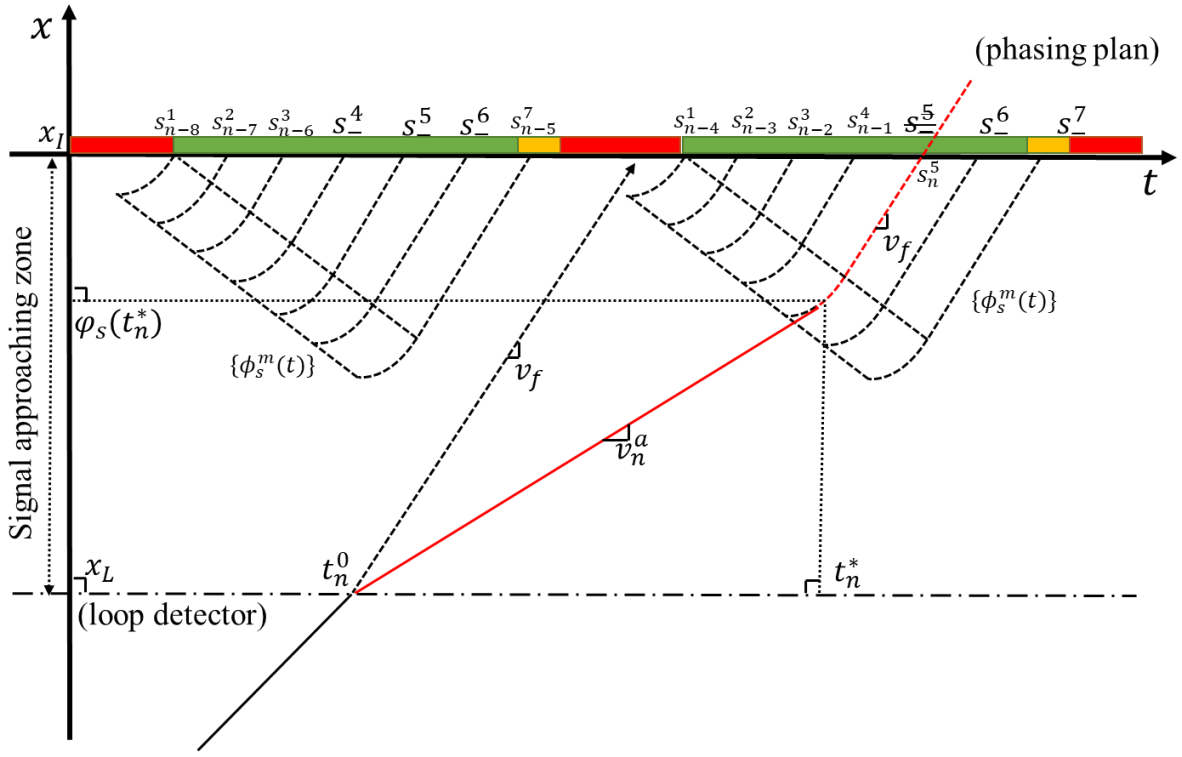

(b)

Figure 5.4 Advisory Speed and Algorithm Application Duration Operations

Once a passing point is assigned, an advisory speed limit could be generated according to a tangent approach, as elaborated in Section 2.4. With the case shown in Figure 5.4(a), the vehicle just needs to travel through the signal approaching zone and the intersection with the free-flow speed. For the other case, Figure 5.4(b) provides an example showing the process of passing point assignment and advisory speed designs for a connected vehicle (n). The passing point assigned for vehicle n is s_n^5. Its advisory speed limit v_N^{ASL} is designed as the average speed from the loop detector point (t_n^0, x_L) to the ending application point (t_n^*, x_n^*). With the objective of avoiding traffic oscillations shown in Model 2.1, the ending point is set at the point where the estimated trajectory speed gets the value of v_n^a, i.e., the vehicle trajectory with v_n^a is set by the tangent line from the detector location and tangent to the estimated trajectory (ϕ_n^5). The tangent line approach makes the vehicle enter the estimated trajectory smoothly. Once it reaches the estimated trajectory, the vehicle stops applying the advisory speed limit and would accelerate along the trajectory and enter the intersection.

$$\phi_{s\to n}^{m}(t_n^*) = x_n^* \tag{5.11}$$

$$\left(\frac{d\phi_{s\to n}^{m}(t)}{dt}\right)_{t_n^*} = v_n^a \tag{5.12}$$

$$v_n^a = \frac{x_n^* - x_L}{t_n^* - t_n^0} \tag{5.13}$$

The advisory speed limit (v_n^a) and ending application time (t_n^*) could be derived from Eq. (5.11) to Eq. (5.13). Eq. (5.11) shows the tangent point is in the estimated trajectory for vehicle n ($\phi_{s\to n}^{m}$). Eq. (5.12) shows the apply ending application point should be the moment when reaching the tangent point. Eq. (5.13) ensures v_n^a is the average speed from the detector location to the ending application point.

5.3. Numerical experiments

5.3.1 Simulation setup

The effectiveness of the proposed eco-driving algorithm in signalized intersections is evaluated in this section. A fleet of vehicles are traveling on the road, with the parameter settings shown in Table 5.1.

For the simulation setup road section, this study considers a flat ring road with the signalized intersection at the end of the road. According to a previous study (Ubiergo and Jin, 2016), the ring road is equivalent to an infinitely long road with the signalized intersections evenly distributed. The ring road length is set to be $1400m$, where each vehicle position would return to 0 when it passes through the stop bar. The ring road section is shown in Figure 5.5.

Table 5.1 Simulation Settings for the Control Algorithm Applied at the Signalized intersection

Parameters	Values
X_r, Ring road length	1200 m
x_I, Intersection location	1200 m*
x_L, Loop detector location	1000 m
T, Total simulation time	1000 sec
GL, Green interval	25 sec
RL, Red interval	25 sec
YL, Yellow interval	6 sec
AL, All-red interval	6 sec
N, The number of vehicles in the ring road	30
τ, Time gap between vehicles	1.5 sec
v_f, Free-flow speed	20 m/s (45 mph)
a, Bounded acceleration rate	2 m/s^2 (6.56ft/s^2)
L, The vehicle length	7 m
Δt, Simulation time step	0.2 sec

* The intersection location is at the end of the ring road.

According to the simulation testbed introduced in Chapter 3, assume vehicles accelerate at a constant rate, which is the bounded acceleration rate, and each vehicle tends to move as fast as it could in the simulation. This study also assume that when vehicles approach the signal during the yellow interval, if there is no algorithm applied, half of the drivers would decide to pass, and the other half would prepare to stop, i.e., the degree of aggressiveness (δ) is 50%.

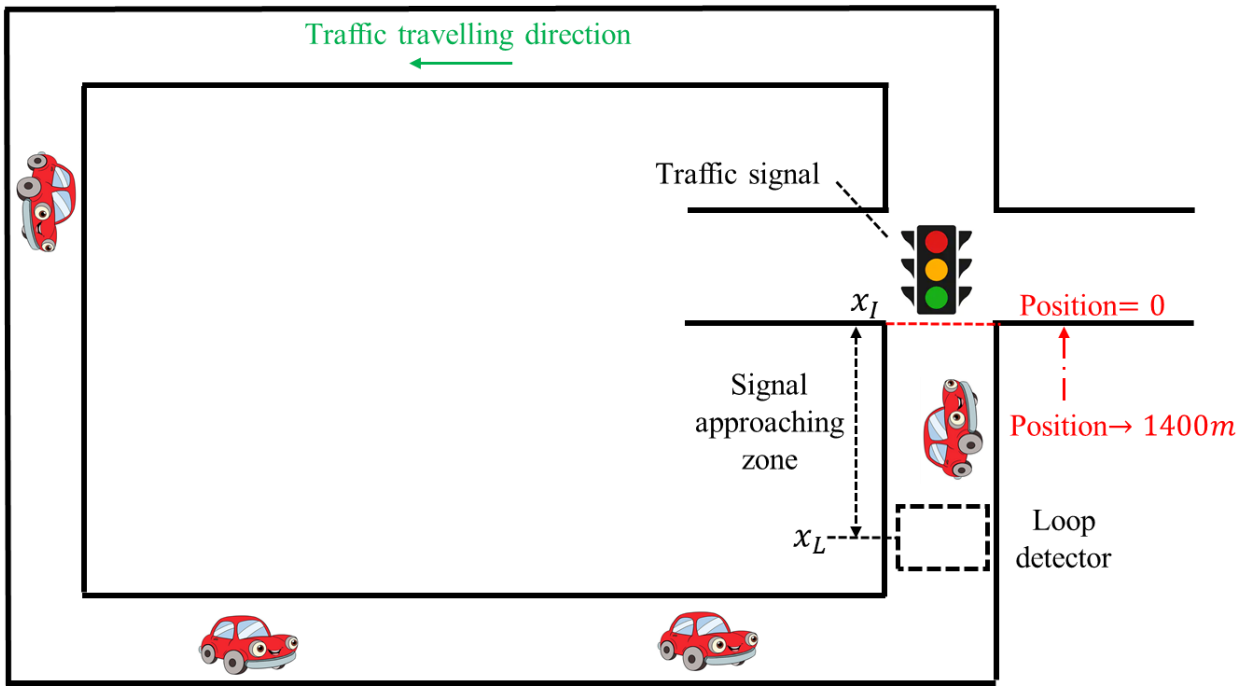

Figure 5.5 The Road Section in the Signalized Intersection Simulation

5.3.2 Vehicle trajectory comparations

A set of comparations on vehicle trajectories are shown from Figure 5.6 to Figure 5.8. In both of the figures, the traffic flow-rate in the ring road is set to be 1200 vph. The loop detector is installed $400m$ ahead of the intersection stop bar, i.e., the length of the signal approaching zone is $400m$. Although the total simulation time is 1000 sec, the vehicle movements become periodic after 100 sec of simulation. In addition, to make the trajectories clearer in the figure, the following figures plot the trajectories from $t = 100\ sec$ to $t = 300\ sec$.

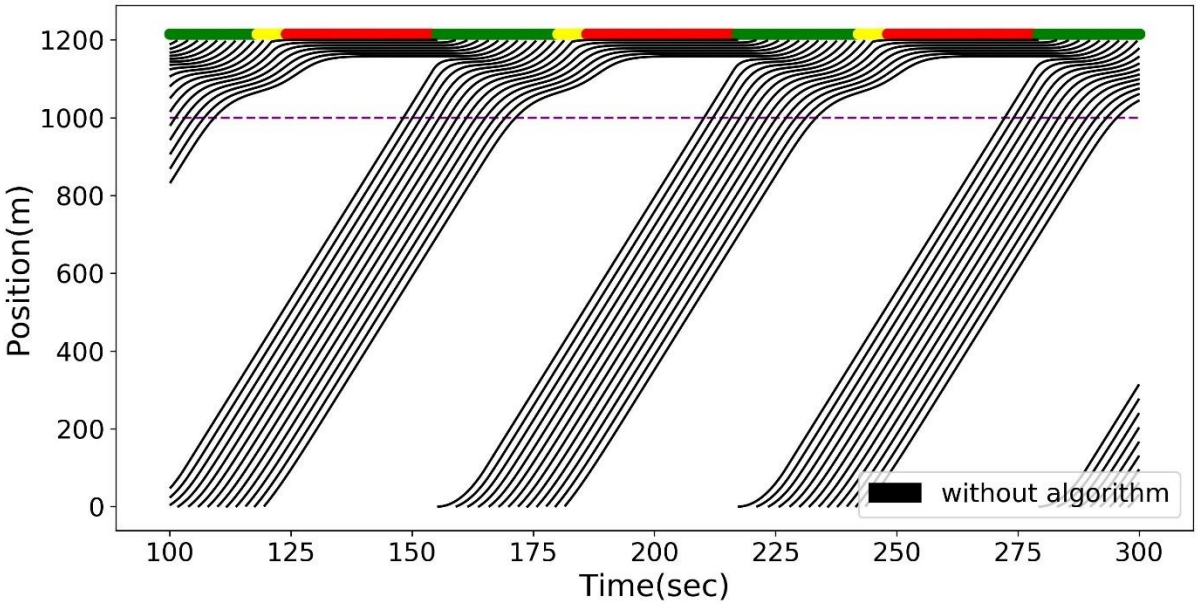

Figure 5.6 Vehicle Trajectories before Appling the Algorithm at Signalized Intersections

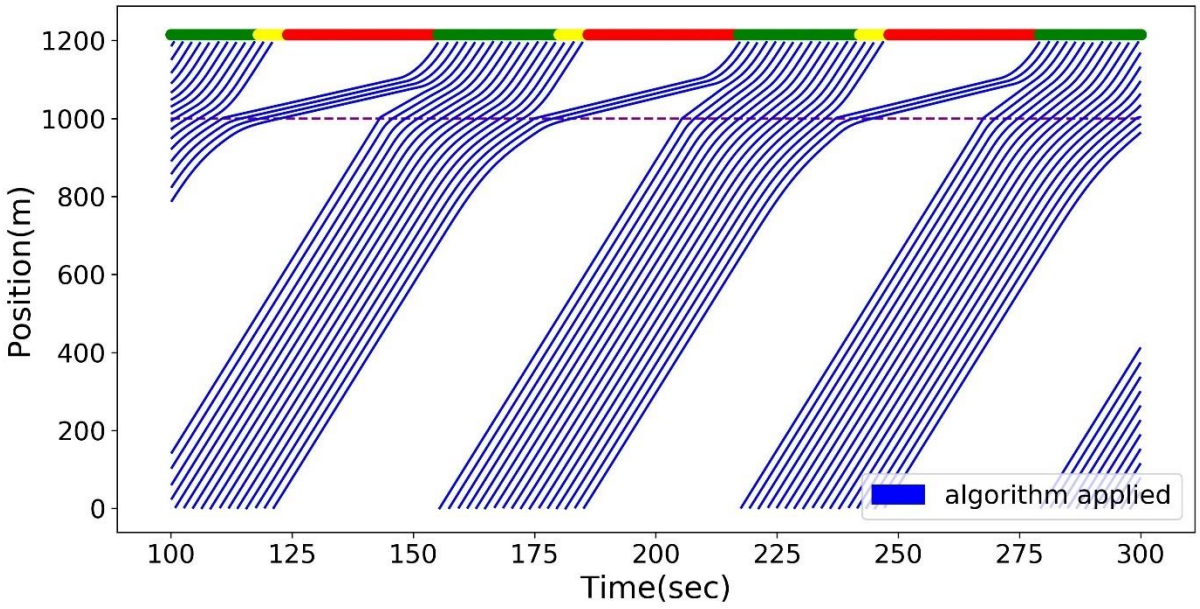

Figure 5.7 Vehicle Trajectories after Appling the Algorithm at Signalized Intersections

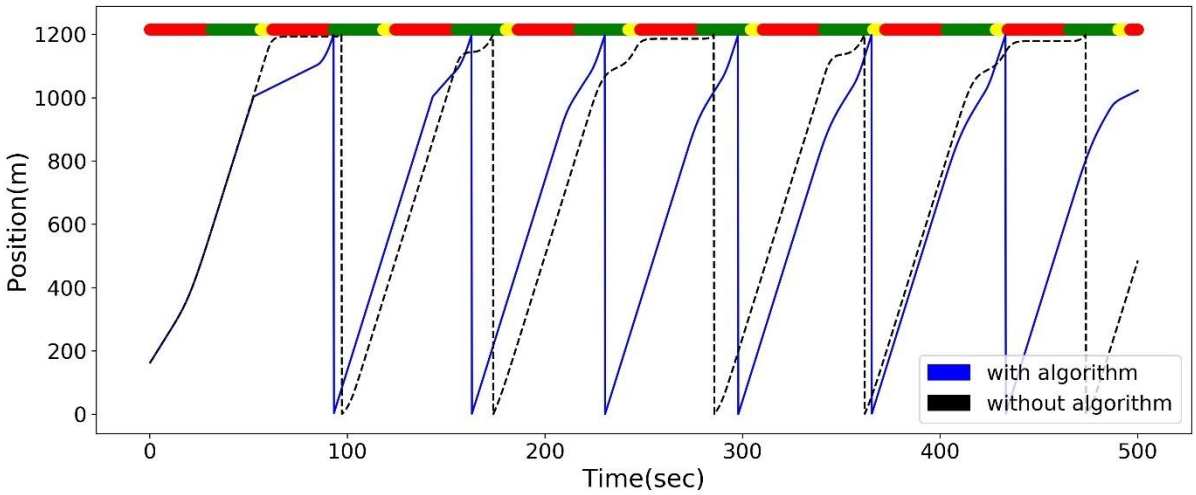

Figure 5.8 Single vehicle Trajectory Comparations at Signalized Intersections

Figure 5.6 plots the vehicle trajectories without applying the algorithm. From the result, all vehicles could experience stops at the intersection, and some vehicles need to wait at the signal for more than one cycle. This result shows the flow-rate of $900vph$ exceeds the capacity of one signal cycle. Figure 5.7 shows the vehicle trajectories after applying the algorithm during the same time period. Compared with Figure 5.6, no vehicle would stop at the signal, and vehicles could pass through the intersection with the free-flow speed (v_f). Since the passing point could be created during yellow intervals, and they assigned with the minimum headway, vehicles could fully utilize the intersection capacity. In addition, vehicle trajectories are much smoother than before.

Figure 5.8 plots the trajectories of the same vehicle with and without applying the algorithm. Although the vehicle has the same initial position and speed at the beginning of two simulations, the vehicle with the algorithm travels longer during the same time period. Before and after applying the algorithm, the vehicle starts travelling from the same initial location. During the first 500 sec of the simulation, the vehicle travels more than one cycle in the ring road (extra distance of around 1500 m) if the algorithm is applied. From the comparisons above, this algorithm could make all connected vehicles could pass through the signal with the free-flow speed, and increase the number of vehicles passing through the intersection regarding the same signal plan in one signal cycle. What's more, the traffic oscillation approaching the signal also decreases.

5.3.3 The algorithm performance evaluations

In this subsection, the performance of the algorithm is analysed at the signalized intersection where the approaching traffic flow has different flow-rate levels and the initial traffic in the ring road is uncongested. The flow-rate changing range is from $60\ vph$ (where only one vehicle travels at the ring road) to $1200vph$ (where applying the algorithm, the green and yellow intervals are fully utilized in all signal cycles). The flow-rate increasing gap is $60\ vph$. As introduced in the Chapter 3, the performance evaluations of the algorithm are from three aspects, i.e., the reduction in speed oscillation (the average speed variance); the improvement on traffic efficiency (average speed during the simulation); and the decrease of environmental impacts (fuel consumptions). The results of the evaluations are shown in Figure 5.9. The data of the evaluation performance result at each flow-rate level is shown in ***Appendix B***.

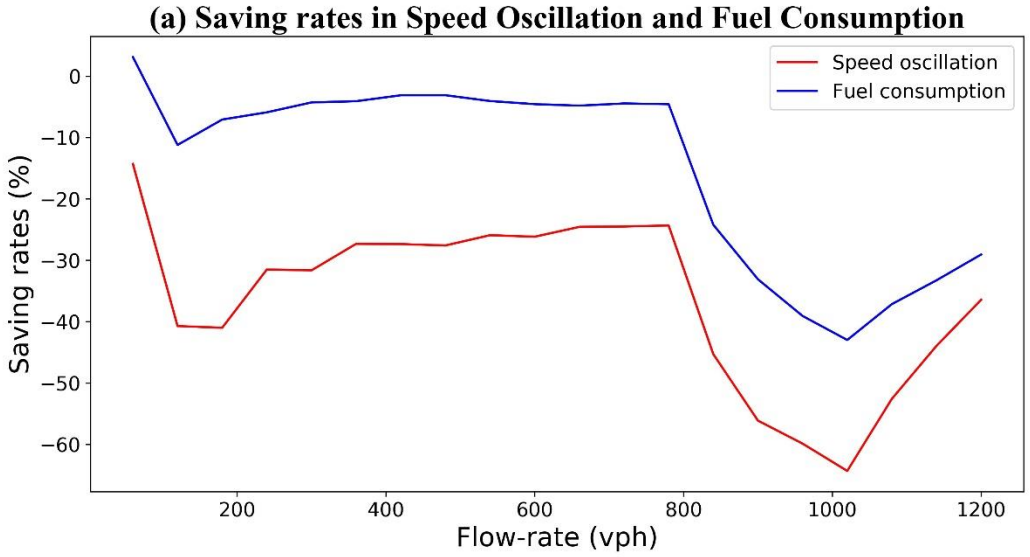

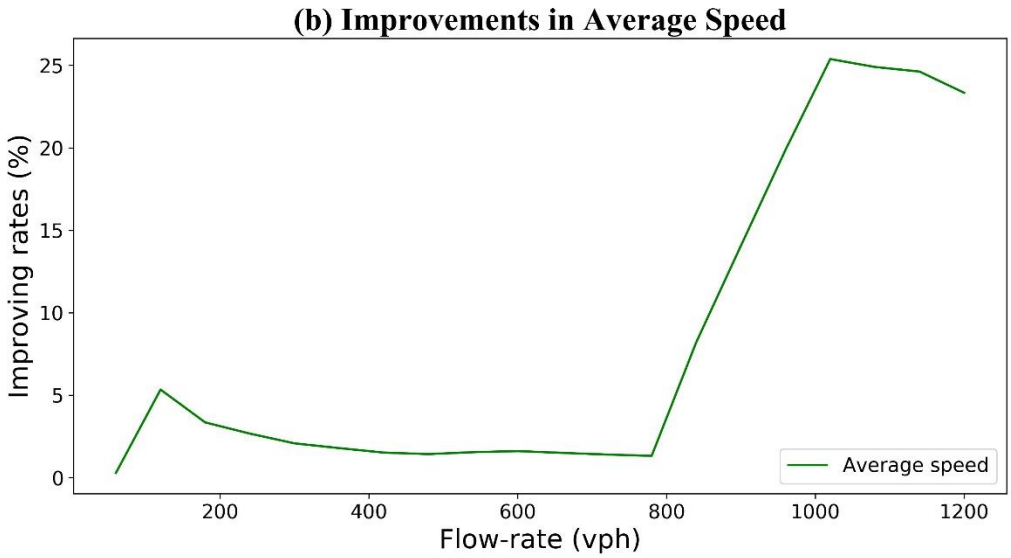

Figure 5.9 Algorithm Performance Evaluations in the Signalized Intersection

Figure 5.9(a) shows the algorithm performances in vehicle speed variance and fuel consumption reductions, and Figure 5.9(b) plots average speed improvement the algorithm brings under each flow-rate level. From the results, the algorithm could bring a reduction on both speed oscillation and improve the traffic efficiency (except for a 0.94% of fuel consumption increasing when the flow-rate is $60\ vph$). When the flow-rate is less than $800\ vph$, the reduction of the speed variance is averagely 31.5% and the savings in fuel consumption are around 7%. When the flow-rate is more than $800\ vph$, the algorithm performances become more significant, and reach the most significant when the flow-rate is at $1020\ vph$, where the algorithm brings as much as 42.6% fuel consumption savings, 66.2% of the speed oscillation reduction, and 25.3% of average speed improvement.

All evaluation results show the same tendency. With a low flow-rate level, since the vehicle moving behaviour is less influenced by intersection, i.e., vehicles could pass through the most of the intersections without stopping, the performance is not obvious in the test group, compared with the control group. As the traffic flow approaching the intersection with a higher flow-rate, more vehicles would stop and wait at the red phasing as the flow-rate reaches the signal capacity in the control group (i.e., with more than $800\ vph$). In contrast, as the algorithm improves the number of vehicles which could pass through the intersection within

the given signal cycle, vehicles applying the algorithm could still pass through the intersection within one signal cycle, which makes the algorithm performances more significant. When the flow-rate reaches more than $1020\ vph$, even the algorithm is applied, the number of vehicles that could pass through the intersection within one signal cycle still reaches the maximum value (c_{max}). In this case, although vehicles could still pass through the intersection by the minimum headway (h_{min}), they still potentially need to wait more than one signal cycle by approaching the intersection with a low average speed. As a result, the algorithm performances in three evaluations become less significant as the flow-rate, with more than $1020\ vph$, goes even higher. In conclusion, the simulation results show that the algorithm could bring an improvement from three aspects under different flow-rate levels.

5.4 Summary

This chapter proposes an eco-driving control algorithm at signalized intersection, which provides advisory speed for each connected vehicle, along with generating the control duration. The algorithm objective is to improve the signalized intersection mobility, smooth traffic oscillation as well as being more environmentally friendly. Based on the estimated trajectories for each passing point in the green and yellow intervals, this chapter first demonstrates that the traffic capacity would be fully improved when all vehicles from one phasing could pass through the stop bar of the intersection with the free-flow speed. According to the theorem, this study proposes the processes of creating and updating passing points, as well as estimating the trajectories for vehicles to reach the free-flow speed before entering the intersection. Based on passing point assignment and the corresponding trajectory, the advisory speed and control duration is determined and applied for the upcoming vehicle.

The effectiveness of the eco-driving algorithm is further tested by a set of numerical examples. From the trajectory comparisons, all vehicles operating with the algorithm would never stop before the intersection, and would enter the intersection with the free-flow speed. The number of vehicles that could pass through the intersection also increases. In addition, the traffic oscillation is reduced while approaching the intersection. The sensitivity analysis is conducted to test the algorithm performances in traffic oscillation, mobility, and environment impacts, when the upcoming traffic flow has various flow-rate levels. From the simulation result, the

algorithm would bring averagely -35%, -18%, and $+9\%$ of the changings in speed variance, fuel consumption, and the average speed respectively, which shows the algorithm could be beneficial in decreasing traffic oscillation, reducing environmental impact, and improving traffic efficiency as well.

Chapter 6

The Eco-driving Algorithm at a Non-signalized Intersection

6.1 Introduction

According to the simulation results of the algorithm introduced in Chapter 4, each vehicle could smoothly cut into the estimated trajectory by applying the advisory speed during the specific application time. Also, the passing point settings and the estimated trajectory designs could make the vehicles pass through the intersection at the designed time point (i.e., the assigned passing point) with the free-flow speed. From the intersection control perspective, the algorithm along with the cruise control system in each vehicle could independently realize a real-time and potentially efficient intersection control and guarantee the traffic safety at the intersection. Given a signal cycle at a conventional signalized intersection, each phasing has the red interval when vehicles need to wait before entering the intersection, while vehicles from other conflicted directions may not fully utilize the capacity of the interval. From the points shown above, under certain eco-driving algorithm designs, the traffic signal is not necessary to control the intersection, and even it could potentially decrease the traffic efficiency while increase traffic oscillation. In addition, few current CVIC intersection control studies consider kinematic analysis in the algorithm design. As a result, vehicles could not travel through the intersection with the free-flow speed, which could still bring a lower mobility.

In this chapter, the proposed eco-driving strategy is realized at non-signalized intersections through a control system ($\Theta = \mathcal{U}$). The algorithm is developed with the objectives of fully improving the intersection mobility, as well as decreasing the fuel consumption by smoothing traffic oscillation. Based on V2I communications and the CVIC safety rules, each vehicle is

provided, by the intersection controller instead of signal plans, with both an advisory speed and the application ending time. By applying cruise control, each vehicle follows the advisory speed until the application ending time. For the intersection controller, the advisory speed and application ending time are generated through the earliest feasible intersection entering time and vehicle trajectory redesign. For safety concerns, the intersection controller guarantees that vehicles can enter the intersection only after conflicting vehicles fully leave the intersection. In addition, we assume all vehicles to share the same travel behaviour, and the initial traffic flow is not congested.

For the traffic scenario, although a typical intersection would have several movements (M), this chapter simplifies the intersection into two conflicted movements from two single lane roads ($M \in \{1,2\}$), in order to better explain the algorithm. The intersection geography is shown in Figure 6.1. For each road, a loop detector is installed ahead of the intersection, which could record the time point when the vehicle covers it. This time point becomes the starting point for the vehicle applying the algorithm. The intersection approaching zone of each movement (m) starts from the detector location (x_L^m) to the intersection entrance (x_I^m), where each vehicle adjusts the travel behaviour under the direction of the control algorithm. Instead of the traffic signal or any stop/yield signs, an information hub is installed at the intersection, which could receive the information gathered by loop detectors, operate the control algorithm, and derive the travel information for each vehicle. The V2I communications are applied in real-time between the information hub and each vehicle, when the vehicle passes by the loop detector and begins to apply the cruise control.

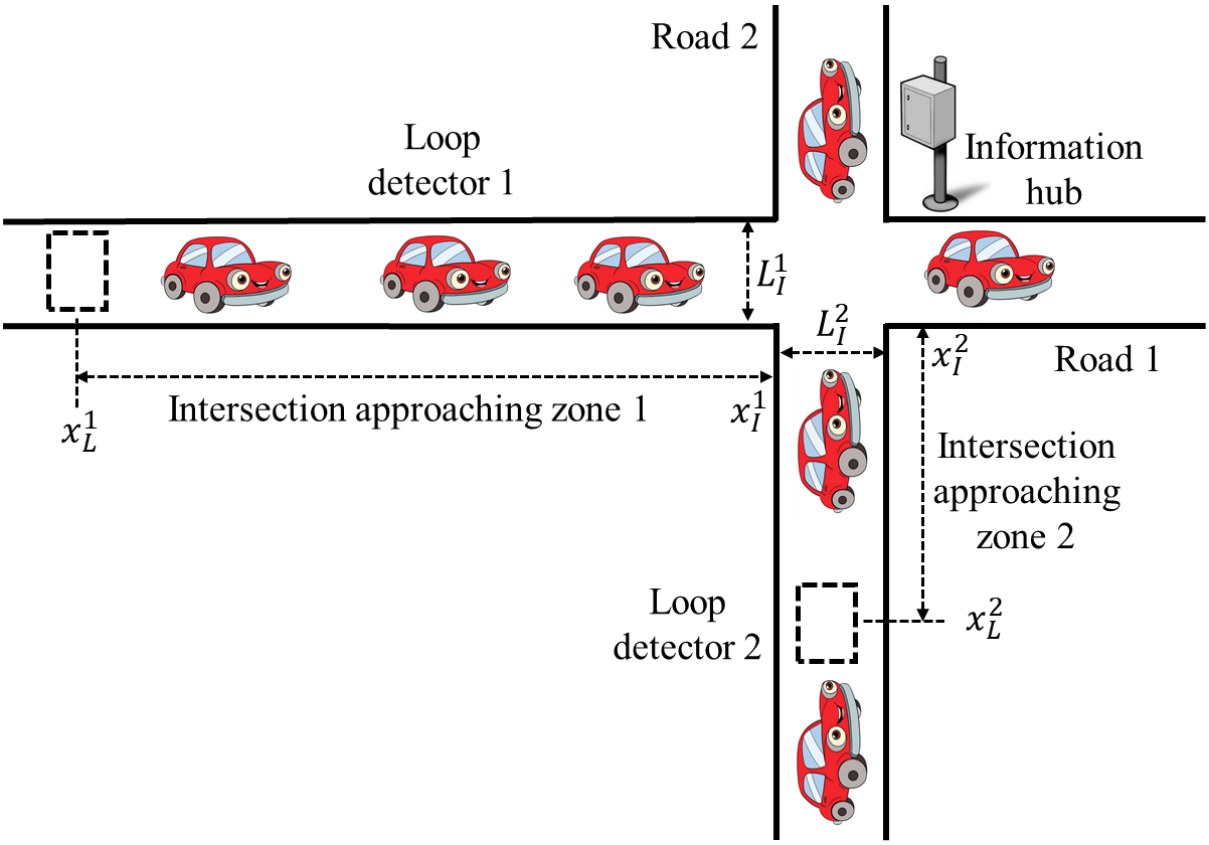

Figure 6.1 The Traffic Scenario at the Non-Signalized Intersection for the Algorithm

6.2 Control algorithm operation

6.2.1Algorithm control framework

In this section, an eco-driving control algorithm is introduced. The control algorithm is applied in a connected vehicle environment with an uncongested traffic condition. The control input is the time when each vehicle passes by the loop detector of the movement, and enters the corresponding intersection approaching zone. The output information which is applied with each vehicle include an advisory speed and ending application time.

The algorithm generates the vehicle travel information (v_n^a and t_n^*) by passing point assignments and updates. The passing points are designed separately for each movement. In this chapter, the passing point for each movement (S_M) is defined as the earliest time when the vehicle could arrive at the intersection entrance without being in conflict or impeded by other

vehicles, in the meanwhile, the vehicle could travel through the intersection with the free-flow speed (v_f). According to the Theorem 5.1, with the objective of fully utilizing the capacity, the passing points, which are designed for one movement, are assigned by the minimum headway (h_{min}). According to Theorem 2.2, for safety concerns between conflicting movements, the time interval between two passing points from conflicting movements should be the minimum intersection clearance time (T_{min}), if all vehicles could travel through the intersection with the free-flow speed. For each passing point, an estimated trajectory (ϕ_M) is designed so that the vehicle could enter the intersection with the free-flow speed when travelling along the trajectory. The estimated trajectories could be derived from the vehicle start-up behaviour to make sure the vehicle could travel along the trajectory without being impacted by other vehicles from any direction.

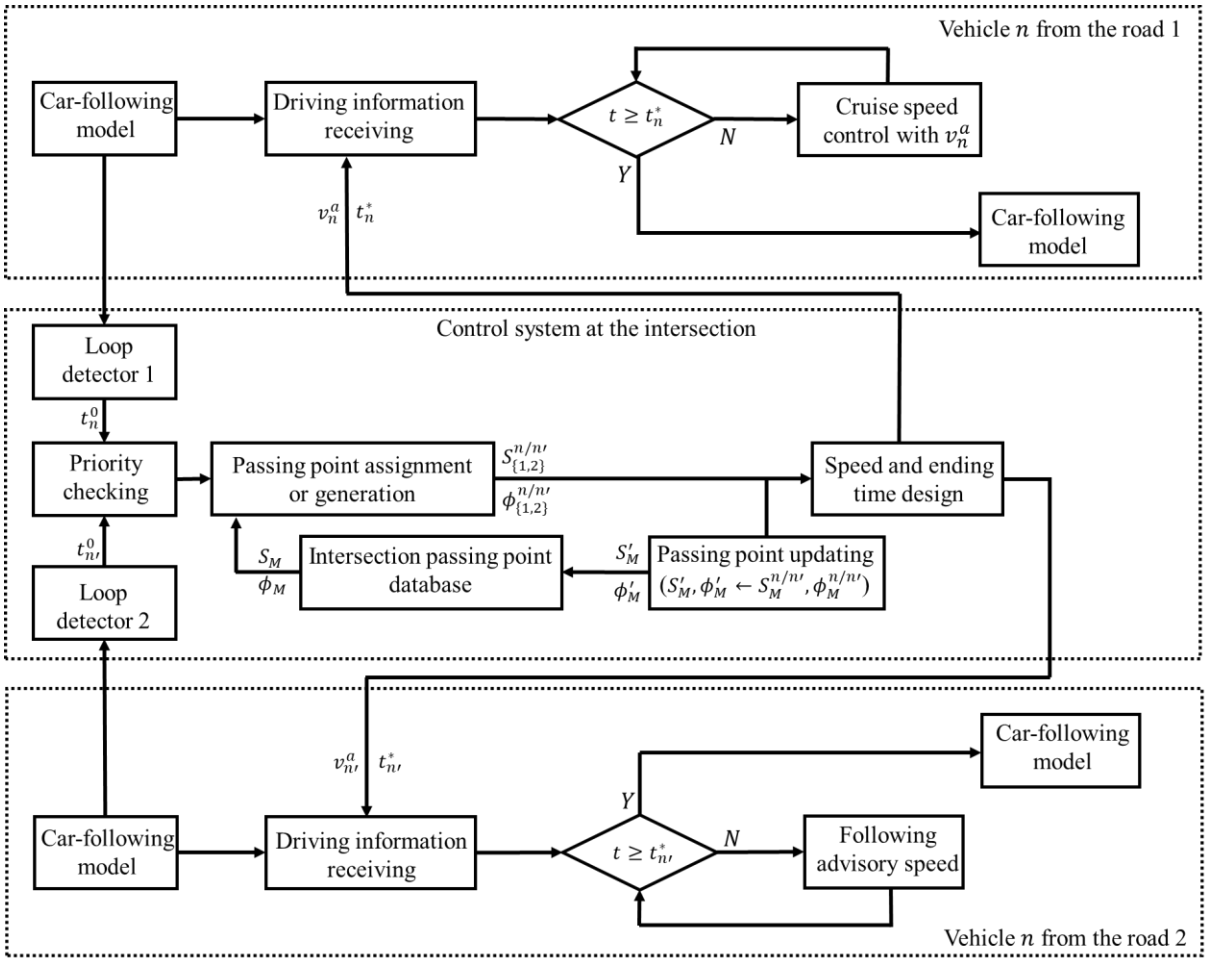

Figure 6.2 The Control System of the Eco-driving Strategy at A Non-Signalized Intersection

The eco-driving algorithm is realized through the control system with feedbacks provided in Figure 6.2. When a vehicle coming from one direction passes the loop detector, the algorithm first checks if another vehicle from a conflicting direction is passing a loop detector at the same time. The algorithm would first assign the vehicle from direction with a higher priority. After checking the priority, the algorithm would determine the earliest feasible time when the vehicle could enter the intersection with the free-flow speed. Meanwhile, the intersection controller would update the earliest time points (S'_M) for all directions. The feasible arriving time determination and the passing point update are elaborated in Section 6.2.2. For each vehicle entering the intersection approaching zone (i.e., passing the loop detector), an advisory speed with the time application ending time is generated by and controller and sent to the vehicle through V2I communication, so that the vehicle could apply the advisory speed until the application ending time. The advisory speed and application ending time design is introduced in Section 6.2.3.

6.2.2 Passing point update and estimated trajectories creating

In this algorithm, the passing point (S_M) and estimated trajectory information for each direction (ϕ_M) are restored in the intersection controller database. The corresponding S_m and ϕ_m could be retrieved when the vehicle from direction m passes the detector. Then the algorithm compares the passing point in the database (S_m) and the minimum vehicle travel time within the intersection approaching zone (E_n^m). The earliest feasible time for the vehicle arriving at the intersection (S_n^m) should be the later one of the two moments above (E_n^m and S_m). Eq. (6.1) defines the estimated earliest arrival time, when the vehicle traveling with the free-flow speed of the direction (v_f^m). Eq. (6.2) determines the earliest feasible time (S_m^n).

$$E_n^m = t_n^0 + \frac{x_I^m - x_L^m}{v_f} \qquad (\forall m \in M, \forall n \in N) \tag{6.1}$$

$$S_m^n = \max\{S_m, E_n^m\} \qquad (\forall m \in M, \forall n \in N) \tag{6.2}$$

Based on the earliest feasible time (S_m^n), the passing point of each direction (S_M) should be updated according to Eq. (6.4). Consider a scenario when vehicle n is coming from the direction m, and its speed when passing through the intersection is v_f. After setting the feasible intersection arriving time, the passing points of all directions should be updated in order not to conflict with the vehicle n. For the direction m, the next passing point should be h_{min} later than S_m^n; while for conflicting directions, the next passing point should be right after vehicle n totally leaves the intersection, which should be T_{min} later than S_m^n. In addition, with the algorithm in operation, the passing point for each road direction couldn't be updated earlier than the previous.

$$S'_{m'} = \begin{cases} \max\{S_m^n + T_{min}^m, S_{m'}\} & (m' \neq m) \\ S_m^n + h_{min}^m & (m' = m) \end{cases} \qquad (m', m \in M) \tag{6.4}$$

The corresponding estimated trajectory for each passing point ($\phi_{m \in M}$) is designed based on vehicle start-up behavior with their acceleration trajectory. All the trajectories include an acceleration trajectory ($X(t) = F(t, t_1)$) from stopped state to reaching the free-flow speed. The vehicle acceleration trajectory is derived from a set of functions shown from Eq. (6.5) to Eq. (6.9), where the vehicle starts from $v(t_0) = 0$ until reaching the free-flow speed at t_1 ($v(t_1) = v_f$) with the acceleration function of $\Psi(\cdot)$.

$$F(t, t_1) = \int_{t_0}^{t_1} v(t)dt \tag{6.5}$$

$$F(t_1, t_1) = x_I^m \tag{6.6}$$

$$v(t) = \int_{t_0}^{t_1} \Psi(v(t))dt \tag{6.7}$$

$$v(t_1) = v_f \tag{6.8}$$

$$v(t_0) = 0 \tag{6.9}$$

After deriving the acceleration trajectory, the estimated trajectories are arranged according to vehicle start-up behaviour. For direction m where vehicle n comes, the estimated trajectory (ϕ'_m) is derived from Eq. (6.10). ϕ'_m is updated from the previous estimated trajectory of S_m^n (i.e., ϕ_m^n), by increasing h_{min} unit temporally and decreasing wh_{min} unit spatially. The acceleration trajectory would be arranged along the rarefaction wave after the spatiotemporal translation. In addition, ϕ'_m continues to reach the point ($S_m^n + h_{min}^m, x_I$), i.e., the updated passing point, with the slope of v_f^m.

$$\phi'_m = \begin{cases} \phi_m^n(t) - wh_{min} & (t_1 + h_{min} \le t \le t_2 + h_{min}) \\ v_f(t - G(t_2 + h_{min})) & (t_2 + h_{min} \le t \le \frac{x_I^m}{v_f} - G(t_2 + h_{min})) \end{cases} \tag{6.10}$$

The estimated trajectory of the conflict direction ($\phi'_{m'}$) is updated from Eq. (6.11). If the passing point ($S_{m'}$) changes, $\phi'_{m'}$ is the vehicle acceleration trajectory reaching $v_f^{m'}$ at the spatiotemporal point ($S_{m'}, x_I$). Otherwise, $\phi'_{m'}$ stays the same.

$$\phi'_{m'} = \begin{cases} F(t, S'_{m'}) & (S'_{m'} = S_{m'}) \\ \phi_{m'} & (S'_{m'} = S_{m'}) \end{cases} \tag{6.11}$$

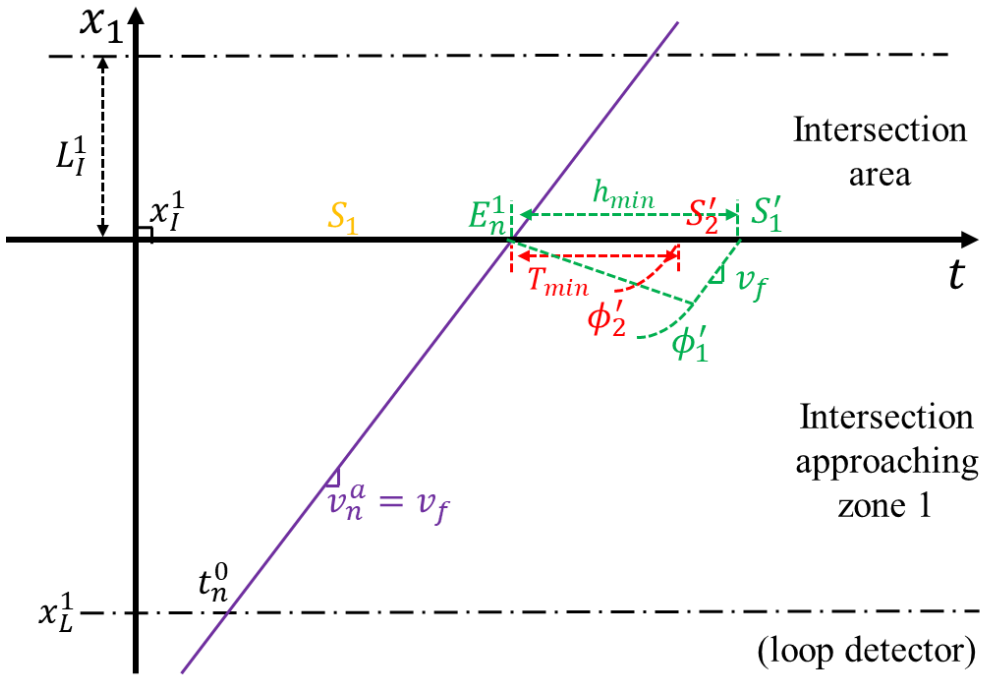
x_1
L_I^1
x_I^1
S_1
E_n^1
h_{min}
S_2'
S_1'
t
T_{min}
v_f
ϕ_2'
ϕ_1'
Intersection area
Intersection approaching zone 1
$v_n^a = v_f$
t_n^0
x_L^1
(loop detector)

(a)

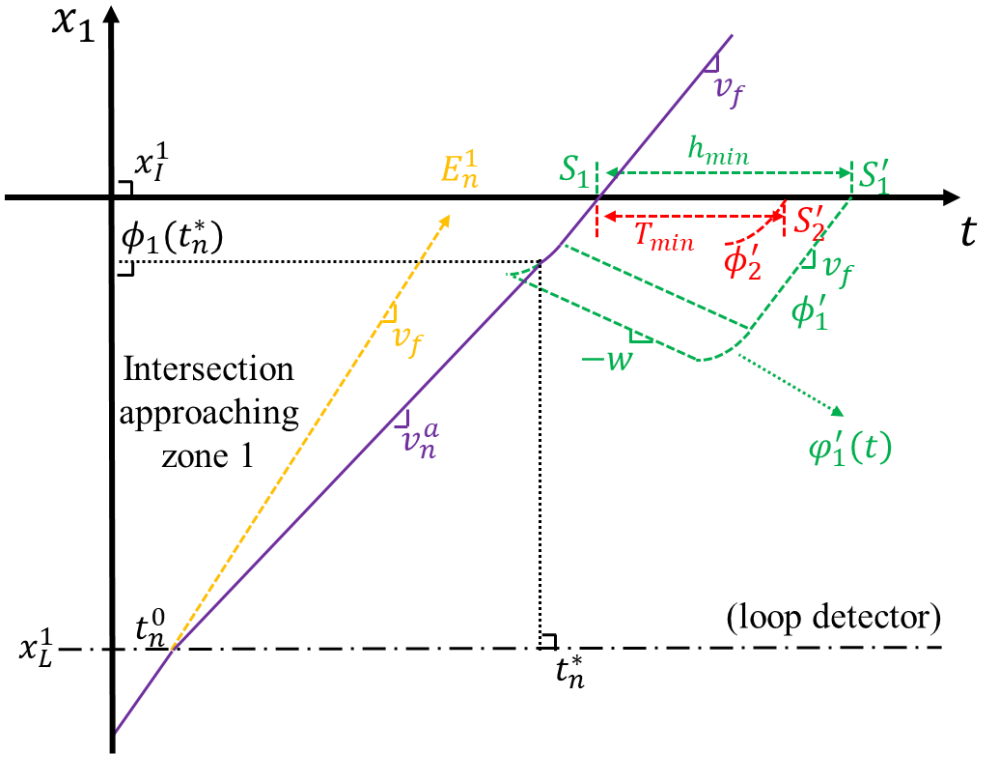
x_1
v_f
x_I^1
E_n^1
S_1
h_{min}
S_1'
t
$\phi_1(t_n^*)$
T_{min}
S_2'
ϕ_2'
v_f
ϕ_1'
v_f
$-w$
Intersection approaching zone 1
v_n^a
$\varphi_1'(t)$
t_n^0
(loop detector)
x_L^1
t_n^*

(b)

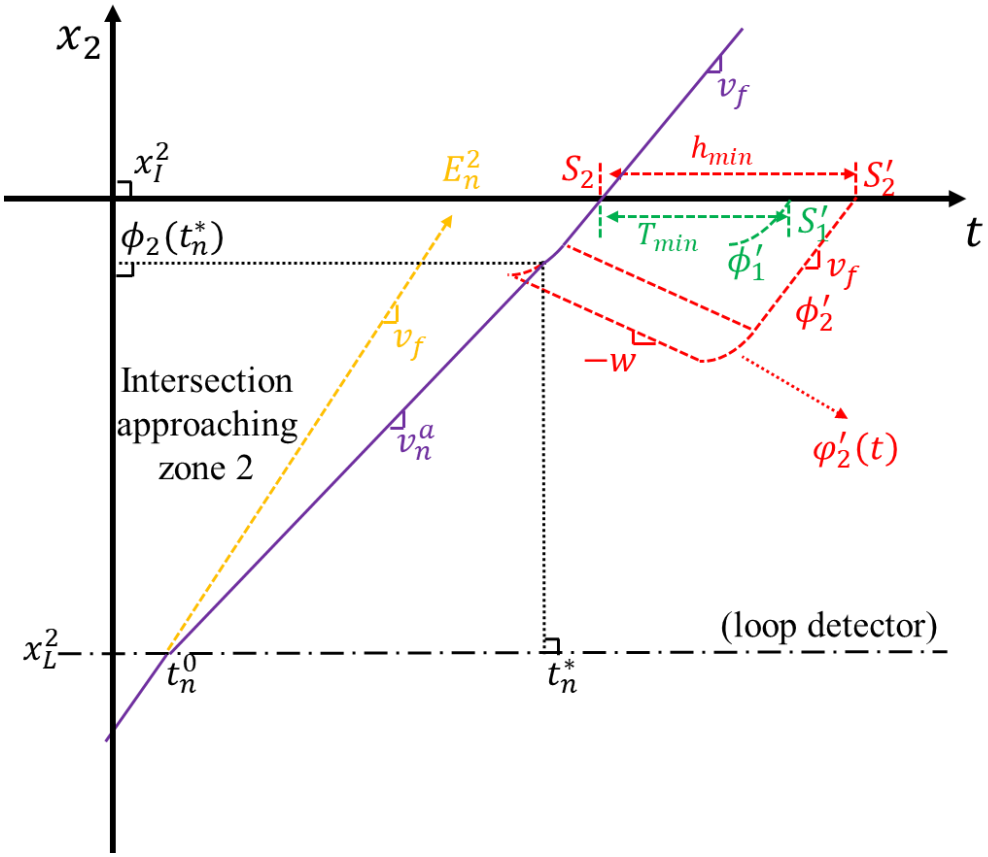

(c)

Figure 6.3 The Passing Point Creating and Updating Process

Figure 6.3 provides an example for passing point assignment and update process when $M = \{1,2\}$. In the Figure 6.3(a), when vehicle n from direction 1 passes through the intersection at E_n^m ($S_1 < E_n^1$), the following vehicle from direction 1 has the earliest safety time for entering the intersection is h_{min} later than E_n^1. For the other direction, the earliest safety time for entering the intersection for vehicles should be T_{min} later than E_n^1. The Figure 6.3(b) and Figure 6.3(c) provide the instances when $S_1 > E_n^1$ and when a vehicle from direction 2 comes respectively. The corresponding estimated trajectories for both directions (ϕ'_M) are updated accordingly. It is worth noticing that $\phi_m^n(t)$ is associated with S_m^n. As the Figure 6.3(a) shows, when $S_m^n = E_n^m$, $\phi_m^n(t)$ only includes the point of (S_m^n, x_I) when updating ϕ_m'.

6.2.3 Advisory speed and application ending time design

The advisory speed and application ending time are designed similar with the algorithm applied in the signalized intersection shown in Chapter 5. The advisory speed and application ending time are designed together through a tangent trajectory which starts from where the vehicle passes the detector (t_n^0) and tangents to the corresponding estimated trajectory (ϕ_m^n), at the tangent point (t_n^*). Once a passing point is assigned, the vehicle should receive and apply the advisory speed towards the non-signalized intersection, and after the application ending time, the vehicle would be back to the normal following behaviour.

$$\phi_m^n(t_n^*) = x_n^* \tag{6.12}$$

$$\frac{d(\phi_m^n(t_n^*))}{dt} = v_n^a \tag{6.13}$$

$$v_n^a = \frac{x_n^* - x_L^m}{t_n^* - t_n^0} \tag{6.14}$$

The advisory speed and the application ending time are derived from Eq. (6.12) to Eq. (6.14). x_n^* is the location where vehicle n finishes applying the cruise control. Eq. (6.12) restricts the vehicle actual trajectory with advisory speed should enter the corresponding estimated trajectory when finishing the algorithm. Eq. (6.13) shows the application ending time (t_n^*) is the tangent point of the estimated trajectory. Eq. (6.14) directs the tangent line starts from the time when the vehicle passes the detector (t_n^0), and the tangent line is regarded as the vehicle trajectory under the control algorithm.

Figure 6.3(b) and Figure 6.3(c) give examples of the vehicle approaching trajectory towards the intersection. Taking the slope of a tangent line as the advisory speed, each vehicle travels stably approaching the intersection, with the decrease of traffic oscillation. Since each vehicle only has to apply a cruise control with providing the application ending time, this approach avoids the complexity in algorithm execution.

6.3 Numerical experiments

6.3.1 Simulation setup

In this section, a set of numerical experiments are conducted to evaluate the control algorithm. The traffic network in the simulation consists of two ring roads, with an intersection at the end of the ring roads. The typical signalized intersection without any control algorithm for vehicles are considered as the control group of the simulation. Two fleets of the vehicles are travelling along each of the road, with the parameter settings shown in Table 6.1.

Table 6.1 Simulation Settings for the Control Algorithm Applied at the General Intersection

Parameters	Values
The intersection settings	
$L_r^{\{1,2\}}$, The length of both roads	1200 m
$x_I^{\{1,2\}}$, The intersection location of both roads	1200 m*
T_s, Total simulation time	500 sec
τ, Time gap between vehicles	1.5 sec
$v_f^{\{1,2\}}$, Free-flow speed of both roads	20 m/s (45 mph)
a, Bounded acceleration rate	2 m/s^2 (6.56 ft/s^2)
L, The vehicle length	7 m
Δt, Simulation time step	0.2 sec
The intersection with the control algorithm (the test group)	
$L_I^{\{1,2\}}$, Intersection length	13 m
$x_L^{\{1,2\}}$, The location of each loop detector	1000 m
The typical signalized intersection (the control group)	
GL, Green interval for both roads	25 sec
RL, Red interval for both roads	*25 sec*
YL, Yellow interval for both roads	6 sec
AR, All-red interval for both roads	*6 sec*
δ, Degree of aggressiveness	*50* %

* The intersection location is at the end of each ring road.

The traffic network used for the simulation, is shown in Figure 6.4(a). The network consists of two flat one-way ring roads with the intersection at the end of each road ($x_I^1 = x_I^2 = 1200\ m$). The ring roads are single lane with one direction each at the intersection. Among the two roads, road 1 has priority over road 2. The ring road network contains a steady flow rate in each road and excludes the traffic behaviours which is not considered in the algorithm, such as overtaking and lane changing outside of the intersection approaching zone. In addition, this scenario is equivalent to an arterial network shown in Figure 6.4(b). Each intersection is equally spaced, with the horizontal and vertical distances of L_r^1 and L_r^2, which is the same as the lengths of the ring roads. The link flow rates of horizontal and vertical directions equal the flow rates at the two roads respectively. Before enforcing the algorithm, we assume each intersection to be signalized, which is set as the control group. Similar with the study in Chapter 5, this simulation also assumes that when vehicles approach the signal during the yellow interval, if there is no algorithm applied, half of the drivers would decide to pass, and the other half would prepare to stop, i.e., the degree of aggressiveness (δ) is 50%. When the algorithm is in operation, the intersection is not signalized, and the signal is replaced by an information controller that could retrieve and record the information from vehicles and communicate with the detector and each vehicle.

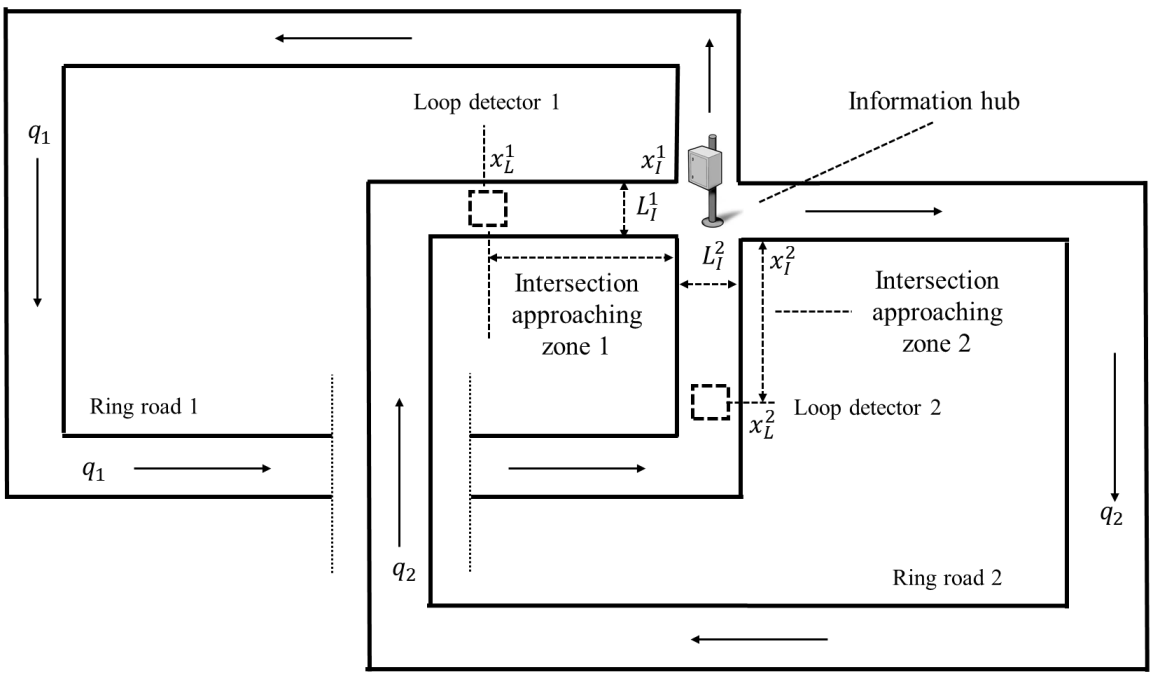

(a)

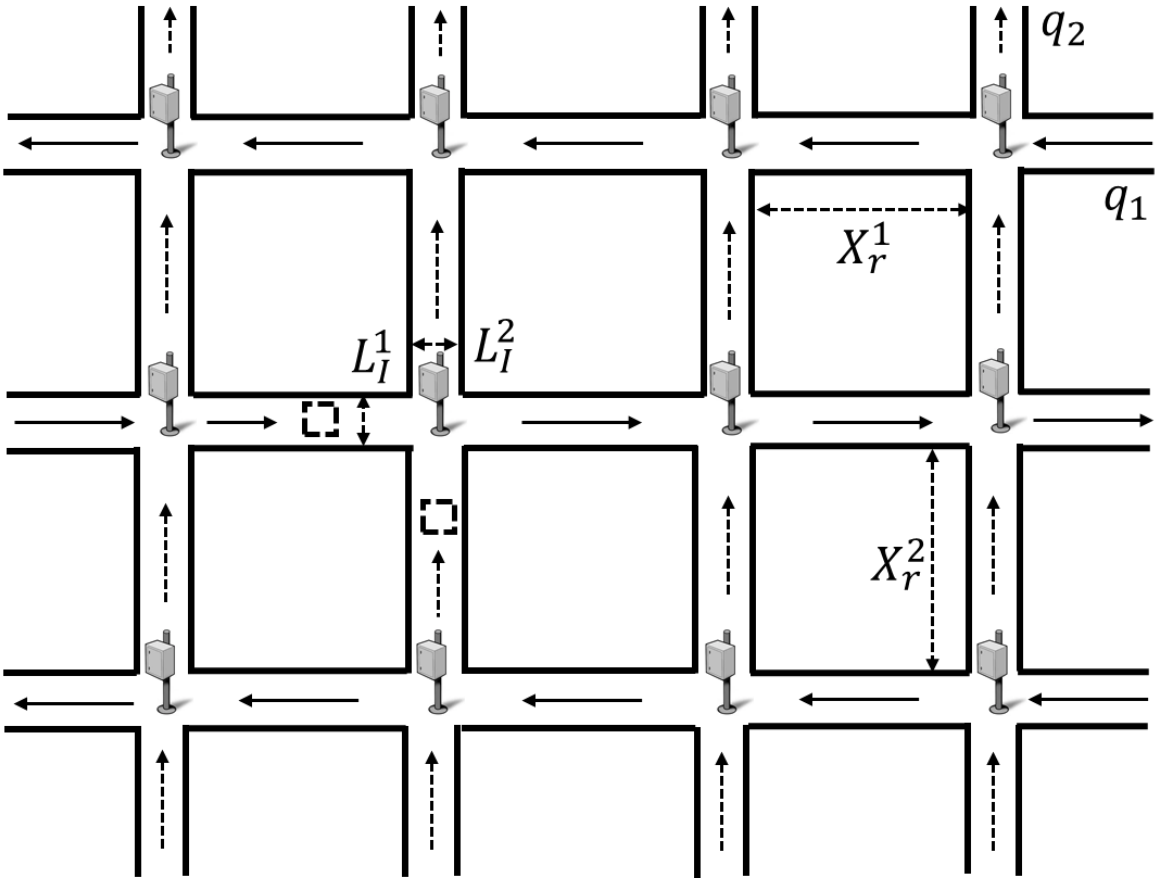

(b)

Figure 6.4 The Road Network in the Non-Signalized Intersection Simulation

6.3.2 Vehicle trajectory comparations

Figure 5 illustrates the trajectories of all vehicles at each ring road before and after applying the control algorithm after the traffic flow stabilizes. The initial flow rate for each ring road is $q_1 = 900vph, q_2 = 600vph$. Figure 6.5(a) and Figure 6.5(b) illustrate the vehicle trajectories on both road 1 and road 2 with conventional signalized intersections respectively. In this case, each vehicle follows the previous vehicle and the signal, which leads to a complete stop and waiting delay during red intervals, and departure delay when the signal changes to green. On the ring road 1, vehicles couldn't pass the intersection within one signal cycle, and the queue always exists ahead of each intersection. If q_1 keeps increasing, the queue length would be longer, which the signal capacity to be exceeded, and the green interval should lengthen. In addition, the departure delay includes the start-up delay (the headway is more than h_{min}), and

the clearance delay (the yellow interval time delay and the passing through time is more than T_{min}).

Figure 6.6(a) and Figure 6.6(b) plot the vehicle trajectories on both roads after applying the control algorithm. The orange moment presents a vehicle from road 1 entering the intersection, while the yellow time moment denotes a vehicle from road 2 entering the intersection. As shown by the vehicle trajectories, every vehicle could pass through the intersection at the free-flow speed. In this case, the trajectories show that both the headway (h) and the traverse time (T) stay at the minimum values. At a steady traffic state, vehicles are more evenly distributed at the ring road comparing with the control group. In addition, each vehicle travels without any conflict with the vehicles from the other direction.

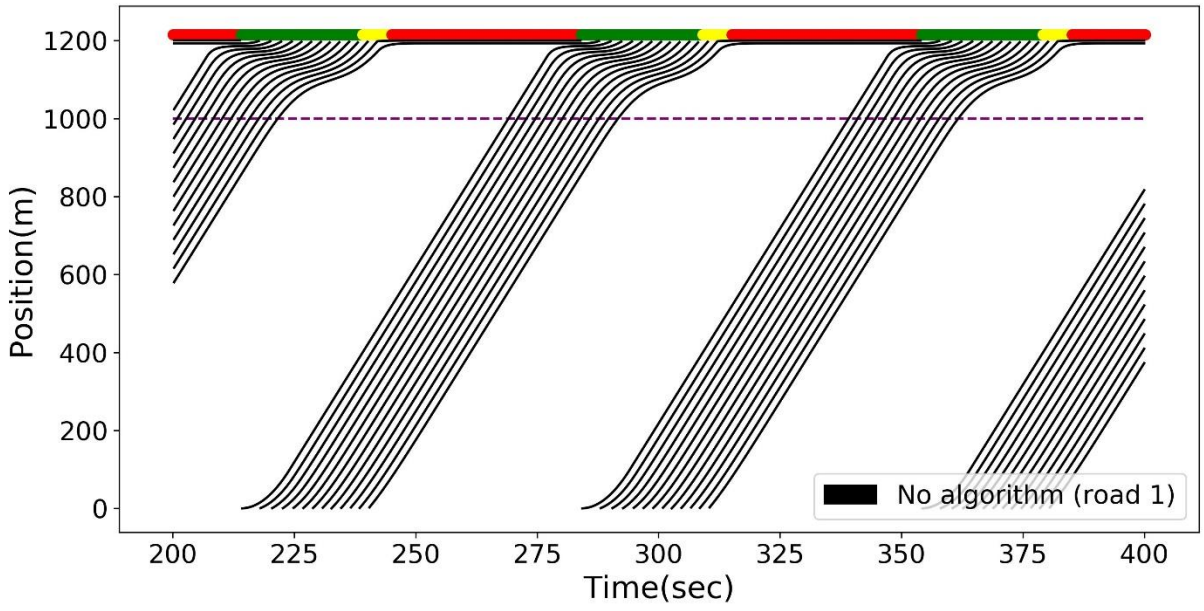

(a)

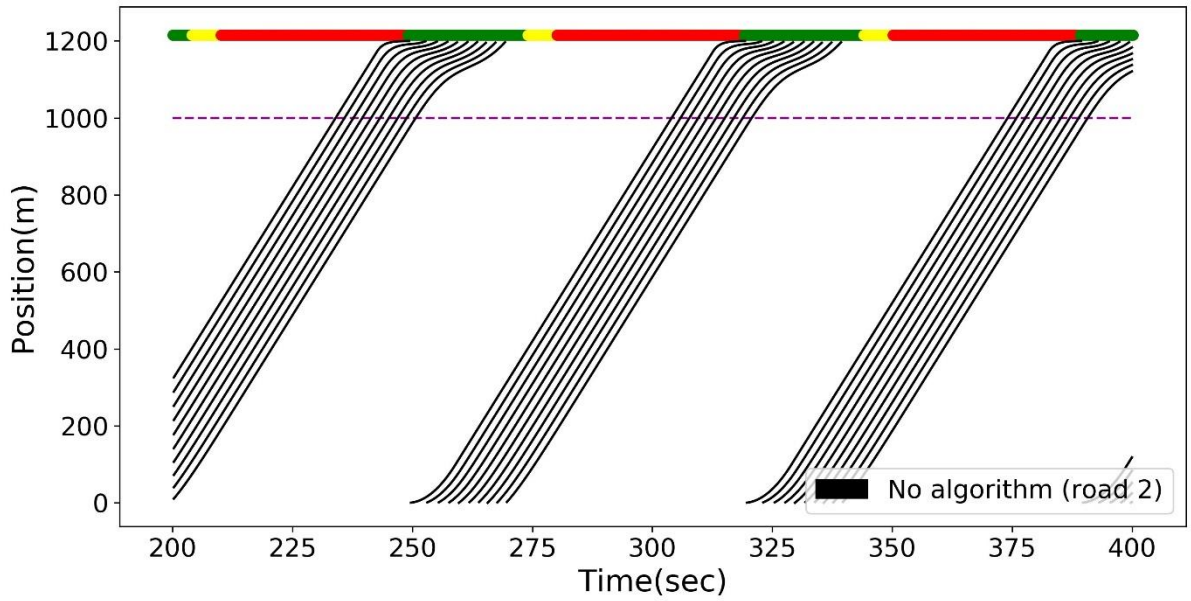

(b)

Figure 6.5 Vehicle Trajectories without the Algorithm at Signalized Intersections

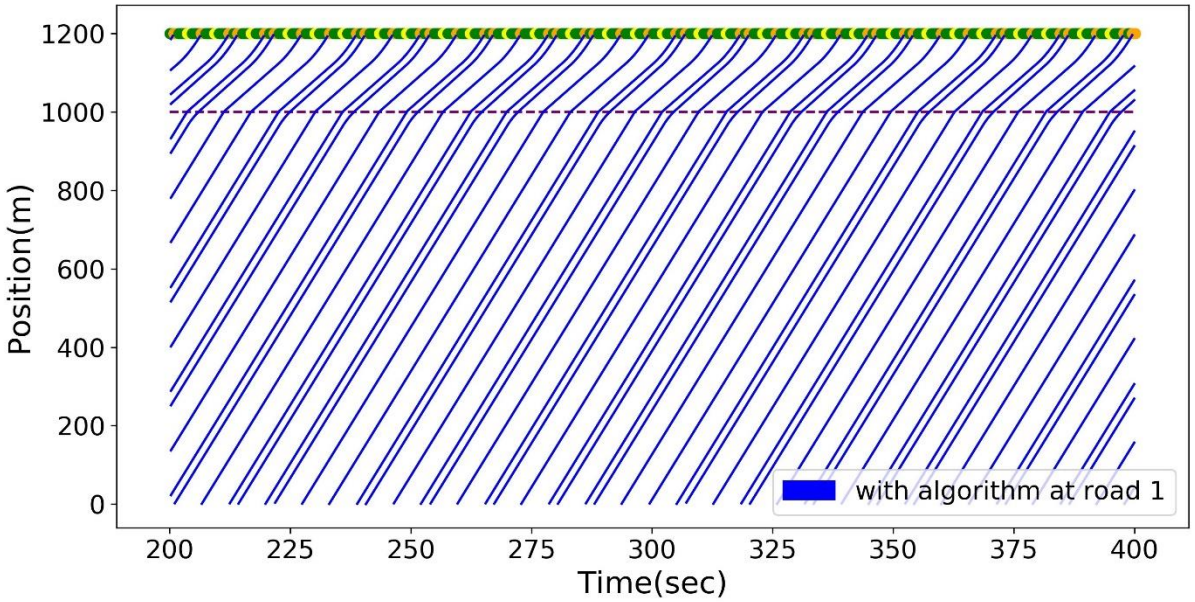

(a)

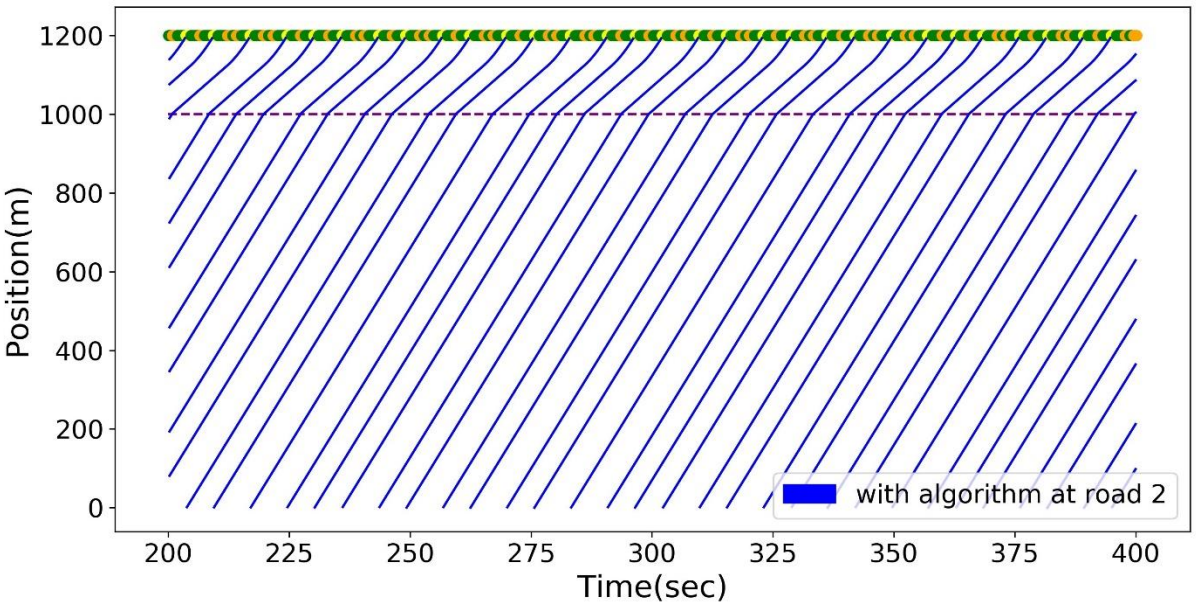

(b)

Figure 6.6 Vehicle Trajectories after Appling the Algorithm at Non-Signalized Intersections

6.3.3 The algorithm performance evaluations

In this subsection, the algorithm performances are analysed under different flow rates of each road. The evaluations are from three aspects, i.e., the reduction in speed oscillation (the average speed variance); the improvement on traffic efficiency (average speed during the simulation); and the decrease of environmental impacts (fuel consumptions). Assuming the algorithm is designed for the traffic flow under an uncongested network, while if any of the flow-rates of the two ring roads (q_1 and q_2) reaches 900 vph, vehicles couldn't pass the intersection within one signal cycle in the control group, i.e., the traffic condition gets to a congested level. Whereas, this study sets the flow-rate range of each ring road is under 900 vph. The simulation results of three evaluations are shown in Figure 6.7, while the data of the evaluation performance results at each flow-rate level is shown in ***Appendix C***.

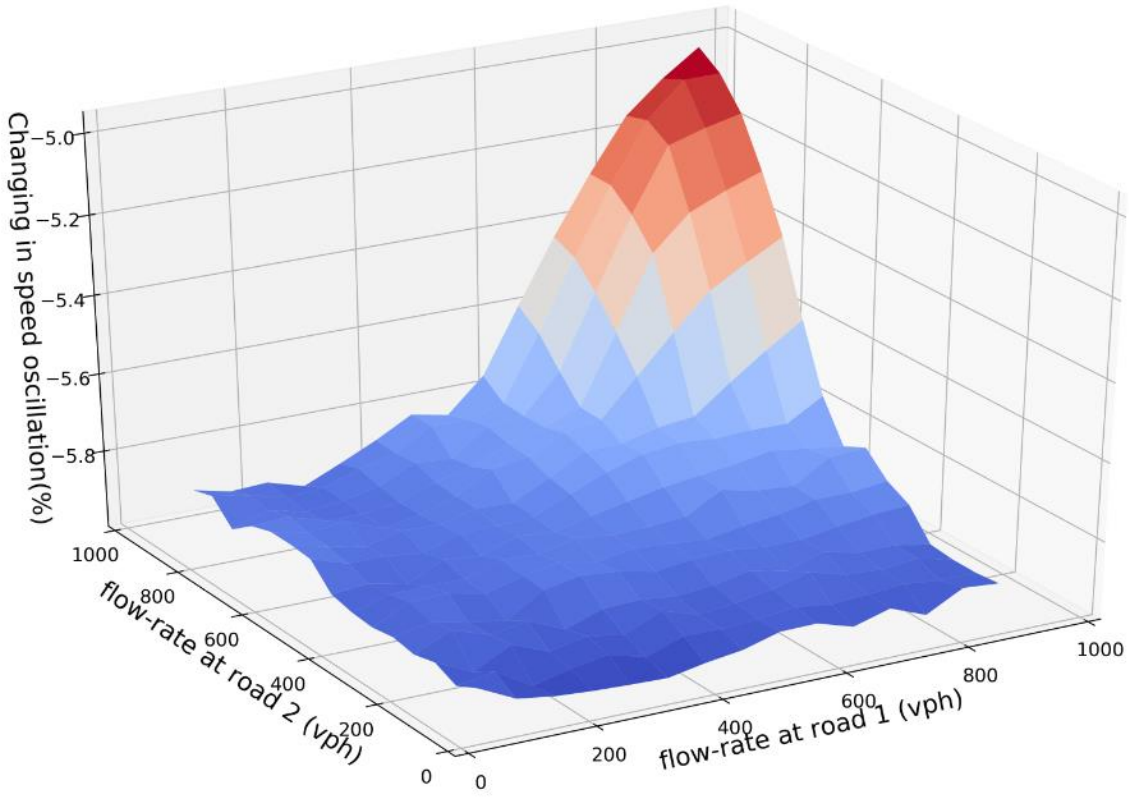
Changing in speed oscillation(%)
−5.0
−5.2
−5.4
−5.6
−5.8
flow-rate at road 2 (vph)
1000
800
600
400
200
0
flow-rate at road 1 (vph)
0
200
400
600
800
1000

(a)

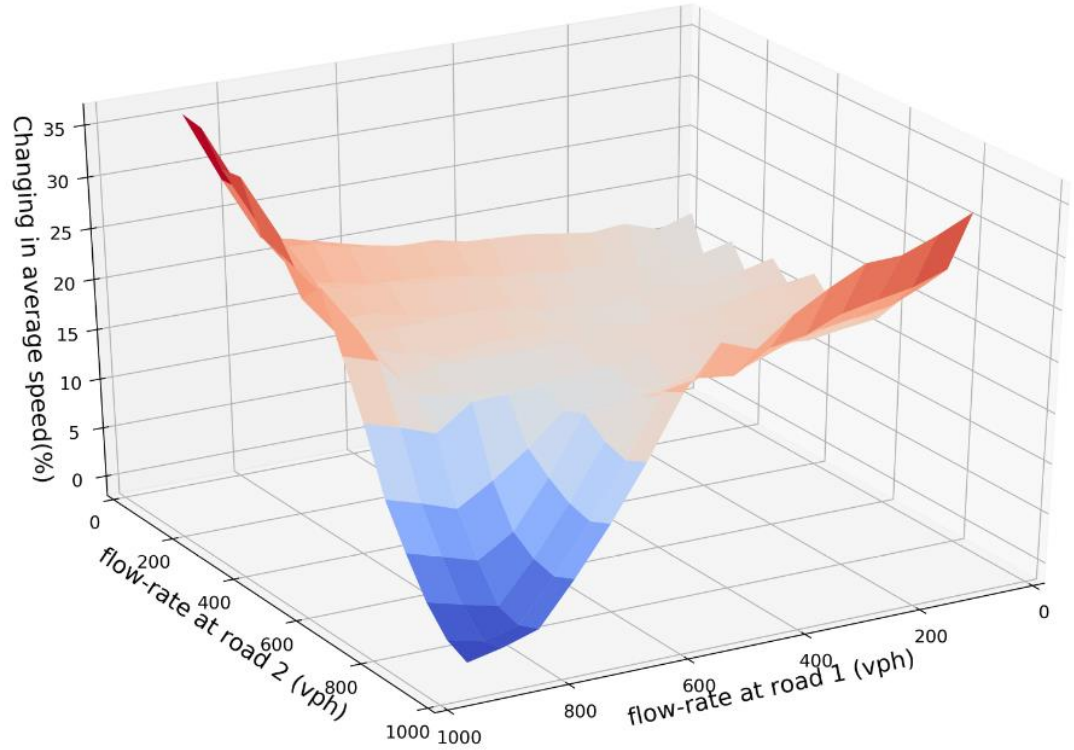
Changing in average speed(%)
35
30
25
20
15
10
5
0
flow-rate at road 2 (vph)
0
200
400
600
800
1000
flow-rate at road 1 (vph)
1000
800
600
400
200
0

(b)

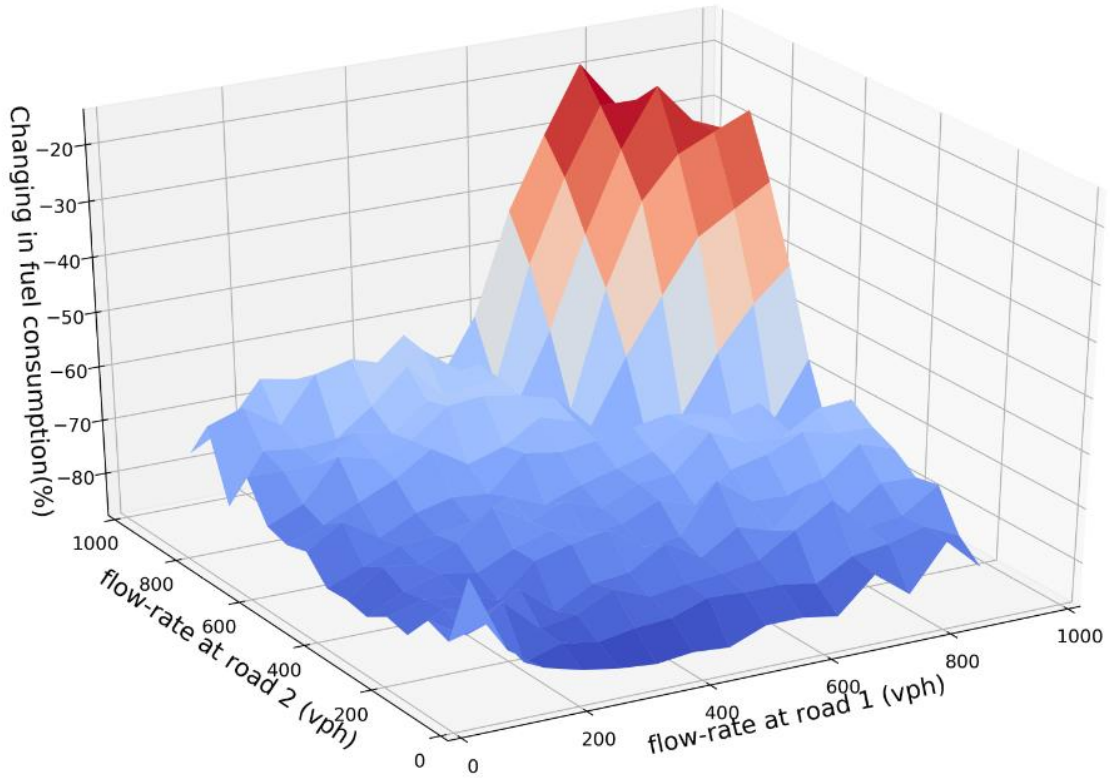

(c)

Figure 6.7 Algorithm Performance Evaluations in the Non-signalized Intersection

It could be observed that a similar tendency is shown of all three simulation evaluations with the flow-rates changing of two road sections, although the values of the improvements are different. Figure 6.7(a) shows the changings in the speed oscillation with the changes in flow-rates of the two ring roads. Overall, the algorithm could reduce the traffic oscillation of more than 5% regardless the flow-rates, while the reduction rate is more significant with lower flow-rate levels.

Figure 6.7(b) shows the improvements in the vehicle average speed during the simulation with different flow rate level of each ring road. When two roads both have relatively low flow rates, the algorithm shows a more significant improvement in the traffic efficiency. The maximum average speed improvement could be as much as 34.95%. In this case, each vehicle from the road with the lower flow-rate could have the advisory speed nearly the same as the free-flow speed, i.e., the vehicle doesn't have to decelerate when approaching and passing through the

intersection. On the contrary, with the signalized intersection case in the simulation control group, vehicles may still have to stop at the signal, which generates greater delays and decrease the traffic efficiency. With the flow rates of both directions increasing, although the average speed improvement becomes less significant, the algorithm could still bring an improvement in traffic mobility. When applying the algorithm, as long as the vehicles which pass through the intersection are continuously from one road, each vehicle would generate a traversing delay of T_{min} which is applied for vehicles of the other direction. As the flow rate increases, the traversing delay would accumulate. In contrast, with a pre-fixed signal as the control group, since a platoon of vehicles are passing through the intersection together during a phase interval, the traversing delay generated by each vehicle is not obvious. Since the savings in start-up and clearance delays is more than the traversing delay, the algorithm still brings an improvement on the traffic mobility with higher flow rates.

In Figure 6.7(c), the savings in fuel consumption shows the same tendency as the intersection delay. With a low flow rate, the saving in fuel consumption could be as much as 86.4%, while with a high flow rate, the saving is more than 15%. Although the traverse delay accumulation is still a reason for generating traffic oscillation, each vehicle stays at a steady speed when applying the advisory speed. Furthermore, the fuel consumption saving becomes more obvious again (with more than 30%) when the control group becomes congested with a higher flow rate. At a congested signalized intersection, vehicles could wait for two signal cycles before leaving the intersection, in which case, these vehicles experience the stop-and-go movements more than twice.

From the result, the priority also has an impact on the improvements. When road 1 (with priority) has a lower flow rate than the other road, the savings are less than the opposite situation, i.e., road 2 has more flow rate than road 1. Since vehicles on road 1 have priority to arrange the passing points, potentially vehicles on the other road have to wait longer and may generate a lower advisory speed. According to the result, the priority should be transferred based on the flow rate of each direction, in order to further improve the performance with the algorithm.

In conclusion, the simulation results at the intersection show that the algorithm could bring an improvement from three aspects under different flow-rate levels. Especially, the algorithm performance becomes more obvious except for the situations where two road are both having a high traffic flow-rates, (i.e., over $800\ vph$). Based on the V2I communications, the algorithm provides an alternative control method to realize the intersection control which is different from the typical signal control. The simulation results show that in an uncongested connected vehicle environment, vehicles could safely pass through the intersections with more traffic efficiency without applying the traffic signal at the intersection.

6.4 Summary

This chapter further proposes an eco-driving CVIC algorithm at the intersection, through which the signal control could be totally replaced by the V2I communications. Instead, an information hub is installed the intersection to operate the control algorithm for each approaching vehicle from all directions. The objectives of the algorithm are to improve the traffic efficiency, reduce the environmental impacts, and decrease the traffic oscillation at a non-signalized intersection. The algorithm could also theoretically avoid any potential traffic conflicts to guarantee the traffic safety at the intersection. According to the kinematic analysis in Chapter 2, vehicles should pass through the intersection with the free-flow speed to fully improve the traffic mobility. Therefore, the passing points for each movement should be created by the minimum headway and the minimum intersection clearance time. Since the intersection doesn't have a signal control, the passing points for upcoming vehicles are purely created and updated according to the previous vehicles passing through the intersection from different directions. The estimated trajectory is still generated for each passing point in order to design the advisory speed and control duration for each vehicle. Through V2I communications, each vehicle could receive the advisory speed from the controller and apply cruise control until the application ending time.

In order to test the algorithm performance, a set of simulations is conducted at a two-road network, where a signalized intersection is simulated as the control group. Firstly, vehicle travelling trajectories of both ring roads are plotted respectively before and after applying the algorithm. From the trajectory comparisons, all vehicles applying the algorithm would never

stop before the intersection, and would pass through the intersection with the free-flow speed. The traffic oscillation when approaching the intersection also decreases. It is worth noticing that vehicles from conflicting movements are passing through the intersection by the minimum intersection clearance time, and no vehicle confliction happens at the intersection. From the sensitivity analysis results, the algorithm could potentially bring an averagely 78.53% improvement in traffic efficient, reduce the fuel consumption by averagely 34.95%, and decrease the speed oscillation for each vehicle by averagely 5.75% under different flow-rate levels. The simulation also suggests a tendency that the improvements of both mobility and fuel consumption become less significant when flow rates increase, especially when two roads have flow rates which over 600 vph.

Chapter 7

Conclusion and Future Studies

This thesis proposes an eco-driving strategy that could be applied into various traffic situations including in a highway road following a moving bottleneck, and at an intersection. The algorithm is applied at a connected vehicle environment where vehicles could receive real-time information via V2I and V2V communications, and autonomously adjust their travel behaviors. Based on kinematic wave analysis at the traffic situations, the algorithm could derive the vehicle's original trajectory in the highway road section by solving the moving bottleneck problem. At the intersection, the algorithm would arrange a set of passing points and estimate the trajectory with the objective of improving the traffic efficiency. According to the optimization model with its heuristic solution, the vehicle trajectory could be redesigned to reduce the speed oscillation of each vehicle. Each connected vehicle would apply a simple cruise control with the advisory speed during the control duration, which would direct the vehicle to travel along the redesigned trajectory.

A set of numerical experiments are conducted to test the algorithm performance at each traffic situation including the trajectory comparison and sensitivity analysis. From the simulation results, in the highway section following a moving bottleneck, the algorithm would reduce the oscillations in the upstream traffic, and thus reduce fuel consumption. As the original trajectories for following vehicles are derived directly from the moving bottleneck problem, where traffic is impeded by the leading vehicle, the algorithm doesn't change the average speed of each following vehicle. At both the signalized and non-signalized intersection cases, vehicles could pass through the intersection smoothly without any conflicts, which guarantees traffic safety at the intersection. In addition, the algorithm would be beneficial on three aspects, including traffic efficiency improvement, traffic oscillation decrease, and environmental impact reduction under different flow-rate levels.

Several further studies could be extended from this study. First, this study assumes that the vehicles are all connected and in communication. A mixed traffic scenario could also be studied where not all vehicles could be under the algorithm's control. Second, this algorithm can be extended to dynamic real-time speed control algorithms with other specific objective functions, while this study focuses more on proposing a heuristic solution and applying the static advisory speed for vehicle trajectory redesign. Third, since the leading vehicle movement estimation and the communications between vehicles can not totally be accurate and timely, other considerations should be included such as communication delays, update of leading vehicle estimation, and communication transmission ranges. In addition, the strategy was applied for uncongested traffic flow situations. The effectiveness would also be tested when the traffic becomes congested. Finally, the algorithm could also be applied into larger networks, and the safety issues can only be studied with detailed and careful field implementations and evaluations.

Some other extension studies could also be explored for each traffic situation. In a highway section, this study focuses on the moving bottleneck case without considering the lane changing behaviours. For a road section with multiple lanes, this eco-driving strategy may also have similar effects on smoothing trajectories and reducing emissions. At a signalized intersection, the algorithm could be extended by combining actuated signal cycles. The algorithm may also further improve the performances at the actuated signalized intersections. At a non-signalized intersection, the intersection could have directions with different passing-through speeds and distances. The algorithm should also be extended to consider such generalized intersections. Also, the algorithm would also be adjusted according to the spatial geometry and traffic channelization when approaching and leaving the intersection. The basic idea behind this study is to make a predictable time and speed for vehicle to eliminate the moving bottleneck effects, and to pass through the intersection. This information provides a theoretical basis to further optimize the traffic flows via V2I, V2V and CAV technologies, which could be applied for various situations. Ultimately, this thesis focused on studying the concept, and not on the myriad practical issues that may develop in implementation, much of which are beyond the thesis scope and not discussed here, even while the author is aware of them. Nonetheless, the successful results certainly indicate that further work that focuses on the practical issues is worthwhile in future.

BIBLIOGRAPHY

Ahn, K., Rakha, H., Trani, A. and Van Aerde, M., 2002. Estimating vehicle fuel consumption and emissions based on instantaneous speed and acceleration levels. *Journal of transportation engineering*, 128(2), pp.182-190.

An, F., Barth, M., Norbeck, J. and Ross, M., 1997. Development of comprehensive modal emissions model: operating under hot-stabilized conditions. *Transportation Research Record, 1587(1)*, pp.52-62.

Al-Dweik, A.J., Mayhew, M., Muresan, R., Ali, S.M. and Shami, A., 2017. Using technology to make roads safer: Adaptive speed limits for an intelligent transportation system. *IEEE Vehicular Technology Magazine, 12(1)*, pp.39-47.

Ban, X., Herring, R., Hao, P. and Bayen, A.M., 2009. Delay pattern estimation for signalized intersections using sampled travel times. *Transportation Research Record, 2130(1)*, pp.109-119.

Barth, M., Mandava, S., Boriboonsomsin, K. and Xia, H., 2011, June. Dynamic ECO-driving for arterial corridors. *In 2011 IEEE Forum on Integrated and Sustainable Transportation Systems (pp. 182-188)*. IEEE.

Dandrea, J., 1986. Coaching the professional driver. *Private Carrier, 23(3)*.

European Commission, 2011. Communication from the Commission to the European Parliament, the Council, the European Economic and Social Committee and the Committee of the Regions Youth Opportunities Initiative.

Fadhloun, K., Rakha, H. and Loulizi, A., 2016. Analysis of moving bottlenecks considering a triangular fundamental diagram. *International journal of transportation science and technology, 5(3)*, pp.186-199.

Gazis, D.C. and Herman, R., 1992. The moving and "phantom" bottlenecks. *Transportation Science, 26(3)*, pp.223-229.

Hurdle, V.F., 1984. Signalized intersection delay models–a primer for the uninitiated. *Transportation Research Record, 971*, pp.96-105.

INRIX (2019) '2018 Global Traffic Scorecard Report', (February). Available at: http://inrix.com/scorecard/.

Jiang, H., Hu, J., An, S., Wang, M. and Park, B.B., 2017. Eco approaching at an isolated signalized intersection under partially connected and automated vehicles environment. *Transportation Research Part C: Emerging Technologies, 79*, pp.290-307.

Jin, W.L., 2019. Nonstandard second-order formulation of the LWR model. *Transportmetrica B: Transport Dynamics, 7(1)*, pp.1338-1355.

Jin, W.L. and Laval, J., 2018. Bounded acceleration traffic flow models: A unified approach. *Transportation Research Part B: Methodological, 111*, pp.1-18.

Krajzewicz, D., Behrisch, M., Wagner, P., Luz, R. and Krumnow, M., 2015. Second generation of pollutant emission models for SUMO. In Modeling mobility with open data (pp. 203-221). Springer, Cham.

Leclercq, L., 2007a. Bounded acceleration close to fixed and moving bottlenecks. *Transportation Research Part B: Methodological, 41(3)*, pp.309-319.

Leclercq, L., 2007b. Hybrid approaches to the solutions of the "Lighthill–Whitham–Richards" model. *Transportation Research Part B: Methodological, 41(7)*, pp.701-709..

Leclercq, L., Chanut, S. and Lesort, J.B., 2004. Moving bottlenecks in Lighthill-Whitham-Richards model: a unified theory. *Transportation Research Record, 1883(1)*, pp.3-13.

Lee, J. and Park, B., 2012. Development and evaluation of a cooperative vehicle intersection control algorithm under the connected vehicles environment. *IEEE Transactions on Intelligent Transportation Systems, 13(1)*, pp.81-90.

Li, L. and Li, X., 2019. Parsimonious trajectory design of connected automated traffic. *Transportation Research Part B: Methodological, 119*, pp.1-21.

Li, X., Cui, J., An, S. and Parsafard, M., 2014. Stop-and-go traffic analysis: Theoretical properties, environmental impacts and oscillation mitigation. *Transportation Research Part B: Methodological, 70*, pp.319-339.

Li, X., Peng, F. and Ouyang, Y., 2010. Measurement and estimation of traffic oscillation properties. *Transportation Research Part B: Methodological,* 44(1), pp.1-14.

Lighthill, M.J. and Whitham, G.B., 1955. On kinematic waves II. A theory of traffic flow on long crowded roads. Proceedings of the Royal Society of London. Series A. *Mathematical and Physical Sciences, 229(1178)*, pp.317-345.

Lin, Q., Li, S.E., Du, X., Zhang, X., Peng, H., Luo, Y. and Li, K., 2018. Minimize the fuel consumption of connected vehicles between two red-signalized intersections in urban traffic. *IEEE Transactions on Vehicular Technology, 67(10),* pp.9060-9072.

Lu, G., Li, L., Wang, Y., Zhang, R., Bao, Z. and Chen, H., 2014, October. A rule based control algorithm of connected vehicles in uncontrolled intersection. *In 17th international IEEE conference on intelligent transportation systems (itsc)* (pp. 115-120). IEEE.

Ma, J., Li, X., Zhou, F., Hu, J. and Park, B.B., 2017. Parsimonious shooting heuristic for trajectory design of connected automated traffic part II: computational issues and optimization. *Transportation Research Part B: Methodological, 95,* pp.421-441.

Mensing, F., Trigui, R. and Bideaux, E., 2011, September. Vehicle trajectory optimization for application in ECO-driving. *In 2011 IEEE Vehicle Power and Propulsion Conference* (pp. 1-6). IEEE.

Newell, G.F., 1998. A moving bottleneck. *Transportation Research Part B: Methodological, 32(8),* pp.531-537.

Newell, G.F., 2002. A simplified car-following theory: a lower order model. *Transportation Research Part B: Methodological, 36(3),* pp.195-205.

Park, S., Rakha, H., Ahn, K. and Moran, K., 2013. Virginia tech comprehensive power-based fuel consumption model (VT-CPFM): model validation and calibration considerations. *International Journal of Transportation Science and Technology, 2(4),* pp.317-336.

Pau, M. and Angius, S., 2001. Do speed bumps really decrease traffic speed? An Italian

experience. *Accident Analysis & Prevention, 33(5),* pp.585-597.

Rakha, H.A., Ahn, K., Moran, K., Saerens, B. and Van den Bulck, E., 2011. Virginia tech comprehensive power-based fuel consumption model: model development and testing. *Transportation Research Part D: Transport and Environment, 16(7),* pp.492-503.

Richards, P.I., 1956. Shock waves on the highway. *Operations research, 4(1),* pp.42-51.

Santa, J., Gómez-Skarmeta, A.F. and Sánchez-Artigas, M., 2008. Architecture and evaluation of a unified V2V and V2I communication system based on cellular networks. *Computer Communications, 31(12),* pp.2850-2861.

Shamir, T., 2004. How should an autonomous vehicle overtake a slower moving vehicle: Design and analysis of an optimal trajectory. *IEEE Transactions on Automatic Control, 49(4),* pp.607-610.

Smulders, S., 1990. Control of freeway traffic flow by variable speed signs. *Transportation Research Part B: Methodological, 24(2),* pp.111-132.

Sun, P., Nam, D., and Jayakrishnan, R., 2021. An Eco-driving Algorithm Based on Vehicle to Infrastructure (V2I) Communications at a Signalized Intersection. *In Proceedings of the Transportation Research Board 100th Annual Meeting* (Submitted).

Sun, P. and Jayakrishnan, R., 2021. A Cooperative Vehicle Intersection Control (CVIC) Algorithm Based on Vehicle-to-Infrastructure (V2I) Communications in a Connected Vehicle Environment. *In Proceedings of the Transportation Research Board 100th Annual Meeting* (Submitted).

Sun, P., Yang, D., and Jayakrishnan, R., 2021. A Dynamic Real-Time Trajectory Smoothing Algorithm for the Vehicles Behind a Moving Bottleneck in Mixed Traffic. *In Proceedings of the Transportation Research Board 100th Annual Meeting* (Submitted).

Sun, P., Yang, D. and Jin, W.-L. 2020. 'Eco-Driving Algorithm with a Moving Bottleneck on a Single-Lane Road', Transportation Research Record. doi: 10.1177/0361198120961381.

Ubiergo, G.A. and Jin, W.L., 2016. Mobility and environment improvement of signalized networks through Vehicle-to-Infrastructure (V2I) communications. *Transportation Research Part C: Emerging Technologies, 68*, pp.70-82.

Vaa, T., 1997. Increased police enforcement: effects on speed. *Accident Analysis & Prevention, 29(3)*, pp.373-385.

Wolshon, B. and Taylor, W.C., 1999. Analysis of intersection delay under real-time adaptive signal control. *Transportation Research Part C: Emerging Technologies, 7(1)*, pp.53-72.

Yang, H. and Jin, W.L., 2014. A control theoretic formulation of green driving strategies based on inter-vehicle communications. *Transportation Research Part C: Emerging Technologies, 41*, pp.48-60.

Yao, H., Cui, J., Li, X., Wang, Y. and An, S., 2018. A trajectory smoothing method at signalized intersection based on individualized variable speed limits with location optimization. *Transportation Research Part D: Transport and Environment, 62*, pp.456-473.

Zhao, W., Ngoduy, D., Shepherd, S., Liu, R. and Papageorgiou, M., 2018. A platoon based cooperative eco-driving model for mixed automated and human-driven vehicles at a signalised intersection. *Transportation Research Part C: Emerging Technologies, 95*, pp.802-821.

Zhou, A., Gong, S., Wang, C. and Peeta, S., 2020. Smooth-Switching Control-Based Cooperative Adaptive Cruise Control by Considering Dynamic Information Flow Topology. *Transportation Research Record*, p.0361198120910734.

Zhou, F., Li, X. and Ma, J., 2017. Parsimonious shooting heuristic for trajectory design of connected automated traffic part I: theoretical analysis with generalized time geography. *Transportation Research Part B: Methodological*, 95, pp.394-420.

Appendix

Appendix A. VT-CFPM model settings

Symbols	Parameters	Values
Q	Fuel lower heating value	$43{,}000{,}000\ J/kg$
N	Engine cylinders number	4
ω_{idle}	Idling engine speed	$700rpm$
d	Engine displacement	$2.354L$
P_{mfo}	Idling fuel mean pressure	$400{,}000pa$
FE_{city}	City fuel efficiency	$22mpg$
T_{city}	Duration of the city travelling	Simulation period
m	Vehicle mass	$1453kg$
η_d	Driveling Efficiency	0.92
ρ	Density of air	$1.2256\ kg/m^3$
C_D	Drag coefficient	0.3
C_h	Correction factor of altitude	1
A_f	Vehicle frontal area	$2.32m^2$
C_r	Rolling coefficient	1.75
c_1	Rolling resistance parameters 1	0.0328
c_2	Rolling resistance parameters 2	4.575

Appendix B. Simulation results at the signalized intersection

		Traffic flow rate (vph)									
		60	120	180	240	300	360	420	480	540	600
Control group	$\bar{F}$ (L /$100km$)	7.19	7.11	6.39	6.57	6.22	6.41	6.16	6.05	6.24	6.15
	σ	279.06	198.98	131.24	121.89	96.35	93.95	79.49	68.87	69.92	62.48
	$\bar{V}$ (m/s)	18.17	18.1	18.74	18.54	18.82	18.66	18.84	18.96	18.77	18.84
Test group	$\bar{F}$ (L /$100km$)	7.41	6.32	5.94	6.18	5.96	6.15	5.97	5.86	5.99	5.87
	σ	239.14	117.94	77.43	83.48	65.86	68.27	57.74	49.86	51.79	46.13
	$\bar{V}$ (m/s)	18.22	19.07	19.37	19.03	19.22	18.99	19.12	19.23	19.06	19.14

		Traffic flow rate (vph)									
		660	720	780	840	900	960	1020	1080	1140	1200
Control group	$\bar{F}$ (L /$100km$)	6.33	6.24	6.24	7.95	8.98	10.05	10.74	11.39	12.15	12.64
	σ	63.47	57.79	53.17	76.12	88.27	99.3	105.28	109.74	114.5	116.76
	$\bar{V}$ (m/s)	18.67	18.72	18.76	17.41	16.53	15.6	14.92	14.31	13.63	13.14
Test group	$\bar{F}$ (L /$100km$)	6.03	5.97	5.95	6.03	6.01	6.12	6.12	7.16	8.11	8.97
	σ	47.88	43.63	40.23	41.63	38.72	39.83	37.55	52.04	64.18	74.21
	$\bar{V}$ (m/s)	18.95	18.99	19.01	18.84	18.85	18.7	18.7	17.87	16.98	16.2

Appendix C. Simulation results at the non-signalized intersection

For the control group

F $(L$ $/100km)$	Traffic flow rate at direction 1 (vph)														
	60	120	180	240	300	360	420	480	540	600	660	720	780	840	900
60	0.51	1.15	1.4	2.23	2.52	3.35	3.63	4.5	4.94	5.64	6.09	6.75	7.53	8.25	9.24
120	1.17	1.81	2.07	2.89	3.18	4.02	4.3	5.17	5.6	6.3	6.75	7.41	8.2	8.91	9.9
180	1.95	2.59	2.85	3.67	3.96	4.8	5.08	5.95	6.39	7.08	7.53	8.2	8.98	9.69	10.68
240	2.71	3.35	3.61	4.44	4.72	5.56	5.84	6.71	7.15	7.85	8.29	8.96	9.74	10.45	11.44
300	3.48	4.12	4.38	5.2	5.49	6.32	6.61	7.47	7.91	8.61	9.06	9.72	10.5	11.22	12.21
360	4.24	4.88	5.14	5.96	6.25	7.09	7.37	8.24	8.67	9.37	9.82	10.48	11.26	11.98	12.97
420	5.12	5.76	6.02	6.84	7.13	7.97	8.25	9.12	9.55	10.25	10.7	11.36	12.15	12.86	13.85
480	5.96	6.6	6.86	7.68	7.97	8.81	9.09	9.96	10.4	11.09	11.54	12.2	12.99	13.7	14.69
540	6.77	7.41	7.67	8.49	8.78	9.62	9.9	10.77	11.2	11.9	12.35	13.01	13.79	14.51	15.5
600	7.57	8.21	8.47	9.29	9.58	10.42	10.7	11.57	12.0	12.7	13.15	13.81	14.6	15.31	16.3
660	8.37	9.01	9.27	10.09	10.38	11.21	11.5	12.36	12.8	13.5	13.95	14.61	15.39	16.11	17.1
720	9.17	9.81	10.07	10.89	11.18	12.02	12.3	13.16	13.6	14.3	14.75	15.41	16.19	16.91	17.9
780	9.97	10.61	10.86	11.69	11.98	12.81	13.09	13.96	14.4	15.1	15.54	16.21	16.99	17.7	18.69
840	11.35	11.99	12.25	13.07	13.36	14.19	14.48	15.34	15.78	16.48	16.93	17.59	18.37	19.09	20.08
900	12.53	13.17	13.43	14.25	14.54	15.38	15.66	16.53	16.97	17.66	18.11	18.78	19.56	20.27	21.26

Traffic flow rate at direction 2 (vph)

Traffic flow rate at direction 2 (vph) \ Traffic flow rate at direction 1 (vph)															
σ	60	120	180	240	300	360	420	480	540	600	660	720	780	840	900
60	364.02	346.85	190.95	181.23	134.0	128.88	106.26	103.2	89.7	87.95	78.95	77.79	76.52	77.38	83.94
120	328.4	324.43	204.19	193.88	151.59	144.91	123.02	118.59	104.92	102.05	92.66	90.6	88.56	88.61	94.13
180	278.51	285.31	191.63	184.59	148.75	143.13	123.6	119.52	106.92	104.11	95.25	93.15	91.08	90.98	96.06
240	237.9	250.34	175.04	170.95	140.6	136.36	119.23	115.85	104.5	102.06	93.93	92.04	90.16	90.12	94.98
300	206.58	221.72	159.4	157.51	131.54	128.51	113.46	110.79	100.6	98.59	91.18	89.57	87.93	88.01	92.73
360	183.08	199.25	146.36	145.96	123.4	121.3	107.96	105.88	96.7	95.06	88.29	86.93	85.51	85.71	90.31
420	164.51	180.96	135.18	135.84	116.0	114.63	102.72	101.12	92.82	91.5	85.31	84.17	82.97	83.27	87.78
480	149.41	165.72	125.49	126.9	109.28	108.48	97.78	96.59	89.04	88.0	82.32	81.39	80.38	80.79	85.2
540	137.09	153.04	117.22	119.16	103.35	103.0	93.31	92.45	85.55	84.75	79.52	78.77	77.92	78.42	82.75
600	126.78	142.26	110.03	112.34	98.04	98.04	89.21	88.63	82.29	81.7	76.86	76.26	75.56	76.13	80.39
660	118.01	132.97	103.7	106.28	93.25	93.54	85.45	85.09	79.25	78.83	74.34	73.88	73.3	73.95	78.12
720	110.46	124.89	98.12	100.88	88.94	89.45	82.0	81.84	76.43	76.15	71.97	71.63	71.17	71.87	75.96
780	103.87	117.78	93.12	96.02	85.01	85.7	78.81	78.81	73.78	73.64	69.74	69.5	69.13	69.88	73.9
840	104.08	117.1	93.93	96.62	86.16	86.76	80.15	80.08	75.22	75.02	71.22	70.93	70.53	71.21	75.04
900	103.96	116.23	94.4	96.92	86.97	87.5	81.15	81.05	76.35	76.11	72.42	72.1	71.66	72.28	75.95

Traffic flow rate at direction 2 (vph) \ $\bar{V}(m/s)$	Traffic flow rate at direction 1 (vph)														
	60	120	180	240	300	360	420	480	540	600	660	720	780	840	900
60	17.86	16.67	17.53	16.8	17.29	16.76	17.08	16.65	16.88	16.51	16.69	16.36	16.07	15.61	14.85
120	17.5	16.7	17.38	16.8	17.22	16.76	17.05	16.66	16.87	16.53	16.69	16.39	16.11	15.69	14.96
180	17.28	16.68	17.25	16.77	17.14	16.74	17.0	16.66	16.85	16.54	16.69	16.4	16.14	15.74	15.06
240	17.11	16.64	17.13	16.73	17.06	16.71	16.95	16.64	16.82	16.53	16.67	16.41	16.16	15.78	15.13
300	16.96	16.58	17.02	16.68	16.98	16.67	16.89	16.61	16.78	16.51	16.64	16.4	16.17	15.8	15.18
360	16.83	16.52	16.91	16.61	16.9	16.62	16.83	16.57	16.73	16.48	16.61	16.38	16.16	15.82	15.22
420	16.71	16.44	16.81	16.55	16.81	16.56	16.76	16.52	16.67	16.45	16.57	16.35	16.14	15.82	15.25
480	16.6	16.37	16.71	16.48	16.73	16.5	16.69	16.47	16.62	16.41	16.52	16.32	16.12	15.81	15.27
540	16.5	16.3	16.61	16.41	16.64	16.44	16.62	16.42	16.56	16.36	16.47	16.28	16.1	15.8	15.29
600	16.4	16.22	16.52	16.33	16.56	16.37	16.55	16.36	16.5	16.31	16.42	16.24	16.07	15.79	15.29
660	16.31	16.15	16.43	16.26	16.48	16.31	16.48	16.3	16.44	16.26	16.37	16.2	16.04	15.77	15.29
720	16.22	16.08	16.35	16.2	16.4	16.24	16.41	16.25	16.38	16.21	16.32	16.16	16.0	15.74	15.29
780	16.14	16.01	16.27	16.13	16.33	16.18	16.34	16.19	16.32	16.17	16.27	16.11	15.97	15.72	15.28
840	15.26	15.2	15.48	15.4	15.63	15.52	15.7	15.59	15.74	15.61	15.73	15.61	15.48	15.26	14.85
900	14.49	14.48	14.79	14.74	14.99	14.92	15.13	15.04	15.2	15.11	15.24	15.14	15.04	14.84	14.46

For the test group

F $(L$ $/100km)$	Traffic flow rate at direction 1 (vph)														
	60	120	180	240	300	360	420	480	540	600	660	720	780	840	900
60	0.18	0.25	0.33	0.41	0.49	0.57	0.64	0.79	1.08	1.17	1.34	1.95	1.59	2.79	2.45
120	0.25	0.43	0.4	0.63	0.68	0.82	0.96	1.05	1.47	1.47	1.68	2.13	2.48	3.21	2.98
180	0.33	0.4	0.69	0.7	0.81	1.07	1.1	1.36	1.4	1.85	2.44	2.35	2.64	3.05	4.05
240	0.41	0.59	0.65	1.01	0.87	1.17	1.42	1.57	1.8	2.29	2.54	2.98	2.91	4.15	4.19
300	0.49	0.68	0.84	0.9	1.33	1.52	1.94	1.82	2.11	2.88	2.97	3.09	3.65	4.63	4.14
360	0.57	0.86	1.15	1.25	1.62	1.86	1.88	2.29	2.26	2.74	3.72	3.85	4.6	4.69	4.61
420	0.73	1.05	1.18	1.49	1.94	1.91	2.3	2.28	3.09	3.21	4.12	4.27	4.16	5.2	5.7
480	0.81	1.35	1.42	1.98	1.81	2.19	2.31	2.73	3.24	3.93	4.3	4.68	5.04	4.85	4.67
540	1.11	1.49	1.63	1.85	2.05	2.67	2.83	3.13	3.59	3.98	4.39	4.08	4.04	4.61	6.54
600	1.24	1.65	1.89	2.43	3.1	2.65	3.11	3.58	3.98	3.56	3.82	4.16	6.22	8.07	9.86
660	1.27	1.7	2.46	2.42	2.83	3.46	4.09	4.3	4.39	3.82	5.69	7.48	9.09	10.85	12.5
720	1.98	2.23	3.08	3.43	3.01	3.88	3.99	4.55	4.54	4.41	7.48	10.15	11.86	13.38	15.16
780	1.65	2.51	2.64	2.81	3.45	4.5	4.16	5.04	3.91	6.22	9.36	11.86	14.17	14.0	14.33
840	2.83	3.05	3.08	3.78	4.53	4.79	5.2	4.44	4.61	8.07	10.85	13.38	14.0	13.47	13.83
900	2.36	2.95	3.97	4.08	4.6	5.15	5.7	4.67	6.73	9.68	12.3	14.8	14.38	13.8	14.11

Traffic flow rate at direction 2 (vph)

Traffic flow rate at direction 2 (vph) \ Traffic flow rate at direction 1 (vph)															
σ	60	120	180	240	300	360	420	480	540	600	660	720	780	840	900
60	35.55	23.7	17.77	14.22	11.85	10.16	8.89	9.94	13.78	13.93	12.52	10.93	7.57	11.88	11.5
120	16.69	27.56	10.01	23.43	16.3	18.1	13.61	12.35	12.91	13.59	12.66	13.23	11.51	12.11	10.85
180	10.21	8.16	18.89	16.54	12.93	18.23	13.96	10.06	13.17	12.06	14.13	10.8	9.78	10.29	11.53
240	7.07	12.88	10.67	17.99	10.11	14.53	13.33	14.91	11.68	14.02	10.36	10.66	10.7	10.85	8.76
300	5.26	14.87	12.82	10.03	17.29	17.1	16.18	13.19	14.32	13.18	11.64	11.35	12.05	13.29	12.37
360	4.12	8.21	9.37	14.1	18.41	17.95	14.84	15.93	14.06	15.03	13.84	14.02	15.4	14.95	15.95
420	6.71	13.62	14.36	13.66	16.17	15.03	16.39	14.38	13.93	13.98	17.78	15.47	14.41	18.94	19.89
480	8.09	12.26	9.65	11.56	13.2	15.91	14.61	15.93	16.89	17.59	18.3	18.36	19.18	18.31	17.64
540	11.13	12.08	10.19	11.76	13.69	14.47	14.08	17.08	19.47	21.13	21.23	19.75	19.4	19.78	24.21
600	10.48	12.97	11.42	13.25	13.41	13.02	14.13	17.98	21.13	20.64	21.76	21.71	26.26	31.76	36.77
660	6.42	10.45	13.25	10.32	11.77	13.88	17.87	18.3	21.23	21.76	28.09	34.09	39.14	43.88	48.24
720	9.05	10.5	9.99	12.89	11.3	14.28	15.54	18.53	19.94	21.84	34.09	46.18	50.78	54.6	57.81
780	4.72	10.78	9.0	10.28	12.03	15.4	14.41	19.18	19.49	26.33	39.21	50.78	60.2	63.34	65.81
840	9.98	9.62	9.93	10.32	13.25	15.54	19.21	18.35	19.78	31.76	43.88	54.6	63.34	70.54	72.64
900	9.19	9.57	7.85	8.72	13.96	16.68	19.89	17.64	24.24	36.82	48.22	57.84	65.87	71.68	78.31

Traffic flow rate at direction 2 (vph) \ $\bar{V}(m/s)$	Traffic flow rate at direction 1 (vph)														
	60	120	180	240	300	360	420	480	540	600	660	720	780	840	900
60	19.84	19.89	19.91	19.92	19.93	19.94	19.94	19.91	19.79	19.79	19.76	19.85	19.89	19.75	19.75
120	19.89	19.75	19.92	19.78	19.84	19.81	19.84	19.85	19.74	19.74	19.71	19.74	19.73	19.67	19.67
180	19.91	19.92	19.72	19.82	19.82	19.71	19.77	19.81	19.77	19.7	19.62	19.75	19.69	19.64	19.6
240	19.92	19.82	19.86	19.65	19.84	19.73	19.76	19.64	19.72	19.57	19.65	19.67	19.62	19.58	19.67
300	19.93	19.84	19.8	19.83	19.6	19.62	19.56	19.64	19.56	19.52	19.52	19.58	19.49	19.39	19.49
360	19.94	19.85	19.77	19.68	19.54	19.48	19.55	19.5	19.54	19.47	19.41	19.4	19.27	19.32	19.24
420	19.89	19.79	19.72	19.72	19.56	19.53	19.41	19.51	19.49	19.44	19.21	19.29	19.36	19.0	18.88
480	19.89	19.74	19.77	19.65	19.64	19.48	19.49	19.36	19.28	19.22	19.14	19.09	19.0	19.06	19.11
540	19.77	19.73	19.75	19.69	19.58	19.51	19.47	19.27	19.11	18.99	18.93	19.01	19.03	18.95	18.49
600	19.76	19.7	19.69	19.57	19.5	19.53	19.42	19.2	18.99	19.04	18.93	18.87	18.42	17.98	17.58
660	19.79	19.7	19.61	19.63	19.5	19.4	19.2	19.14	18.93	18.93	18.37	17.91	17.51	17.13	16.76
720	19.84	19.76	19.64	19.5	19.57	19.32	19.28	19.06	18.99	18.86	17.91	17.1	16.71	16.35	16.03
780	19.87	19.71	19.69	19.63	19.48	19.26	19.36	19.0	19.02	18.41	17.5	16.71	16.02	15.67	15.37
840	19.73	19.68	19.63	19.58	19.38	19.22	18.94	19.05	18.95	17.98	17.13	16.35	15.67	15.09	14.78
900	19.74	19.68	19.67	19.65	19.28	19.1	18.88	19.11	18.48	17.56	16.76	16.03	15.37	14.8	14.27